Title
A Mathematical Model of a DC Machine

Author
Chuang, N

Bibliographic citation
Chuang, N (2005). A Mathematical Model of a DC Machine. University Of Tasmania. Thesis.
https://doi.org/10.25959/23213066.v1

Is published in:

A MATHEMATICAL MODEL OF A DC MACHINE

By

Ning Chuang, B.E.(Hons), MIEAust, CPEng

School of Engineering

Submitted in fulfillment of the requirements for the degree of

Master of Engineering Science (Research)

UTAS

UNIVERSITY
OF TASMANIA

2004

Statement of Originality

I declare that this thesis presents my own original work and contains no material which has been accepted for a degree or diploma by any university or other institution, except by way of background information and duly acknowledged in the thesis, and to the best of my knowledge and belief no material previously published or written by another person, except where due acknowledgement is made in the text of the thesis.

……………………………….

Ning Chuang
October 2004

Statement on Authority of Access

……………………………….

Ning Chuang
October 2004
School of Engineering
University of Tasmania, TAS 7005
Australia

ABSTRACT

This research aims to determine how a mathematical model may predict the effects of a shorted and/or opened armature coil on a d-c machine. A mathematical model and a simulating computer were developed for a particular 0.375 kW d-c machine under both healthy and faulty conditions.

The model was based on the coupled-coil theory, with a set of first order differential equations that were solved in the time domain. New techniques for measuring inductances on a particular d-c machine were implemented in order to acquire data for development of a simulation. The research found that measurements of armature current waveform, including commutator ripple, agreed quite well with the simulated waveform.

Acknowledgement

During my extremely busy but unforgettable period of study for this research, I have received lots of help and support. I wish to take this opportunity to give my thanks to the following organisations and individuals.

Firstly, I would like to thank the Head and the Deputy Head of the School of Engineering, Professor Frank Bullen and Dr Greg Walker, for their support in my research, so that I could complete this work in such a short time.

Secondly, my sincere thanks should be given to my research supervisor, Dr Richard Langman, and my primary supervisor, Dr Tim Gale. I would like to thank them for their understanding, support and very kind help during the difficult time of my studies. Sometimes I kept them very busy with many issues regarding my work and its progress. I have enjoyed working with Richard in the Power Laboratory in solving some difficult problems with the machine. I also received lots of encouragement and suggestions from Tim. I am so glad that I was able to develop a very close friendship with my supervisors, so that my research project could be kept on the right track to meet the tight deadline.

I would also like to thank Dr Martin Ringrose and Associate Professor Michael Negnevisky, for helping and supporting me while I was learning MATLAB/SIMULINK. I very much appreciate the opportunity that enabled me to start using SIMULINK when I was working for Martin last year.

I also would like to thank a number of the technical support staff in the school, Steve Avery, John McCulloch, Glenn Mayhew, Bernard Chenery, Russell Twining and David Benda. Their help with my research has been very much appreciated.

I wish to give special thanks to a retired lecturer in the School of Engineering, my former university supervisor, Bob Wherrett who has given me support and assistance every time I was faced with various problems.

I am also grateful for Dr Sam Ho's kindness in allowing me to have a copy of the reference papers from his research in 1999. I would also like to thank Prof. Dieter Filbert in Germany for sending me a copy of his published papers.

In the School other postgraduates Andrew Barton, Simon Locke, Andrew Greenhill, Warwick Gillespie, Alan Henderson, Tzuu Bin Ng, Phi Anh Phan, Patrick Burke and Mark Lim have given me varied help and moral support. I often had conversations with them, sharing our research experiences or trying to solve technical problems. I would like to extend them my appreciation.

At the beginning of my research, Hydro Tasmania's Peter Fluckiger helped me by translating a paper in German, and TAFE teacher Rosalind Goodsell translated a French paper. These two papers were very useful to my research, and their many hours' work on technical translations relating to electrical machines has been much appreciated. Here also, my thanks should go to them.

While I was working on MATLAB/SIMULINK, I received assistance from the Applications Engineer from Ceanet, David Willingham, in relation to problems with my model. It may have taken longer to get my model working, without his valuable help, and I would like to thank him as well.

I also need to pass my thanks to the Science Librarians of the University, Chris Evans and Sandy von Allmen, for their very kind help when I was searching my references for this research. It was very hard to find appropriate references in this field, but I found most of them with Chris's and Sandy's help.

I would like to thank SEMF drafter David Belanich for helping me to learn AutoCAD, so that I could draw my many circuit diagrams in CAD within a short time.

Finally, my thanks should be given to my loved dog, Smudge, even though he could not directly help me in my research. But I always found a solution for the problems in my complicated model when I was out walking with Smudge, so I thought he should also be included in these acknowledgements.

Contents

Contents 1

Chapter 1 Introduction 4
1.1 Background of the research 4
1.2 Summary of this research project 4

Chapter 2 Literature review 6
2.1 Perspective on failure in d-c machines 6
2.2 Condition monitoring techniques for d-c machines 8
2.3 Initial studies on d-c machines 10
2.4 The effect of commutation on d-c machines 15
2.5 Technical methods of measuring machine parameters 20
2.6 Mathematical modelling techniques for d-c machines 20
2.7 Summary of literature review 25

Chapter 3 Equivalent circuits of the Davey machine 27
3.1 Basic Principles of modeling a d-c machine 27
3.2 7-coil and 5-coil equivalent circuits 29
3.3 Analysis of commutation during one revolution 32

Chapter 4 Measurement of inductances on the Davey machine 35
4.1 The need for a d-c inductance measurement 35
4.2 The d-c method of measuring inductance 35
4.3 Modifications of the basic DCIB method for measuring the self-inductance of armature sub-coils 39
4.4 Measuring other self-inductance on the machine 41
4.5 Measuring mutual inductance on the machine 43
4.6 Field current required for the Davey machine 47
4.7 Conclusion 47

Chapter 5 A mathematical model 50
5.1 Establishment of armature voltage equations 50
5.2 Preliminary model design techniques 58

5.3 Varying brush resistance programming in the model 58
5.4 Connection schemes 64
5.5 Implementation of the model in MATLAB 67
5.6 Conclusion of the model 69

Chapter 6 Experimental results 70
6.1 Load testing on the Davey machine 70
6.2 Armature and field current waveforms comparison 70
6.3 Problem solving and sensitivity analysis 75
6.4 Analysis and assessment on model's performance 77

Chapter 7 An armature shorted coil model 79
7.1 Armature winding with one shorted coil 79
7.2 The shorted coil position after 22.5^0 rotation 84
7.3 Implementation of the one shorted coil model for 22.5^0 of rotor movement 85
7.4 Model's outputs for the shorted coil machine 89
7.5 Test results on the Davey machine with shorted coil 91

Chapter 8 Conclusion of this research and further discussion 93
8.1 Overall review of the research work 93
8.2 Measuring inductance method using a d-c source 93
8.3 A model of the healthy Davey machine 93
8.4 A model of the faulty Davey machine with one shorted coil 94
8.5 Working with models in MATLAB/SIMULINK 94
8.6 Recommendations and future directions 95

References 96

Appendix A Measurements of armature inductance using an a-c source 103
A. 1 Measurement errors in the a-c method 103
A. 2 Saturated and unsaturated inductance data 106

Appendix B-1 A model of the healthy Davey machine 107
Appendix B-2 A model of the rotor position selector for the Davey machine 108

Appendix B-3 A model of the 7-coil circuit for the healthy Davey machine................ 109
Appendix B-4 A model of the 5-coil circuit for the healthy Davey machine................ 110

Appendix C-1 A model of the Davey machine with one shorted coil........................... 111
Appendix C-2 A model of the 8-coil circuit for the Davey machine with SC 112
Appendix C-3 A model of the 6-coil circuit for the Davey machine with SC 113
Appendix D-1 Data for the model of the healthy Davey machine................................114
Appendix D-2 Data for the model of the healthy Davey machine................................115

Chapter 1

Introduction

1.1 Background of the research

This research is a continuation of more general research into the condition monitoring of electrical machines by Ho [1]. Ho achieved two main things as a result of his research. Firstly, He designed equipment that would capture relevant current and voltage waveforms on industrial induction motors, and he also monitored currents and voltages on medium size (400 kW) d-c motors. Secondly, Ho modelled the a-c and d-c motors, using coupled coil theory in enough detail, so that the effect on supply currents of a broken motor bar on an induction motor, or a shorted circuit armature coil on a d-c machine could be predicted.

Ho's main study was of induction motors, since they have become the most common motors in industry. His study of d-c motors was very much a preliminary one, and aspects of modelling and solving the simultaneous differential equations were incomplete.

1.2 Summary of this research project

This research aims to examine the d-c machine in more detail. Two of the main aims were to reduce the time required for solving the differential equations (Ho [1] took 26 hours of PC time for 1.5 seconds of generator time), and to measure the inductances on the d-c machine in more detail, to allow correctly for magnetic field saturation.

Chapter 2 is a comprehensive review of the published literature. For the sake of completeness, this covers some general background on d-c machine research in addition to that what is specifically relevant to this research.

The armature winding of the d-c machine was established by two alternative equivalent circuits as discussed in Chapter 3.

The measurement of self and mutual inductances involving new and unusual techniques are presented in Chapter 4.

The differential equations describing the d-c machine were solved using MATLAB/SIMULINK. It might be thought that the solution of the first order simultaneous differential equations would be simple, but the many mutual inductance terms caused considerable difficulties, and how these were dealt with is detailed in Chapter 5.

Experimental results for the healthy machine are given in Chapter 6. There was very good agreement between the model of the healthy machine and experimental tests on the d-c machine. The waveforms of the armature and field currents obtained in the model were analysed and discussed in detail.

A model of the faulty machine with one shorted coil is discussed in Chapter 7. The model was implemented with a rotation in 22.5^0. The outputs of the model were compared with the test results on the d-c machine, with the comparison showing very similar for both the armature and field currents. The shorted-coil current obtained from the model was reasonable and satisfactory as calculated.

Chapter 8 provides a conclusion and further discussion for development in modelling d-c machines.

Chapter 2

Literature review

The purpose of this chapter is to review all recent and relevant literature for d-c machines. This includes some peripheral literature.

To achieve these goals this chapter starts with overview of the previous research work. A mathematical model on a direct-current machine has been regarded as an interesting topic in the field of power electrical engineering. The main objective of this research is to provide an early indication of incipient failures, and to help avoid major motor breakdown and catastrophic failures. Preliminary work on which this thesis was based was previously reported by Ho [1].

Although there was no previous work which covers exactly this research area except Ho [1], the reviewing process has still been carried out in a way that is useful for studying electric machines.

2.1 Perspective on failure in d-c machines

Previous work on failures in d-c machines was reviewed as an initial step. First, relevant aspects of the health and safe operation of electric direct-current machines are considered. The discussion starts with consideration of several types of faults as summarised below.

Due to the nature of the commutation process in d-c machines, the transfer of energy (electrical to mechanical and vice versa) can be accompanied by excessive arcing. It is known that excessive arcing may lead, under certain circumstances, to a shorted and/or open armature coil. A fault in a d-c motor may result in extensive damage and significant costs in repair and plant downtime. Arcing problems, as well as the armature winding integrity, are typically identified as the most critical failure modes that require a proper condition-monitoring strategy. Traditionally, off-line manual techniques are used to check the condition of the d-c motor winding and commutators.

Usually, any catastrophic failures of d-c motors cause substantial financial losses to the business unit who owns and operates those motors. It is very important to maintain and vigorously monitor the condition of these machines for early detection of any incipient fault. The focus of this research project is to develop condition monitoring for a shorted and/or opened armature coil on a d-c machine, using MATLAB as modelling tool.

There are several factors that could cause a failure of a short or an open armature coil on a d-c machine [2], as listed in table 2.1.

	BY CAUSE
1	Insulation degradation
2	Fatigue
3	Loosening
4	Shaft current
5	Foreign matter
6	Contamination
7	Improper maintenance
8	Improper design
9	Improper manufacture
10	Inadequate electrical protection

Table 2.1 List of DC machines dominant failure modes

Predominantly, the failure of d-c machines can be attributed to their armature faults [3]. The main faults that may develop in the armature winding are:

- A short circuit of a coil or coils

If this fault develops when the machine is running, intense local heating of the faulty coil will occur, quite independent of the load on the machine, owing to the large local current that will circulate in the faulty coil. The local closed circuit is the seat of the alternating emf. normally induced in the coil, so the current is limited solely by the impedance of the short-circuited coil. The heavy local current very often results in burn-out of the coil, and the fault then becomes an open circuit. The short circuit may take place between the risers on the commutator, or it may take place between adjacent turns of a multi-turn coil. The heavy current is purely local, so it does not overload the brushes.

- Open-circuited coil

The symptoms of this fault are most spectacular when the machine is loaded, but are insignificant on light load. Due to an open circuit coil, the other coil circuit on the armature lap winding carries double its normal current. The brushes are not overloaded, however, and trouble does not occur until the faulty coil passes under the influence of the brush. In so doing it is transferred from one armature circuit to the other, thereby causing the current in the whole of the sound coils to be changed from double normal value to zero.

- Earthed coil

If only a single earth occurs on the machine no serious symptoms arise. However, if two separate points on the armature winding become earthed, the coils between the two faults become short circuited, and the intense local heating symptoms are those of short-circuited coils. If a number of coils are thus short circuited very violent sparking will take place owing to the marked imbalance of the armature circuits.

As background to the research, it was also necessary to understand the specific nature of the short circuit currents on electric machines. One earlier publication of Concordia [4] was found particularly useful, even though the subject was for synchronous machines. Numerous equations were given in showing the relations of self-inductance and mutual inductance between stator and rotor circuits. Particularly, the flux-linkage relations in both direct axis and quadrature axis were provided.

2.2 Condition monitoring techniques for d-c machines

Publications on the condition monitoring techniques in this field were subsequently reviewed. There is a wide variety of condition monitoring techniques that have been used. This section presents the main published work relating to this field. Condition monitoring (CM) has attracted the interest of power electrical engineers for many decades. The fundamental principle of d-c machines in relation to CM was first considered by Hindmarsh [5] in the 1950's, when he discovered the problems with the complex magnetic relationship of d-c machines. Part 1 of the paper was about the commutation of large d-c machines, but it was part of the theory of the d-c machine commutation process. A main point learnt from this paper is a real criterion – whether or not the commutator and brushes are subject to excessive wear in service. As understood, there may be arcing under the brush and commutator bar by a number of contact points working at extremely high current densities of the order of several thousands of amperes per square inch. The comparison was made based on good commutation, reactance voltage, and effects of speed and energy considerations.

Part 2 of Hindmarsh's paper [5] emphasised modification of commutation theory using damping windings. The effect of commutation on the output equation was introduced in the conditions with damping winding present. Part 3 of his continuous research demonstrated the relevance of damping for large d-c machines. Commutation as a key process was stressed and there were a number of diagrams to show how d-c machines' commutation might be done.

Consecutive research work done by Hindmarsh in the 1950s, [6], [7], [8], [9], [10] and [11] involved understanding and analysis of large d-c machines. His major subject was focussed on large d-c machines, and his series of publications concentrated on this subject. The fundamental principles were first described showing that d-c machines could have flexible operation in terms of speed and energy [8]. The second article of his research focussed on large d-c machines having a volt per bar limit [11]. In this article he outlined evidence of the commutating behaviour from large d-c machine performance. His work involved investigation of several different types of d-c machine winding and the response of large d-c machines was also investigated. His fifth article [10] related to testing d-c machines using a method with interpole and compensating windings, and a linear relation between compole flux and its exciting current was claimed to be found.

Increasing interest in CM techniques for electrical equipment was investigated by Han and Song [12]. A general concept of condition monitoring was defined as a technique or a process to monitor the operating characteristics of machines. In such a way that changes and trends of the monitored characteristics can be used to predict the need for maintenance before serious deterioration or breakdown occurs, and/or to estimate the machine's "health". CM was considered to be of great benefit to customers, with the potential to reduce operating costs, enhance the reliability of operation, and improve power supply and service. The literature was surveyed on developing intelligent CM systems with advanced practicability, sensitivity, reliability and automation. Several areas in power electrical engineering were listed to use CM techniques:

- Power transformers
- Power generators

- Induction motors

The various faults occurring in general power equipment were investigated. Their paper reached conclusions that advanced signal processing techniques and artificial intelligence techniques were indispensable in developing novel CM systems. Following the development of CM techniques, the current research for modelling d-c motors is certainly seen as extending this theme.

Modelling a d-c machine with the simulation of a healthy or a shorted coil of the armature circuit is not easily implemented while the machine is rotating. The difficulties of this test were recognised in previous research by Ho, ([1] and [13]), and considerable difficulties were encountered when his mathematical model was applied to a d-c machine. A severe problem was described on a faulted d-c motor that resulted in burning of the commutator bar. The problem was also recognised by Thompson [14], who previously found that there would be arcing across the mica below the surface of the commutator if only two adjacent bars were discoloured. The problem might be caused by conductive material built-up, such as copper, between commutator bars, which could lead to flashover when bar-to-bar voltage became high.

The emf induced in the armature coils of d-c machines during commutation was investigated by Tustin [15]. An analysis identifying various sources of uncompensated emf and the means for evaluating them were introduced. Such a solution was found to the problem of designing interpoles for d-c machines so as to obtain a prescribed distribution of current between brushes and commutator. His claim indicated that the sources of such uncompensated emf could be recognised and avoided, because that component of emf must sum to zero. The research result in this paper is not directly related to the current research while some concepts were useful.

2.3 Initial studies on d-c machines

This section discusses a number of references relating to initial studies of d-c machines. The initial studies on d-c machines were carried out in relatively few publications (Engelann and Middendorf [16], Clayton and Hancock [17], Say and Taylor [18], Fitzgerald, Kingsley and Umans [19], Sarma [20] and Slemon [21]), which described d-c machine principles and theories as well as their performance and applications. A basic concept was obtained from these references used as a starting point for this research. This assisted the understanding of the complex relationships within a d-c machine, and how each component of a machine performs such as armature windings, commutators and brushes.

Regarding the measurement of mutual inductance between coils in the d-c machine, a survey undertaken by Clayton and Hancock [17] identified a conclusion that the exact calculation of the reluctance of the air gap in d-c machines is a matter of difficulty owing to:

- the gap dimension not being constant over the whole pole pitch, and
- the fact that modern armatures are toothed, so that the flux tends to concentrate upon the teeth.

Clearly, the distributed flux winding circuit is always a complicated concept in the study of d-c machines, and quite different opinions are expressed in the various publications reviewed in this literature survey.

The successful expression of the voltage and torque equations was established by Jones [22]. The performance of the different types of electrical machine under steady state, unbalanced or transient operation was discussed based on a basic two-winding machine. The machine performance could be analysed or predetermined from these voltage and torque equations. Also, an important point to learn from this reference was how to determine the coefficients of self-inductance and mutual inductance depending on saturation conditions.

According to Spannhake and Filbert [23], parameter estimation and modelling could be used to detect faults in small electric motors. Because of the high speed of production of small electric motors a fast and reliable test is necessary. At present testing small electric motors is usually done using a conventional test stand. The test stand consists of two major parts:

(1) the mechanical construction;
(2) the electrical equipment consisting of the power supplies, the electric units for data acquisition, data handling and displays.

A fault could be found if one of the measured quantities exceeds the pre-set threshold, but the test method is quite expensive. Model equations are considered necessary to estimate the parameters of electric machines, but these equations generally do not exactly correspond to the real system. The simple equations for both electrical and mechanical models were discussed in this paper.

Using a model derived from time dependent measurements, a test method to detect a fault if measured quantities exceeded the pre-set thresholds was then derived by Filbert [24]. This method could be beneficial to industry as the cost of the test stand was low and the test time was short. Another model of an advanced fault diagnosis method for the mass production of small power electric motors was also created by Filbert [25], which dealt with the measured signals of voltage, current and speed only. These reference papers covered the development in testing small electric motors and are very significant to this research.

In similar work to this research, another fault diagnosis method for low power electric motors, based on analysing the current signal in the time and frequency domain, was developed by Guhmann and Filbert [26]. A model-based measuring procedure was described in the paper, which was a continuous development from Dreetz (1989) and Filbert (1985). An earlier investigation made by Dreetz used physical model parameters and parameter identification in comparison with the use of state variables. The improvement with their work was the confirmation that information regarding the condition of the rotor was contained mainly in the periodic components of the current signal. Those harmonics are speed dependent and the speed is not constant, and so digitising synchronously with speed was required for the test. This was achieved with data collection synchronous with the speed, as used in on-line monitoring of machines by analysing airborne or impact noise. This method resulted in improvement in the detection of faults, which was applicable to the detection and localisation of faults occurring in the rotor of universal motors. The faults were distinctly different in comparison with behaviour of healthy and faulty motors, and could be identified during the test. The approach for this research involves a similar strategy.

Subsequently, the new methods that could be used for testing low power electric motors were summarised by Filbert and Schneider [27]. To use these methods, a particular test needed to be set up, and it was only suitable for small d-c motors. The objective of this method was the fast and reliable diagnosis of faults and their locations in all parts of the motor. The test used in this method combined a functional test and a vibration test. The functional test provided the nominal values such as torque, speed or power, and the vibration test gave evidence as to whether the acoustic noise of the motor would be acceptable. These model-based diagnostic methods were considered to lead to simpler test stands.

Model equations in relation to fault detection in electric motors were also discussed by Filbert, Schneider and Spannhake [28]. Those equations included the transformation of the measured variables into non-linear variables. The parameters were determined by the least-squares estimator $\underline{q} = [\mathrm{Re}(\underline{X}^T X^*)]^{-1} [\mathrm{Re}(\underline{X}^* T\underline{Y})]$ in the frequency domain. The discussion related to how errors of a model could be affected by parameter estimation in both electrical and mechanical equations. Some examples were given to show the percentage of errors incurred due to the variation of one or more parameters.

Another paper for diagnosing electric motors dealing with analytical redundancy was produced by Bradatsch, Guhmann, Ropke, Schneider and Filbert [29]. In this paper two methods based on technical diagnosis for low power electric motors were described, in which the parameter estimation technique together with a fault sensitive filter bank were used. As a task from the demanding and fast growing motor industry, it could not be fulfilled with conventional test systems, where the measurement techniques were based on direct procedures. The method was considered to achieve a fast and reliable detection and isolation of faults in small power electric motors, and the problem that the relevant components of an electric motor were supervised via one or more sensors was resolved. An advantage was that parameter estimation was based on "*continuous time models*", in contrast to previous "*time discrete models*". The identification formula for both methods was the same:

$$\alpha = \left[X^T X\right]^{-1} X^T Y$$

Parameter estimation in the frequency domain was also discussed in this paper [29]. The main point was that if the input and output signals were periodical, the parameters of the system could be therefore determined in the frequency domain. The common procedure to determine the parameters in the frequency domain was described in the following manner:

- Transformation of the signals into the frequency domain. This is possible with the Fast Fourier Transformation (FFT).
    - **Application of differential operators or integral operators.**

- Calculation of system parameters with the least square method.

The method was provided to avoid a large range of spectral leakage causing errors in the harmonic determination, if the observation interval is not a multiple of the signal period. The modelling for diagnosing electric motors was involved with the development, criteria and verification of models. In use of this model, the design of a prediction error filter design was required to examine the modelling results of the motors.

Further studies on testing electric motors were described by Filbert [30], [31] and [32], in which a technical diagnosis for electric motors and electric drive systems was derived. His research resulted a number of methods for testing and detecting faults in electric motors. The basic theory in these methods could be summarised as follows:

- Parameter estimation
- Spectral analysis
- Parity space methods

These diagnostic methods were provided in a conventional way and comparisons were also given to provide evidence for their similarities and differences. However, some of the methods would require a specific test stand. The used current spectrum method was very similar to the vibration method, depending on whether the faults were in the electrical or mechanical part. These different methods presented some significant improvement, but were not ideal.

A study of how to realise and minimise detrimental nonuniformities found in rotating devices was conducted by Diehl [33]. His research work concentrated on the true effects of machine dissymmetries. Because of the unsuspected causes of harmful effects during commutation, it would lead to mechanical, magnetic, and electrical machine imbalances. Commutating difficulties and external influences were then investigated. A new aspect of commutating difficulties was again considered. All of the foregoing dissymmetry indications appear to be directly related to nonuniformities of the rotating member. However, it was found that such unbalances do not affect all the field coil voltages in the same manner or degree nor at the expected time. The method for measuring and analysing rotating devices was developed from his previous method of commutation observation.

An earlier publication (Hughes [34]) was found to be a particularly good summary of electric machines as the initial study for this research. It gave a detailed explanation on how the brushes and segments handle the alternative currents due to the distribution of flux in a generator with compoles. Making assumptions of machine current directions under magnetic fields was considered reasonable, in relation to the present research. The construction of equivalent circuits of the Davey machine was certainly assisted by his work, in which the portion of armature winding shows the current flow direction during commutation.

2.4 The effect of commutation on d-c machines

A number of references reviewed here discuss the effect of commutation on d-c machines in different ways. Although this research did not deeply address d-c machine commutation, it is nevertheless important to understand the concept, in order to design the mathematical model correctly (specifically, how the 7-coil and 5-coil circuits operate alternatively during commutation).

Due to the significance of the commutation process, many researchers have concentrated their efforts in this area, resulting in many valuable discoveries. An analysis to solve the eddy-current problem was introduced by Hancock [35], as it affects those parts of the armature conductors within the slots. As the flux crossing the slot is everywhere perpendicular to the slot sides, it could be assumed that slot end effects would be negligible. These assumptions were retained in the present treatment. However, there would be complex problems in calculating commutation performance of d-c machines. Hancock's concluding comment in the paper was to facilitate the complex problems of calculating commutation performance or design. He also provided a relatively simple basis for an initial comparison between two ways of treating the slot-impedance problem. Several other idealisations were also embodied in the paper,

Morley and Hughes [36] and Hughes [37] clearly explained the fundamental phenomena of electromagnetic induction in relation to armature windings of d-c machines, in which the effect of brush and commutator functions were discussed for a simple two-pole machine. The writer's interest was particularly in d-c machines with lap windings which are similar to the Davey machine used in this research.

A theoretical discussion on varying brush resistance during commutation was published by Kisch and Smiel [38]. Based on this theory, the relationship between the brush and the commutating current could be linear under certain circumstances, in which case the model would be applicable to d-c machines with wave windings. Their investigation considered that current density under the brushes was evenly distributed along their full width during commutation. The self-inductance and resistance of each coil, and the contact resistance of the brushes, was found to have a relationship that can be described mathematically during commutation. From this paper some ideas were obtained for calculating the varying brush resistance in the model for the Davey machine, specifically their experience with the inverse proportional functions between the interfacing areas and the conductance of the brush-segment.

In relation to the investigation of commutation of d-c machines, some other methods are described for observation of the phenomena of commutation. A method to measure the armature coil current on a d-c machine was described by Sketch, Shaw and Splatt [39]. This method involved triggering an oscillograph time-base by a current reverse on a rotating machine. This method was considered to have the following advantages compared with conventional methods:

- The difficulties of positioning the potential leads, associated with the shunt method, are avoided.
- A signal of reasonable voltage level can be obtained with negligible effect on the electrical symmetry of the armature.
- A simple test can be made to ensure that undesired signals are negligible.

The “Black Band” method of commutation observation on d-c machines was first described by Schroeder and Aydelott [40]. In this method, the measured curves directly indicate certain features of the machine’s adjustment, including the commutating field strength and brush position. When the black-band method is used in the systematic adjustment of a machine for good commutation, it removes much of the uncertainty and variability of commutation. The black band directly indicates only brush position and commutating-zone magnetic conditions, it also indirectly indicates, some information regarding stability of commutator film and friction, a phase of the commutation problem which must still be solved largely by experience.

A factory method for commutation adjustments on a d-c machine was described by Johnson [41]. His work was able to obtain the possibility of sparkless running on machines and the performance of each individual effect and step in the commutation process was detailed. Each individual part of the machine was required to be checked and properly assembled. This included air gaps, brush gear, circumferential brush spacing, brush overlap, brush alignment, fitting the brushes, commutator smoothing, brush pressure setting, brush arm position and interpole strength. Among these, one of the most important tests carried out in the final stages of d-c machine production is the check on commutation.

Operational testing on d-c machines was also described by Johnson [42]. An initial examination and adjustment before running was highly recommended. In this paper, a few testing methods were introduced to diagnose machines under different operating conditions, but the determination of full-load temperature rise was considered as the most important. No-load losses and magnetisation was discussed in detail on an auxiliary driven motor and a compound wound generator. The regulation for the compound wound generator was given by the ratio:

$$\frac{\text{Change in voltage due to load}}{\text{Normal voltage}}$$

An alternative way of carrying out this test is to run the machine fully loaded at normal speed and voltage after the speed has been adjusted to normal.

Another method for comparing the commutating ability of various brushes was established by Lundy [43]. The earlier "Black Band" theory was developed with measurements taken using a suitable electronic voltmeter. The percentages of the rated currents were given in the comparison. The conclusion made in the paper is that these machines rely on the commutating ability of brushes for their proper operation.

It is accepted that the successful operation of a d-c machine is mainly dependent on its ability to run without injurious sparking over its complete load range. A method of assessing this commutating ability by measuring the black-zone of the machine was introduced by Johnston [44]. This method could achieve sparkless operation at any load within the zone by compensating for the field strength that was affected by both compole and compensating winding. The black-zone measurement was first taken from the assessment and an opposite compensating current was then generated to the point where light general sparking begins at the brushes. In practice, the method required a constant speed, so the sparkless commutation was presented within the black-zone.

Motter [45] discussed commutation of d-c machines and its effects on radio influence voltage generation. Radio influence voltage is generated as a result of passing a direct current from a stationary surface (such as a brush) to a revolving surface (such as a slip ring). The main factor interfering with the machine's commutation was radio influence voltage generation due to transient voltages produced during commutation. The research claimed that the magnitude of the conducted radio influence voltage measured across the brushes of a d-c commutating machine is often much greater than measured across slip-ring brushes under identical test conditions.

Another method of analysis of commutation phenomena for large d-c machines (Linville and Rosenberry [46]) dealt with the voltage appearing from bar-to-bar on the commutator during commutation, as a function of time. They compared the calculated results and measured oscillograph curves to verify thier method. The work was focused on the instantaneous values of bar-to-bar voltage that the brushes absorb during commutation. In this method, a basic problem was to write the differential equations for each coil of an armature winding and to solve the resulting equations for the coil currents during commutation. This seems to deal with a similar problem of the complicated differential equations on the Davey machine. The basic solution in analysing a d-c machine's voltage equations is to make assumptions. Self and mutual inductances of armature coils can be determined as functions of space position, or time. The brush contact resistance is one of the most uncertain factors to handle. It has been common practice to treat it as a variable proportional to the area of contact. However, it is known that the brush contact voltage drop is created by concentration of current in a small part of the contact area.

In a conference publication of commutation in rotating machines, Walton [47] introduced an opinion about armature windings and brush gear on d-c machines. The paper documented Walton's view on the commutation limits due to the effects of varying stationary parts on d-c machines. Walton thought that design could be improved by considering the following:

- The effect of brushes and brushgear on the commutation limit

- Extension of the commutation limit
- Means of extending the commutation limit
- Extension of limit by insulation changes
- Extension of limit by strengthened compoles
- The effect of stationary parts

The final conclusion was that a low volts per segment value results in a generator which ought to be somewhat less demanding in respect of maintenance.

The Unified Machine Theory (Jones [48]) was also discussed in the same conference. The expression in the transformed voltage equations was derived in matrix form. The presence of the variable rotor angle θ in the equations is non-linear. The solution presents the purely mathematical problem of devising a transformation matrix that eliminates θ, but this method was not used in this research, instead a SIMULINK solution was used to model the Davey machine.

The studies of the influence of commutating coils on the main pole flux of a d-c machine was introduced by Tarkanyi [49]. He stated that there was an additional mmf in the direct axis produced by the combined effect of currents in the coils short circuited by the brushes. This claim was supported by such a theory that additional mmf always contains a component that is proportional to the load and affects the stable operation of the machine.

Taylor [50] made a patent application on how to improve commutation in d-c machines, by delaying the onset of the sparking which occurs if electromagnetic conditions are not perfectly balanced. He stated that this could be achieved by using flux traps in conjunction with inter-poles. The method was considered to work quite well in practice, but there was loss of space for active copper in the slot. Taylor also discussed a number of different types of d-c machine construction in relation to the magnetic fluxes. Using flux traps was found to be the best, and even though there were penalties to be paid for this method, it was still considered acceptable. The main point raised by Taylor was that using traps in a machine could obtain some reasonable quantitative agreement between the effects of traps as measured by a-c bridge and the commutation performance.

Schroder and Oberretl [51] claimed the important point that the quality of a d-c machine was significantly affected by its commutation characteristics. The geometry of the stator and rotor of a machine, the brush contact resistance, self-inductance and mutual inductance were used to determine as Fourier series to calculate the field harmonic elements. The result obtained was that the large field harmonics would yield all the voltage and currents, and comparison was made between the measurements and their calculation. The harmonic theory described in the paper was expanded in terms of the voltage, current and flux on a d-c machine. The determination of self-inductance, mutual inductance and brush contact resistance was also provided in detail.

A new method using harmonic field theory for calculation of commutation of d-c and universal motors was described by Doppelbauer [52]. Coil currents and commutator segment voltages in a 32 kW d-c motor were calculated with respect to time, taking the iron saturation into account, and compared to measurements, with good results. Calculations of commutation with several different procedures for unbiased determination of spark borders were presented. The effects of rotor skew, slot scattering, overhang leakage flux and brush dimensions were studied.

Recently, a paper on assisted commutation was published by Goyet and Benalla [53]. In the paper a method of electronic assistance for d-c machine commutation was introduced. The assistance depended on several parameters such as the type of windings, the dimensions of the brushes and commutators and the voltage during the commutation. Experimental implementation resulted in commutation without any spark under the brushes.

2.5 Technical methods of measuring machine parameters

Obviously, the difficulty in condition-monitoring d-c machines can be partly attributed to the lack of machine parameter measurements for self-inductance and mutual inductance between coils due to the difficulties in establishing their rotating positions. To date, this basic difficulty still remains. Some key research findings have been collected and reviewed in this section.

In Ho's research [1], a method of measuring d-c machine current was developed using "Rogowski" coil theory. The method used in analysis of this coil was derived by Ramboz [54]. He found that typical Rogowski coils are suitable for measuring high amplitude a-c current. In Ramboz's paper a "Machinable Rogowski" coil was introduced, which was mainly used for machine applications. A detailed discussion was presented including coil design, test and calibration. The positionally related errors in this method were considered to have been improved on the original method of Rogowski coil current measurements.

In relation to the "Rogowski" coil, another paper written by Destefan [55] was also found to be relevant. His work involved the development of working standards for calibration and testing of resistance welding current monitors. The test equipment and methods could be used to evaluate current-sensing coils and weld-current monitors. The Machinable Rogowski Coil was one of the methods used to achieve accuracy by comparing positional errors for various-sensing coils. While the measuring method of the "Rogowski" coil was applied in Ho's work [1], but it was not used in this research and a new method was developed.

As an alternative method, Krause [56] established a way to calculate the mutual inductance for a-c machines. This method should also be applicable to d-c machines. In the theory, self-inductance was determined by computing the flux linking a winding due to its own current, and the determination of mutual inductance was necessary to compute the flux linking one winding due to current flowing in another winding. This is a very important point which gives us a fundamental understanding of the calculation of d-c machine self-inductance and mutual inductance. Chapter 4 of this thesis presents the details of this method for measuring inductance.

2.6 Mathematical modelling techniques for d-c machines

This section reviews research relating to mathematical modelling of d-c machines.

The Unified-Machine Theory was established by Jones [58], which gives a logical treatment for commutator primitive machines. His theory was a new method of measuring self-inductance and mutual inductance on d-c machines, based on a machine's electromagnetic and mechanical equations. The derivation of those equations was significantly developed in measuring inductance on a d-c machine. The theory was based on a complete impedance matrix solving the torque equation $T = \frac{1}{2} i_t \frac{dL}{d\theta} i$ where the current in the commutating coils of such a machine is provided by the external currents and voltages over a period which is an integral multiple of the commutation time. The theory provided very useful in assisting experimental tests for the machine parameter measurements in this research. The great merit of this theory is that the very complicated relationships on the machines' inductances are treated in a logical way. The magnetic circuits on the armature winding were established for measurement of mutual inductance between the armature-with-interpoles and shorted-circuited turns. Hence a method in use of a d-c source was therefore based on Jones' Unified –machine Theory for this research.

A general concept for modelling electric machines was described by Thaler and Wilcox [59]. They used a circuit model consisting solely of a number of electric circuits comprising resistance and self-inductance. These circuits were inductively coupled and each circuit produced a magnetic field. A number of circuit equations were used to calculate machine performance. The model coils were chosen to be stationary, and the coils on the physical machine could be handled in the mathematics.

A traditional solution, dynamic circuit theory, was also reviewed. This solution provided a simple and unified basis for the treatment of rotary machines, established by Messerle [60]. His main points in the theory were the following:

- The electrical circuit equations
- Electromechanical energy conversion relations
- The equations of motion

The established equations could directly present the equivalent circuits of a machine, which was the method applied in Ho's model [1]. There was no need for any complex mathematical skill to establish the basis of dynamic circuit theory, and even matrices could be left out of the initial study. The method was derived from basic armature winding circuit, in which saturation effects were neglected if the inductance's were taken as constant.

In an area of dealing with model data, analysis of failure states of a d-c machine was represented by a mathematical model in Glowacz's paper [61]. A d-c machine with loop and wave rotor windings by approximating equivalent resistance circuits was modelled. The model equations were solved in the FORTRAN language using the effective implicit integration method. The result from this model indicated that the coil currents, voltages and electromagnetic torque depended on the character of failures and the parameters of d-c machines. Mathematical model of a d-c machine formed in this manner was a set of stiff nonlinear differential equations. This model took into detailed consideration the width of brushes. Inductance's of coils were determined by means of the air-gap permeance function and then expressed in Fourier series. The set of system failures includes among other the shorted and broken rotor coils (partly and totally).

Burth, et. al [62] considered the concept of non-linear approach to fault diagnosis. A physical model was developed to predict the current spectrum of an universal motor with a faulty bearing. The important point raised was that the current or voltage ripple of a motor could be used as a diagnostic signal. A few parameters of testing a motor, in which “fast signal processing” and “short test time” were taken into consideration. The measurement of a few revolutions was considered sufficient. The classification results were proven on the healthy and faulty motors. The pseudo-side-bands around the shaft frequency and its 4th harmonics were evaluated.

Filbert and Guhmann [63] also diagnosed faults in electric motors, but the model described in their paper was based on the estimation of the current spectrum. This model was implemented with MATLAB/SIMULINK using a Runge-Kutta integration algorithm. Numerical simulations were compared with measurements and the results were used to find significant features for the classification.

Filbert and Bradatsch [64] produced a paper describing a personal computer based system for fault detection in electric motors. The method of this model was based on a mathematical theory using Fourier Series, and it was formed as polynomial approximations in terms of differentiation. The model described could solve for nonlinear parameters. The model-based measurement needs a mathematical description of the physical system. This method was claimed to have the advantages of a short test time and being easy to handle with no additional load required.

Poignet, et al. [65] described how to design a model in MATLAB. This article dealt with an alternative approach to mechanical machine tool axis - a new way of modelling and improvement of the simulation accuracy in terms of mechanical structure control. In Poignet’s paper, a number of descriptions were given from the point of view of control schemes in a MATLAB/SIMULINK environment. It was found to be essential to understand the nature of the simulation before considering the mathematical equations.

The model was introduced with different orientation of applications, and it was used to aim the control parameters and to predict the closed loop performances of the machine.

In the study of d-c machine, a shorted and/or opened armature winding of a d-c machine has been one of the prime concerns of power electrical engineers. Model-based measuring procedures such as those of Ho [1] have been developed for a d-c generator. The initial development in his work was restricted to the case where a 2-pole, ½ HP, 16 slot and 48 segment d-c machine was modeled. Ho's model used the coupled coil theory and all three sub coils on the adjacent segments were in one slot and were treated as a single coil. The equivalent circuits on the machine's armature winding were either 7 concentrated coils or 5 concentrated coils while the machine was running. Attempts were made to solve the equations based on these equivalent circuits using MATLAB software. Certain measurements on the machine were taken with the machine stationary, and some reasonable assumptions were also made from experience. His approach was to regard the problem as one of coupled circuits. It was assumed that self-inductance and mutual inductance between the coils in the same slot would be the same. This then gave a coupling factor of exactly 1.000, and it turned out that the equations could not be solved. This was overcome by assuming only 1 coil per slot (with 3 turns as many turns). Mutual inductance between coils adjacent slots were assumed to be equal $L_1 \times \cos(\theta)$, where L_1 is the self-inductance of one coil and θ is the slot-pitch angle. This was not confirmed by the measurement, and his model was not able to solve the differential equations in relation to the equivalent circuits.

It is instructive to take a preliminary look at the references commonly used in measuring inductance (Ghoneim, Fletcher and Williams [66]). The self- and mutual inductance variation of the armature winding with respect to the rotor position can be expressed as:

$$L_{ij}(\theta) = N_i^{\,2} \, \frac{u_0 l_{ax} r}{\mathrm{l_g}} \, \beta L_{ij}(\theta)$$

$$M_{ij}(\theta) = N_i \, N_j \, \frac{u_0 l_{ax} r}{\mathrm{l_g}} \, \beta M_{ij}(\theta)$$

$$M_{ij}(\theta) = M_{ji}(\theta)$$

Where: $\beta L_{ij}(\theta)$ and $\beta M_{ij}(\theta)$ were the inductance overlap angles, $i \neq j$; $\mathrm{l_{ax}}$, $\mathrm{l_g}$ were the machine axial length and the airgap length respectively, m; r was the arithmetic mean airgap radius, m; N_i, and N_j were the number of turns in the *i*th and *j*th coils, respectively.

The above equations were developed for general doubly salient reluctance machines, but should also be applicable to d-c machines, as their physical modes are identical. Having followed this concept, both self-inductance and mutual inductance are functions of the angles and lengths of a machine. Hence, they should vary during the rotation. As predicted, the mutual inductance should be smaller than its self-inductance, due to the impact of flux density in the air gap, in which the permeability u is much smaller than the ferromagnetic material in the magnetic field, resulting in higher reluctance. The paper [66] also pointed out that the air gap reluctance with slotted d-c machine armatures would exceed that of corresponding smooth core machines, and it would not be a constant in the magnetic field.

Two publications have been found useful for modeling electric machines using MATLAB. Lyshevski [67] performed comprehensive analysis of electric machines. The key element introduced in this publication was how a model is related to machine dynamic behaviour using MATLAB functional blocks. However, MATLAB's users were cautioned that the multi-disciplinary functionality of electrical or mechanic systems would not allow researchers to successfully approach the challenging problem through "design-by-discipline" philosophy, but other related components would need to attain to the desired degree of adaptation and functionality. Another publication by Cathey [68] was relevant to a range of electric machines in MATLAB. One chapter specifically discussed d-c machines in various ways, and continued with the script files in MATLAB for analysing the machines' problems. The most important concept stated in the publication was to analyse the machine's performance through every operational step. The model was then implemented in the MATLAB environment.

2.7 Summary of literature review

There has not been much literature published on d-c machines especially over the last 40 years. Only limited knowledge appears to be available regarding the relative merits of modeling of d-c machine armature windings, with respect to their commutating ability. The most economical and practical means of obtaining useful data is by detailed measurements on a number of small two pole machines having windings and commutating characteristics similar to those of larger machines.

The literature review can be briefly summarised as the following:

- Why we need condition monitoring (CM) techniques for d-c machines
- How d-c machines are affected by various faults during the operation
- What the important concepts are on d-c machines for the research
- How commutation works and is related to d-c machine's performance
- How the mathematical model and the measuring inductance method are established
- Which testing method is most suitable for the Davey machine

Regarding the measuring method for a d-c machine, Jones [58] was found to be the most useful reference for the present research. This method was used to take all data required into the mathematical model. For the purposes at hand, the references by Ho [1] and Jones [58] gave considerable assistance in this research.

Chapter 3

Equivalent circuits of the Davey machine

3.1 Basic Principles of modeling a d-c machine

The aim of this research is to be able to predict the current in a short-circuited armature sub-coil. Hence the armature winding cannot be represented by just one equivalent coil, as is customary for a healthy d-c machine. Instead, every armature sub-coil was modelled.

There are many types of armature windings, but the author did not attempt to model a general case. A small direct-current laboratory motor was selected for the modelling. The measured inductances of this machine were used as the input data for the mathematical model.

A small power d-c machine - Davey, 2-pole, ½ HP 1440 rpm 16 slots and 48 segments with lap winding, - was especially utilised for this research. It was a machine with salient poles on the stator, which produced the main magnetic field. This field was fixed in space and did not vary with time except during transient disturbances. The rotor was a cylindrical structure, wound with 48 coils in 16 slots and with connections made from these coils to the 48 segments of the commutator, as shown in Figure 3.1.

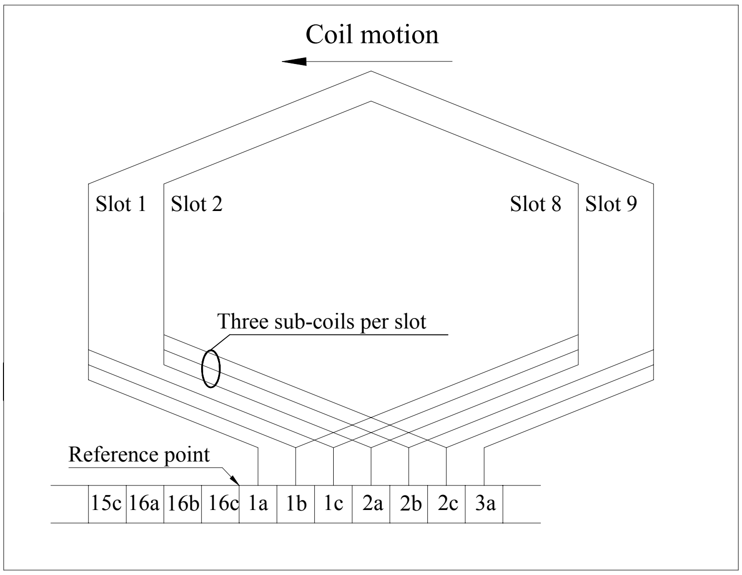

Figure 3.1 The armature circuit of the Davey machine

The author confronted a problem if using the actual 48 commutating segments of the machine. This problem occurred due to a numerical relationship with the mutual inductance resulting from having three sub-coils per slot. As they had the same physical structure and position, the flux linkages of these sub coils remained the same. Due to their very close or almost equal mutual inductance, it was not possible to numerically solve the differential equations with a coupling coefficient k ≈ 1 (Ho [1]). As $k = \frac{M}{\sqrt{L1 * L2}}$ is required to be less than 1 in the theory. Hence, an important new idea was introduced when establishing the model's circuits, in which every three segments were merged into one commutator segment in the model. This assumption did not affect modelling accuracy, because every three sub coils were always commutated at the same time.

On the actual machine, there were 48 segments and 16 slots. Each coil of a single segment was modelled as occupying 7.5 degrees of the rotor's angular position, and so the three merged segments were modelled as 22.5 degrees instead of the actual 7.5 degrees per segment on the machine. The width of the brush was modelled as 30 degrees. In visualising this it is perhaps helpful to picture a brush whose width is exactly equal to that of one and one-third commutator segments (Figure 3.2).

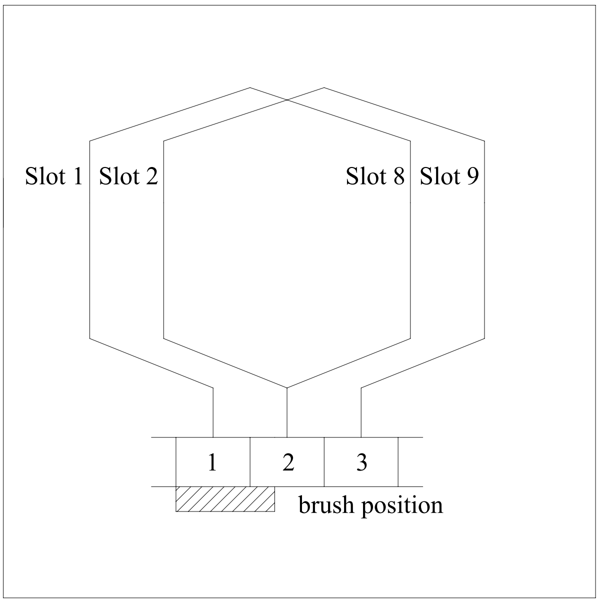

Figure 3.2 Modified 16 segment model of the Davey machine

3.2 7-coil and 5-coil equivalent circuits

The physical meaning of 7-coil and 5-coil equivalent circuits on the Davey machine is best visualised with the help of Figure 3.3 and Figure 3.4.

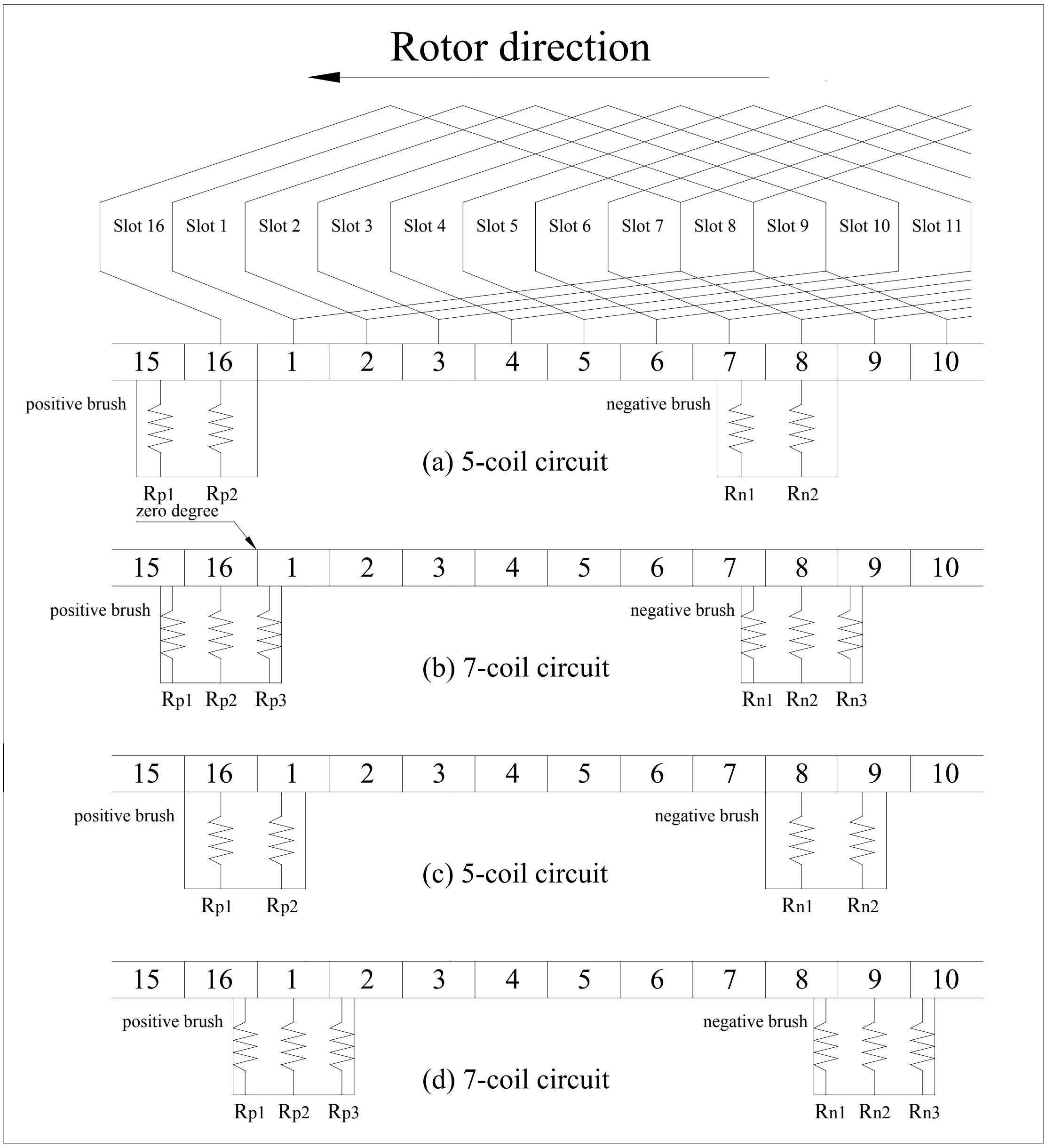

Figure 3.3 The commutating process on the Davey machine

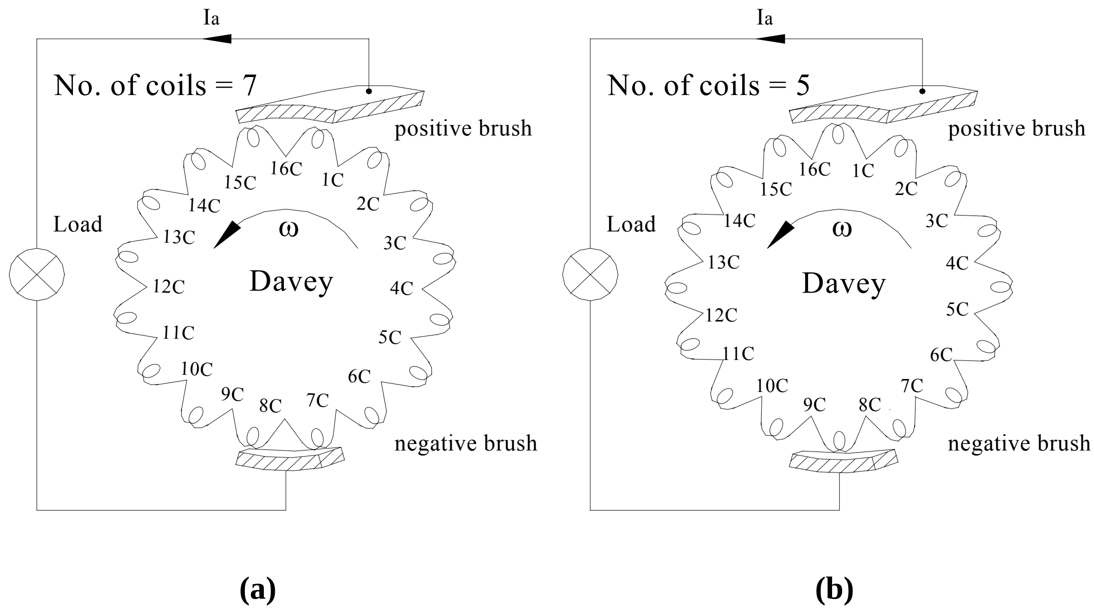

Figure 3.4 Establishing equivalent circuits process

The related 7-coil and 5-coil equivalent circuits are given in Figure 3.5 and Figure 3.6.

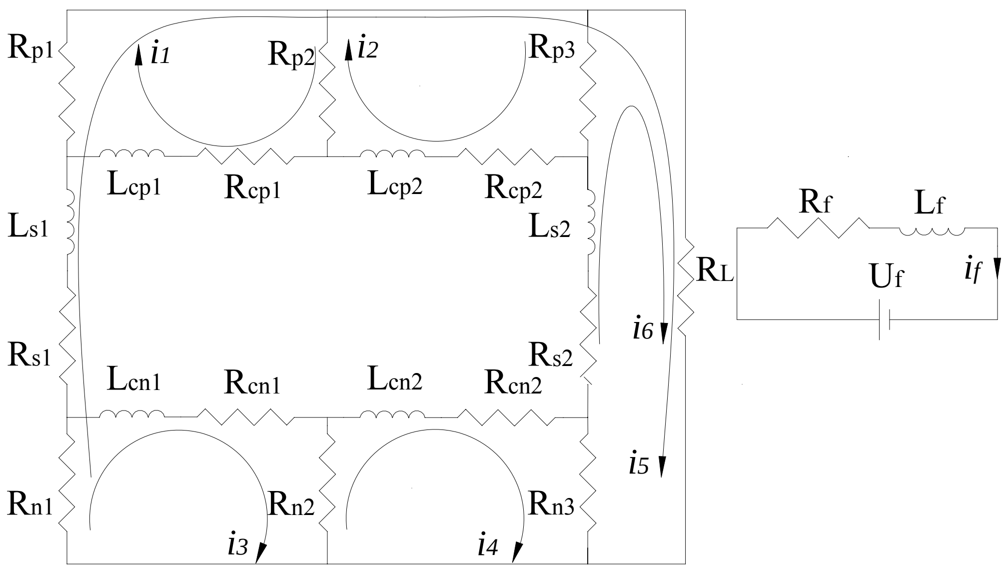

Figure 3.5 7-coil equivalent circuit of the Davey machine

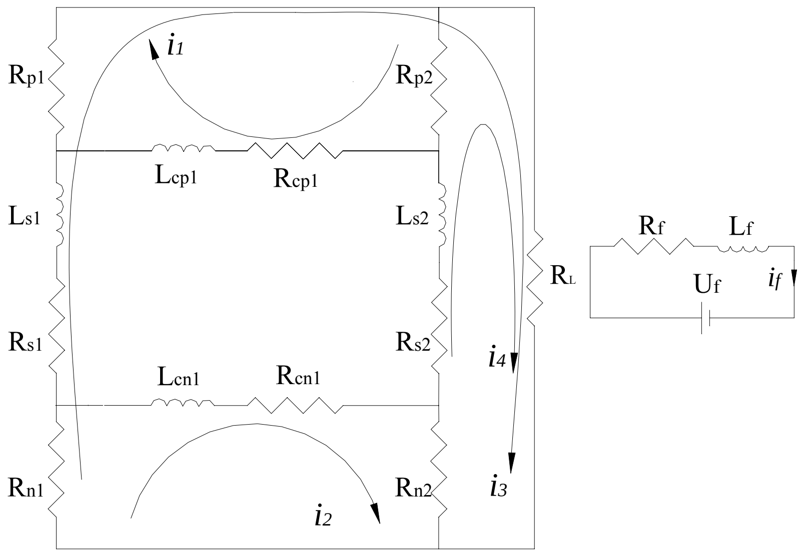

Figure 3.6 5-coil equivalent circuit of the Davey machine

<u>7-coil equivalent circuit</u>

Referring to Figure 3.3 (b), each brush contacts three segments (15, 16 and 1 under the positive brush, and 7, 8 and 9 under the negative brush) - Figure 3.4 (a). At that time the armature winding is modelled as a 7-coil circuit, with four of one coil under commutation, two each of six coils in series and also one coil of the field. Figure 3.5 shows the 7-coil equivalent circuit.

<u>5-coil equivalent circuit</u>

Referring to Figure 3.3 (c), each brush is shorting the contact surface of two segments (16 and 1, 8 and 9). This phenomenon is considered as a 5-coil circuit. Another way of explaining these equivalent circuits is given in Figure 3.4 (b). The armature is modelled as five coils, with two each of one coil under commutation, two each of seven coils in series, and the field coil on the stator. The 5-coil equivalent circuit diagram is shown in Figure 3.6.

The 7-coil and 5-coil equivalent circuits represent the machine during a certain period of rotation. Namely as a 7-coil, the armature winding is presented by 7 coils all together, as both positive and negative brushes are contacting three segments at the same time. Alternatively, there are 5 coils presented on the armature of the machine if only two segments are under commutation. The notation in Figure 3.5 (7-coil equivalent circuit) and Figure 3.6 (5-coil equivalent circuit) is explained in Section 3.3.

3.3 Analysis of commutation during one revolution

The following discussion is concentrated on the machine's commutation performance during one revolution. An angle θ is defined as a reference of the rotor's position between axes fixed to the moving coil on the rotor. Assume the machine starts at 0° of the rotor's initial position shown in Figure 3.3 (a). Then the armature winding is performing as a 7-coil equivalent circuit first, with the positive brush contacting with coils 15, 16 and 1, as described in Figure 3.3 (b) for this at the commutating time. The corresponding movement of the armature winding can then be modelled as a 7-coil equivalent circuit, which they are represented by L_{s1} and L_{s2} (two parallel paths of 6 coils in series in the d-axis), L_{cp1}, L_{cp2}, L_{cn1} and L_{cn2} (two coils on each side of the commutation by both positive and negative brushes) and the coil L_f in the field circuit. Therefore, the total number of coils is 7.

The 7-coil equivalent circuit's operation goes only from 0° to 7.5° in the model. As soon as the brush bar leaves coil 15 due to the rotor movement in a right direction, as shown in Figure 3.3 (c), then the 5-coil equivalent circuit takes over.

Once the 5-coil circuit is active in the model the 7-coil is disabled. The 5-coil circuit is active for two times longer than the 7-coil circuit. The rotor will travel from 7.5° to 22.5° during this operating time.

With this revolution of the machine, the brush position will move back to the 7-coil circuit again when the rotor's position has passed one interval of 22.5°, as shown in Figure 3.3 (d). Thus, the model will consist of a 7-coil circuit again during the next 7.5° rotation and its behaviour is the same as for the rotation from 0° to 7.5°.

The 5-coil circuit will then turn on again at a rotor position of 30°. The operation of the 5-coil circuit is repeated as discussed above.

The 7-coil circuit and 5-coil circuit simulate the armature winding's performance at each time alternately. Each of them should be active 16 times during one revolution of the machine. Their required simulation parameters for each rotor position are listed in the following Table. 3.1.

Rotor positionin θ in deg	Pos. brush coil	Neg. brush coil	d-axis uncommutated coil number S1/S2	Equivalent circuit
$0^{\circ} < \theta \leq 7.5^{\circ}$	16 & 1	8 & 9	10, 11, 12,13,14,15 / 2,3,4,5,6.7	7
$7.5^{\circ} < \theta \leq 22.5^{\circ}$	1	9	10, 11, 12,13,14,15,16 /	5
$22.5^{\circ} < \theta \leq 30^{\circ}$	1 & 2	9 & 10	11, 12,13,14,15,16 / 3,4,5,6.7,8	7
$30^{\circ} < \theta \leq 45^{\circ}$	2	10	11, 12,13,14,15,16,1 / 3,4,5,6.7,8,9	5
$45^{\circ} < \theta \leq 52.5^{\circ}$	2 & 3	10 & 11	12,13,14,15,16,1 / 4,5,6.7,8,9	7
$52.5^{\circ} < \theta \leq 67.5^{\circ}$	3	11	12,13,14,15,16,1,2 / 4,5,6.7,8,9,10	5
$67.5^{\circ} < \theta \leq 75^{\circ}$	3 & 4	11 & 12	13,14,15,16,1,2 / 5,6.7,8,9,10	7
$75^{\circ} < \theta \leq 90^{\circ}$	4	12	13,14,15,16,1,2,3 / 5,6.7,8,9,10,11	5
$90^{\circ} < \theta \leq 97.5^{\circ}$	4 & 5	12 & 13	14,15,16,1,2,3 / 6.7,8,9,10,11	7
$97.5^{\circ} < \theta \leq 112.5^{\circ}$	5	13	14,15,16,1,2,3,4 / 6.7,8,9,10,11,12	5
$112.5^{\circ} < \theta \leq 120^{\circ}$	5 & 6	13 & 14	15,16,1,2,3,4 / 7,8,9,10,11,12	7
$120^{\circ} < \theta \leq 135^{\circ}$	6	14	15,16,1,2,3,4,5 / 7,8,9,10,11,12,13	5
$135^{\circ} < \theta \leq 142.5^{\circ}$	6 & 7	14 & 15	16,1,2,3,4,5 / 8,9,10,11,12,13	7
$142.5^{\circ} < \theta \leq 157.5^{\circ}$	7	15	16,1,2,3,4,5,6 / 8,9,10,11,12,13,14	5
$157.5^{\circ} < \theta \leq 165^{\circ}$	7 & 8	15 & 16	1,2,3,4,5,6 / 9,10,11,12,13,14	7
$165^{\circ} < \theta \leq 180^{\circ}$	8	16	1,2,3,4,5,6,7 / 9,10,11,12,13,14,15	5
$180^{\circ} < \theta \leq 187.5^{\circ}$	8 & 9	16 & 1	2,3,4,5,6,7 / 10,11,12,13,14,15	7
$187.5^{\circ} < \theta \leq 202.5^{\circ}$	9	1	2,3,4,5,6,7,8 / 10,11,12,13,14,15,16	5
$202.5^{\circ} < \theta \leq 210^{\circ}$	9 & 10	1 & 2	3,4,5,6,7,8 / 11,12,13,14,15,16	7
$210^{\circ} < \theta \leq 225^{\circ}$	10	2	3,4,5,6,7,8,9 / 11,12,13,14,15,16,1	5
$225^{\circ} < \theta \leq 232.5^{\circ}$	10 & 11	2 & 3	4,5,6,7,8,9 / 12,13,14,15,16,1	7
$232.5^{\circ} < \theta \leq 247.5^{\circ}$	11	3	4,5,6,7,8,9,10 / 12,13,14,15,16,1,2	5
$247.5^{\circ} < \theta \leq 255^{\circ}$	11 & 12	3 & 4	5,6,7,8,9,10 / 13,14,15,16,1,2	7
$255^{\circ} < \theta \leq 270^{\circ}$	12	4	5,6,7,8,9,10,11 / 13,14,15,16,1,2,3	5
$270^{\circ} < \theta \leq 277.5^{\circ}$	12 & 13	4 & 5	6,7,8,9,10,11 / 14,15,16,1,2,3	7
$277.5^{\circ} < \theta \leq 292.5^{\circ}$	13	5	6,7,8,9,10,11,12 / 14,15,16,1,2,3,4	5
$292.5^{\circ} < \theta \leq 300^{\circ}$	13 & 14	5 & 6	7,8,9,10,11,12 / 15,16,1,2,3,4	7
$300^{\circ} < \theta \leq 315^{\circ}$	14	6	7,8,9,10,11,12,13 / 15,16,1,2,3,4,5	5
$315^{\circ} < \theta \leq 322.5^{\circ}$	14 & 15	6 & 7	8,9,10,11,12,13 / 16,1,2,3,4,5	7
$322.5^{\circ} < \theta \leq 337.5^{\circ}$	15	7	8,9,10,11,12,13,14 / 16,1,2,3,4,5,6	5
$337.5^{\circ} < \theta \leq 345^{\circ}$	15 & 16	7 & 8	9,10,11,12,13,14 / 1,2,3,4,5,6	7
$345^{\circ} < \theta \leq 360^{\circ}$	16	8	9,10,11,12,13,14,15 / 1,2,3,4,5,6,7	5

Table 3.1: Equivalent circuits vs rotor angle of Davey machine

The basic elements in both the 7-coil circuit and 5-coil circuit are the resistors and the self-inductances. The suffix ‘p’ and suffix ‘n’ are used for the resistors and self-inductances of the coils being commutated under the positive and the negative brushes accordingly. As the brushes are set in the q-axis (or ‘neutral axis’), only changes in slot and overhang leakage fluxes need to be considered in calculating the emf in a coil undergoing commutation. The emf results from changes in the self flux and the mutual flux set up by currents in adjacent coils that are being simultaneously commutated, as shown in Figure 3.7.

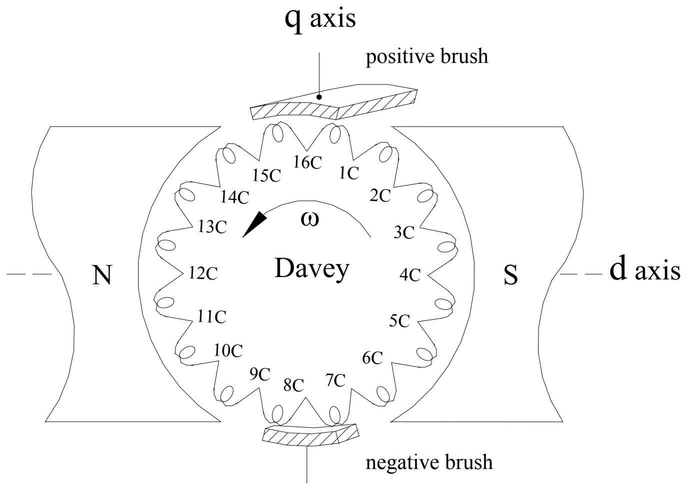

Figure 3.7 Commutation and flux position of the 7-coil circuit on the machine

The armature coils in series under the poles (d-axis) for the commutation interval are in parallel paths presented by L_{S1} and L_{S2} in both 7-coil and 5-coil circuits in Figure 3.5 and Figure 3.6. The generated voltage at the brushes (q-axis) is constant until the next commutation interval when L_{S1} and L_{S2} will change to 6 or 7 coils in series alternatively.

These equivalent circuits were used in the development of the model.

Chapter 4

Measurement of inductances on the Davey machine

4.1 The need for a d-c inductance measurement

The usual method of measuring inductance is to use an alternating supply on the inductance, measure the current and voltage, and calculate the impedance finding both real and imaginary parts.

However, this a-c method does not work on the Davey machine. In order to obtain flux conditions close to the flux on the actual machine while it is running, it requires a constant field current of 0.2A in this particular case. This causes magnetic saturation in the machine.

When a separate d-c source is connected to the field coil to achieve this measurement together with the a-c source supplied into the armature, an a-c current is induced in the field. The impedance measured on the armature then is too low. This analogy is like trying to measure the no load impedance of a transformer when there is a load connected to the secondary. Two solutions to this problem are to use a much lower frequency of supply to the armature, which is impractical, or to use a true d-c method. The latter was the method employed for the measurements and its principle is described in this chapter

4.2 The d-c method of measuring inductance

The initial idea for measuring self-inductance is based on the method of Jones [22], which uses a Wheatstone Bridge circuit. The self-inductance to be measured (L_1 Henry, R_1 Ohm) is connected with three non-inductive resistors shown in Figure 4.1

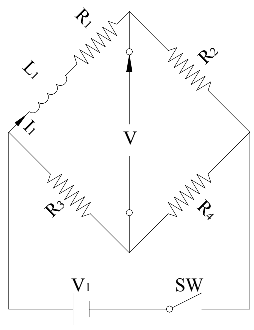

Figure 4.1 Wheatstone Bridge measuring self-inductance circuit

Within the Wheatstone Bridge circuit a d-c supply V_1 is used. The bridge is in a balanced state when V = 0. The supply voltage is removed by opening the switch at time t = 0. The inductance can be given in Equation 4.1

$$L_1 = \frac{1 + R_1/R_2}{i_1} \int_0^\infty V dt \qquad (4.1)$$

The derivation of Equation 4.1 is obtained by considering its steady state and transient conditions. The steady state of the Wheastone Bridge is reached after the switch has been closed and R_2, R_3 and R_4 are adjusted until V = 0. Their steady state values are then given by $R_1/R_2 = R_3/R_4$.

The transient state of the Wheastone Bridge starts at time t = 0, and the current i_1 through the inductor is initially at its steady value I_1, and it then decays to zero, flowing through the bridge circuit as shown in Figure 4.2

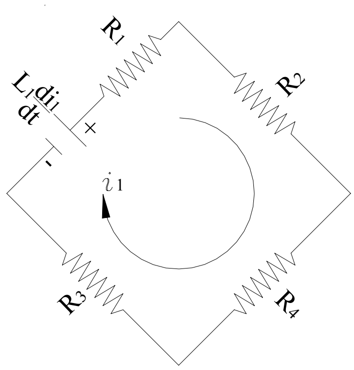

Figure 4.2 Wheatstone Bridge transient-state

The inductor yields a voltage source $L_1 \frac{di_1}{dt}$ and i_1 keeps in the same direction as in the steady-state condition. The bridge voltage is therfore

$$V = L_1 \frac{di_1}{dt} - (R_1 + R_3)\, i_1$$

Also, $V = (R_2 + R_4)\, i_1$. Hence, substituting for i_1

$$V = L_1 \frac{di_1}{dt} - \frac{R_1 + R_3}{R_2 + R_4} V = L_1 \frac{di_1}{dt} - \frac{R_1/R_3 + 1}{R_2/R_4 + 1} V$$

With $\frac{R_1}{R_3} = \frac{R_2}{R_4}$, the equation simlifies to

$$V = \frac{1}{1 + R_1/R_2} L_1 \frac{di_1}{dt}$$

Integrating,

$$\int_0^\infty V dt = \frac{1}{1 + R_1/R_2}\int_0^\infty L_1 \frac{di_1}{dt} = \frac{1}{1 + R_1/R_2}\int_0^{I_1} L_1 di_1 = \frac{L_1 \times I_1}{1 + R_1/R_2}$$

where I_1 is the steady current (in amps) through L_1 before the switch is opened.

$$L_1 = \frac{1 + R_1/R_2}{I_1}\int_0^\infty V dt$$

Therefore, L_1 can be obtained once $\int_0^\infty V dt$ is measured.

Likewise, a mutual inductance M can also be measured using the similar Wheatstone Bridge circuit shown in Figure 4.3.

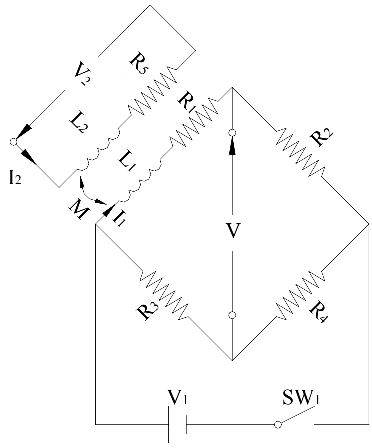

Figure 4.3 Wheatstone Bridge measuring mutual inductance circuit

The mutual inductance can be obtained by

$$M = \frac{1 + R_1/R_2}{I_1}\int_0^\infty V_2 dt \qquad (4.2)$$

It is not in fact necessary to use a Wheaststone Bridge for the mutual inductance case. All that is needed to reduce I_1 from its initial value to zero, whilst integrating V_2, and this can be achieved by the circuit in Figure 4.4.

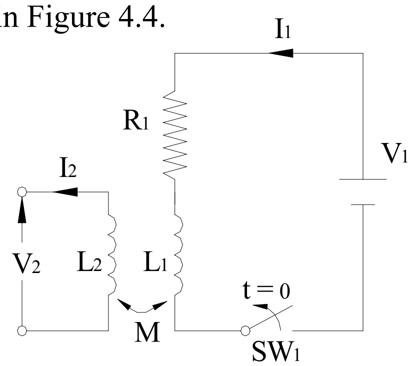

Figure 4.4 Measuring mutual inductance circuit

Then,

$$M = \frac{1}{I_1}\int_0^{\infty} V_2 dt \tag{4.3}$$

Figure 4.1 to Figure 4.4 do not show the constant field current of 0.2A supplied from a separate d-c generator in our measuring method. It is known that, during the integration transient, the field current would be altered slightly by small ripples of a-c in the field current (Ho [1]), but because the initial and final values always stay at 0.2A, the integrated voltage is not affected by this. A constant field current at 0.2A was required to keep a saturated magnetic field.

In practice, errors due to residual flux are avoided by reversing I_1 during the integrating period, in which

$$M = \frac{1}{2\times I_1}\int_0^{\infty} V_2 dt \tag{4.4}$$

The Wheatstone Bridge method of measuring self and mutual inductance had already been developed into a complete unit, called a Direct Current Inductance Bridge (DCIB) in the power laboratory of the School of Engineering. The tests were carried out using the DCIB. The DCIB unit consists three main parts: a Kelvin Double Bridge (instead of a Wheatstone Bridge), an electronic integrator, and a digital voltmeter (DVM). The circuit diagram in Figure 4.5 describes the connections between the DCIB and the inductance to be measured.

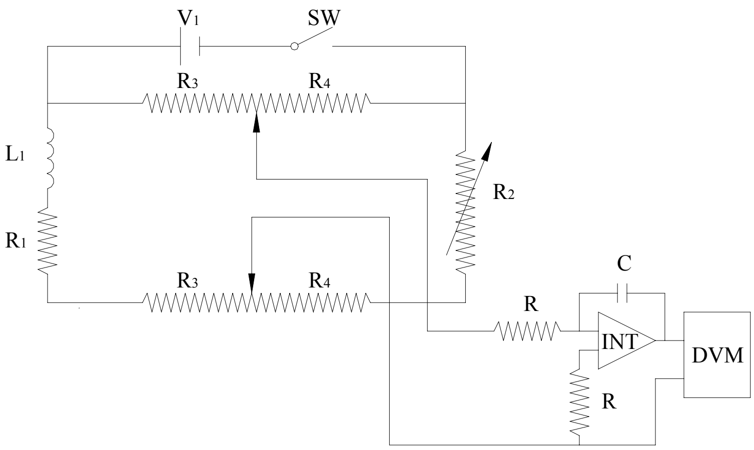

Figure 4.5 Direct Current Inductance Bridge (DCIB) Connections

A Kelvin Double Bridge is a part of the DCIB circuit, which is one of the best available for the precise measurement of low resistance. It is a development of the Wheastone bridge to eliminate the errors due to contact and lead resistances. These are connected to form two sets of ratio arms R3/R4 as shown in Figure 4.5. In this DCIB circuit, however, an electronic integrator is used to replace a sensitive galvanometer in a normal Kelvin Double Bridge. The ratio R3/R4 is kept the same on the both arms. These ratios being varied until zero output reading of the integrator is obtained.

4.3 Modifications of the basic DCIB method for measuring the self-inductance of armature sub-coils

As discussed in Chapter 3, the established equivalent circuits require measurement of their self-inductances

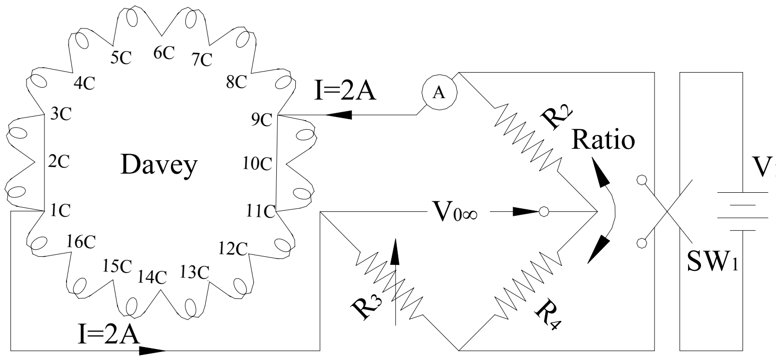

Figure 4.6 Connection of measuring self-inductance for 7-coil circuit

The 16 armature sub-coils were permanently connected with each other to form a closed loop. To measure the self-inductance of the six sub-coils in series for the 7-coil circuit, the connection to the DCIB in Figure 4.6 was made for this purpose. It can be seen that the segments from 1C to 3C and from 9C to 11C are shorted out and carry zero current in this circuit. The series connected coils 9C - 3C and 11C - 1C have 1A current flowing through them from the supply V_1, and the DCIB measures self-inductance of two sets of the six sub-coils in parallel. In this diagram, the field circuit is not shown, but it carries 0.2A d-c during the measurement.

In order to work out the paralleled inductances being measured in Figure 4.6, it is necessary to first look at the direction of flux produced by current in the sub-coils. Refer to Figure 4.7

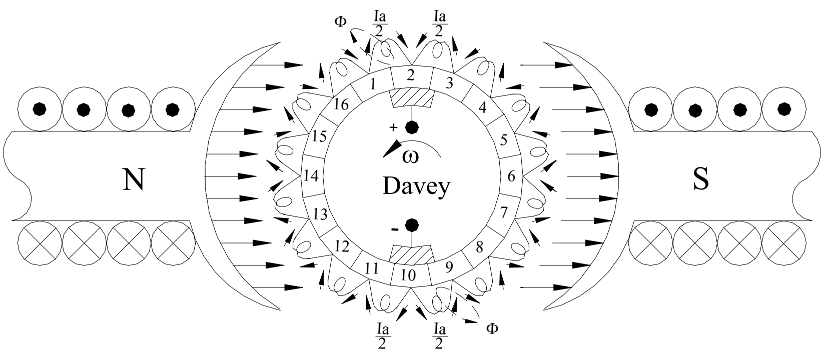

Figure 4.7 Flux directions in the Davey machine as a generator

Based on the theory of the convention in a generalised machine, the m.m.f. of a coil is along its axis. The currents in sub coils 9C – 3C and 11C-1C both produce m.m.f. and flux vertically, and are of course mutually coupled.

Before further discussion about the measurements, an analysis of the flux linkage is needed. As specified 2A to be the armature current I_a generated by the Davey machine, the elements in this circuit can simply be considered as only L and R, as shown in Figure 4.8, and they are desirable symmetrical and balanced as assumed.

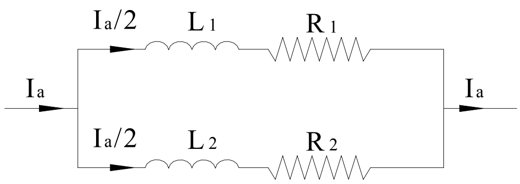

Figure 4.8 Flux and current distribution diagram

Figure 4.8 shows the essential arrangement of measuring two parallel self- inductances L_1 and L_2 of six sub-coils in series ($L_1 = L_2$). Suppose that $I_a/2$ flowing only in L_1, produces flux Φ through L_1, likewise in L_2. In practice, $I_a/2$ in both inductances produces 2Φ through L_1 and L_2. The DCIB gives an integrated voltage V' proportional to 2Φ. Thus V'/2 is proportional to Φ. Referring back to Equation 4.1, I_1 is now I_a, the total current flowing in the parallel combination of sub-coils.

It is now necessary to discuss the effect of magnetic saturation on the measurement of inductance. The 0.2A field current produces approximately the same amount of flux as 5A in the complete armature. This was verified by using the DCIB and a 20-turn coil that was temporarily wound around one pole of the machine. The inductance was measured with 0.2A in the field coil. It was found that the different armature currents from 1A to 3A did not vary the inductance significantly (ie. only a few percent difference), which was close to the inherent error in this method. A sub-coil inductance was then measured under a similar flux condition to what would exist when the motor is running.

Under the unsaturated condition (ie. a zero field current) the self-inductance of the total armature winding varies with angular position. Referring to Figure 4.7, the self-inductance measured between the segments 2 and 10 was found to vary almost sinusoidally between 0.15H and 0.31H as the rotor was turned. By contrast, when there was 0.2A field current, the armature self-inductance was 0.07 ± 0.01H, almost independent of the rotor position. Thus, the self and mutual inductances of the armature sub-coils can be assumed to be constant and independent of the armature current used and their location on the rotor.

4.4 Measuring other self-inductance on the machine

For less than six armature coils in series of the machine, the concept of measuring self-inductance remains the same. The only modification is to add a piece of wire into the armature, which will short some coils depending on how many coils of self-inductance are needed to be measured. For example Figure 4.9 is the connection to measure a two coil self-inductance in the 7-coil circuit of the Davey machine's armature.

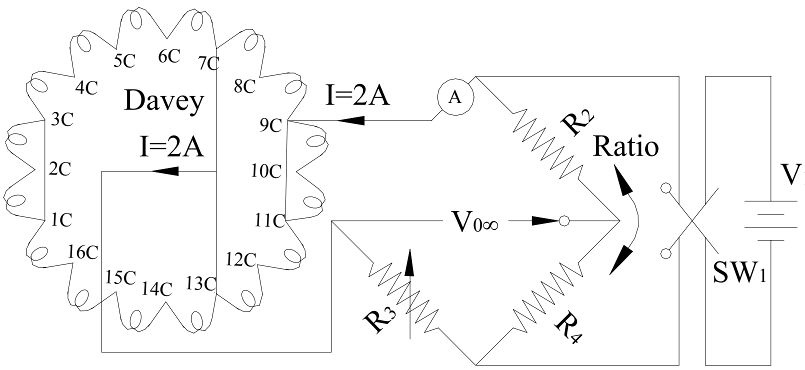

Figure 4.9 Measuring self-inductance on different coils of the 7-coil circuit

In this circuit, a short lead is connected between 7C and 13C on the machine's armature. $I_a = 2$A, which is fed from the commutated coils 9C and 11C. Each $I_a/2$ (1A) flows from 9C to 7C and also from 11C to 13C. Although the two coils between 1C and 3C are also shorted during the commutation, there is no current going through both coil sides of the armature (coil numbers from 7C to 3C and from 13C to 1C in Figure 4.9).

In the same way, one to five coil self-inductances for the 7-coil circuit can be measured. The only modification needed is just to move the short lead along the paralled coils, connect it between 8C and 12C, 7C and 13C, 6C and 14C, 5C and 15C, and 4C and 16C respectively. The purpose of measuring these different coil self-inductance is for obtaining other self-inductance value as required data in the model of the Davey machine with one shorted coil, which will be discussed further later.

To measure self-inductance in the 5-coil equivalent circuit, the changes made in this connection were to short one coil at both ends, as required by the commutating condition. Because there is only one coil being shorted (10C-9C and 2C-1C), shown in Figure 4.10, the uncommutated 7 coils of the parallel paths are in series. Similiarly, the measurement of the self-inductances from one to seven can be done in the same way as for the 7-coil circuit.

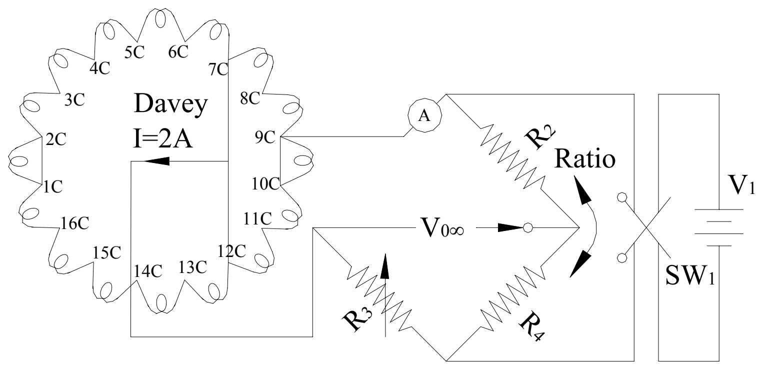

Figure 4.10 Measuring self-inductance on different coils of the 5-coil circuit

The field current in the generator (Davey machine) is almost constant at 0.2A, but it contains a ripple. Thus an incremental self-inductance is required during the test. To measure this, a slightly indirect method was used. An additional 20-turn coil was wound around one of the poles. The complete self-inductance (ie. non-incremented) of the field was measured with the DCIB by reversing 0.2A in it, and the mutual inductance between the field and the 20-turn coil was also measured at the same time. This enabled the 20 turn coil to be calibrated, so that the self-inductance of the field coil could be calculated from the mutual inductance obtained between them.

Then a 100Ω resistor was connected in series with the 1100Ω field coil and the 220V field supply, which reduced the current to $220/(1100+100) \approx 0.18$A. The 100Ω resistor was then shorted out, and the incremental mutual inductance between the field and the 20-turn coil was obtained. This enabled the measurement to be calculated for the incremental self-inductance of the field circuit as $47.7 \pm 1\text{H}$.

4.5 Measuring mutual inductance on the machine

The new method used for measuring mutual inductance for the 7-coil equivalent circuit is in Figure 4.11.

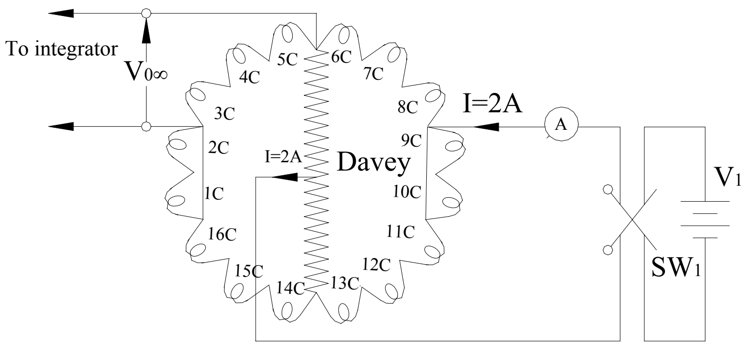

Figure 4.11 Measuring mutual inductance on different coils of the 7-coil circuit

In this example of the 7-coil circuit shown in Figure 4.11, the integrated voltage $V_{0\infty}$ on three coils from 3C to 6C is attributed to the current flowing through from 9C to 6C. Thus, it is considered that the mutual inductance is produced between these two circuits, and it can be called M_{33} in this case for the mutual inductance generated on the three coils from 3C to 6C in series depending on the current in another three coils from 9C to 6C.

A problem arose initially with a short circuit connection between the segments 6C and 14C. Because of non-zero lead resistances, there was a small voltage (ie. only a few millivolts) between 6C and 3C. This adversly affected the total voltage of the integrator, as explained in more detail in section 4.6. This problem was solved by adding a 1.6Ω rheostat between 6C and 3C as shown, and then carefully adjusting the slide position until there was less than 1mV aross 3C-6C before the current was reversed.

Similiarly, each different mutual inductance on the machine was measured based on this method. Before measuring, the armature current I_a was adjusted to 2A. Equation 4.2 for multual inductance looks very much like the equation for self-inductance in Equation 4.1. However, the voltage $V_{0\infty}$ is the integrated voltage from the other sub-coils. This is the major difference between these two equations.

Refering to Figure 4.11, the measured results of the mutual inductance on the Davey Machine with I = 2A can be summarised in Table 4.1

Connected Coils	Measured $V_{0\infty}$ (Volt)	$M = \frac{1+\text{Ratio}}{2\times I\times \text{Rate}} V_{0\infty}$ (mH)	Notation. of MI
3C - 4C	0.105	2.625	M_{31}
3C - 5C	0.29	7.25	M_{32}
3C - 6C	0.57	14.25	M_{33}
4C - 5C	0.20	5.0	M_{31}
4C - 6C	0.48	12.0	M_{32}
5C - 6C	0.28	7.0	M_{31}

Table 4.1 Measuring three coils mutual inductance in the 7-coil equivalent circuit

In the above table, each mutual inductance is denoted with a last number subscript for a number of coils affected by the flux linkage of the current through from 9C to 6C. It will be noticed that the measured mutual inductances of M_{31} or M_{32} in the different coil positions are obviously different. Thus, a question may be raised in here – can these parameter's values be validated? The answer is "more or less". The single coil, for example, between 3C and 4C, 4C and 5C or 5C and 6C is magnetically coupled by a different flux linkage depending on the angular θ. Therefore, the flux linkage associated mutual inductance to each single coil is given to cosθ, as presented in Figure 4.12.

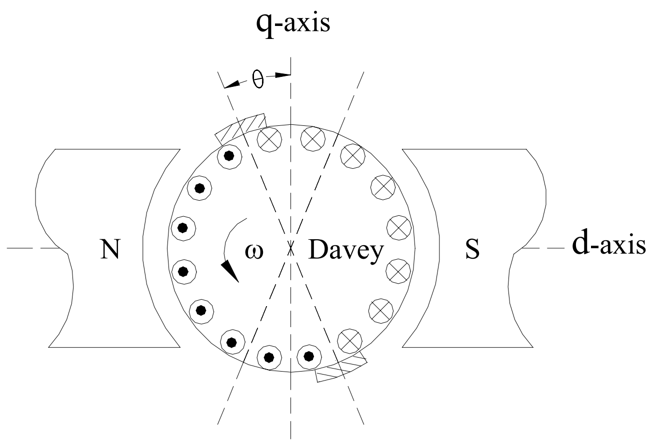

Figure 4.12 Rotating position θ definition

Before it's further progress, it is necessary to verify the above measurements. As previously stated, each segment was 22.5° apart on the armature for this 2 pole/16 slot machine. Hence the mutual inductance M_{31} defined between 9C-6C and 5C-6C can be written as $M_{31MAX} \times \cos 22.5^{\circ}$ with the current direction from 9C to 6C. Also M_{31} of 9C-6C with 4C-5C and 3C- 4C can be given as $M_{31MAX} \times \cos 45^{\circ}$ and $M_{31MAX} \times \cos 67.5^{\circ}$.

Theoretically, these mutual inductances should be expected including the term of $\cos\theta$ as:

$$\frac{M_{31MAX} \times \cos 22.5^{\circ}}{M_{31MAX} \times \cos 45^{\circ}} = \frac{0.924}{0.707} = 1.306$$

$$\frac{M_{31MAX} \times \cos 45^{\circ}}{M_{31MAX} \times \cos 67.5^{\circ}} = \frac{0.707}{0.383} = 1.846$$

The measured value of M_{31} for 5C - 6C was 7.0 mH, and M_{31} for 4C - 5C was 5.0 mH. Thus we have 7.0/5.0 = 1.4.

This answer is close to the value of 1.306 from the calculation. Thus, an error obtained for this is (1.4-1.306)/1.306 = 0.072. The percentage of the error in this case is 7.2% which is quite minor.

If the measured value 2.625 is substituted to M_{31} on 3C - 4C, then 5.0/2.625 = 1.905 is obtained. It can be considered that the measurement is also close to the calculated $\frac{M_{31MAX} \times \cos 45^{\circ}}{M_{31MAX} \times \cos 67.5^{\circ}}$ which is 1.846, and the absolute error envolved here is 1.905-1.846 = 0.059. The error can then be given as (1.9 – 1.846)/1.846 = 0.029 and its 2.9 % error should be tolerable in here.

In order to clarify the magnetic relationship between the coils on the armature winding of the Davey machine, the following Figure 4.13 can represent in a more clear way the current and flux directions.

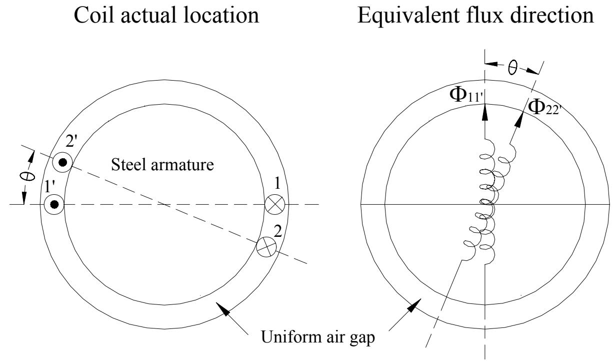

Figure 4.13 Armature coil current and flux directions

To use the same example as previously discussed, the mutual inductance M_{31} between 8C - 6C (3 coils) and 3C (1 coil), as shown in Figure 4.14.

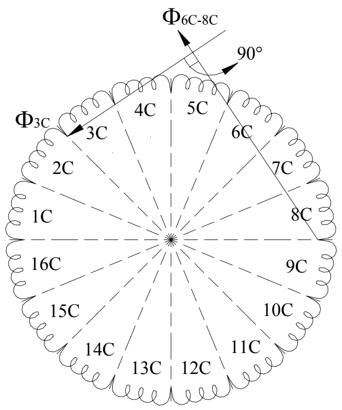

Figure 4.14 Explanation of a mutual inductance angle with the flux directions

From Figure 4.14, it can be seen that the flux directions of 8C-6C and 3C form a 90° angle. This is another way to explain these angles. So the given angles in the calculations about the mutual inductances on the armature winding can be verified, and are found to exist in intervals of 22.5°, such as 22.5°, 45°, 67.5° and 90° etc. Figure 4.14 is just a particular case if the mutual inductance between a 3-coil inductance (8C-6C) and 1-coil inductance 3C, shown as an example of the 90° angular between them.

The generated voltage terms in the model equations are of the form $\omega_r I_f \frac{dM}{d\theta}$, where M is the mutual inductance between 6 subcoils (ie. for the 7-coil model) and the field. This was measured as a function of θ, and a θ value of $\frac{dM}{d\theta}$ or 0.1H/degree (0.2πH/radian) was used in the model equations. With I_f = 0.2A, the mutual inductance for the 7 sub-coils in series in the 5-coil model had the same value, within the limits of experimental error. Note that each mutual inductance was measured during the complete reversal of the 0.2A field current.

4.6 Field current required for the Davey machine

To ensure all the self and mutual inductances were measured under the same field flux, the d-c field current in the generator (Davey machine) was supplied by an independent source. It was convenient to use another generator in our power laboratory, which was able to constantly produce 0.2A field current to the Davey machine while testing.

For a detailed discussion in relation to the field current of the Davey machine, refer to Chapter 6 Experimental results.

4.7 Conclusion

This new method of measuring inductance using a d-c source has demonstrated the feasibility of taking measurements on a d-c machine. However, the existence of this method was not perfect. Some difficulties were encountered during the experimental tests and may still remain in the machine modelling later. These difficulties were identified as follows:

(1) The integrator in the DCIB had its output voltage drift over the test period. This reduced the accuracy of measuring small values of inductances. One example could be given here when a single coil self-inductance was measured, shown in Figure 4.15.

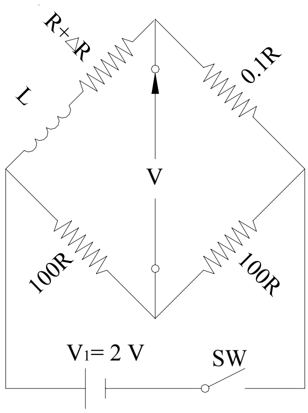

$R = 1\Omega$

DCI Bridge Integration Rate = 10

$V_{0\infty} = \int V dt$

Figure 4.15 An example of measuring a small value self-inductance

With a gain (ie. Rate) of 10, the output voltage of the integrator with a short on the input can be adjusted to be steady to about 1mV change in 5 seconds. Therefore, the readout of $V_{0\infty}$ for a self-inductance gives 1mH with $\pm 2A$, which is, in theory

$2L \times I = 2 \times 10^{-3} \times 2 = 4$ mV

Errors also occur because the current heats up the coil and this leads to a change of the measured R. Eg. if R = 1Ω and 1^oC changes it by approximate 0.4 %, then a voltage drop of 8 mV is obtained by 0.4 % of 2V. Thus, $V_{0\infty}$ will change by $10 \times 8 = 80$ mV/sec in this case.

Obviously, the bridge can be continually balanced, but the limit for useful measurement of an self-inductance is around 2 mH at $\pm 2Amp$, with an error of a few percent.

This problem was encountered during the test, where there was no input signal to the integrator, its output voltage tended to 'drift' steadily with time. Also this drift would be fastest on the highest integration rate. To minimise the drifting, an OffSET knob on the DCIB should be used.

(2) It is difficult to predict the effective value of mutual inductances due to the physical location of the armature windings on the machine. In fact the d-axis of the field will only effect those mutual inductances with angle in terms of cosθ, varing with the rotor position during the rotation. The real situation in the magnetic field on a d-c machine may therfore be more complicated than it is considered.

Although there were unavoidable errors in the data, care was taken during the tests and all parameters were measured with sufficient accuracy for this research. The estimated maximum error in the above two study cases was only 7.2% for measuring the small value of inductances. It should be understood that the less accurate value only occurs while measuring a small value of inductance. For accurate results, the inductances must be measured under conditions approximating as closely as possible to those of normal operations. The following photo in Figure 4.14 shows the unassembled Davey machine under the test for its measurement.

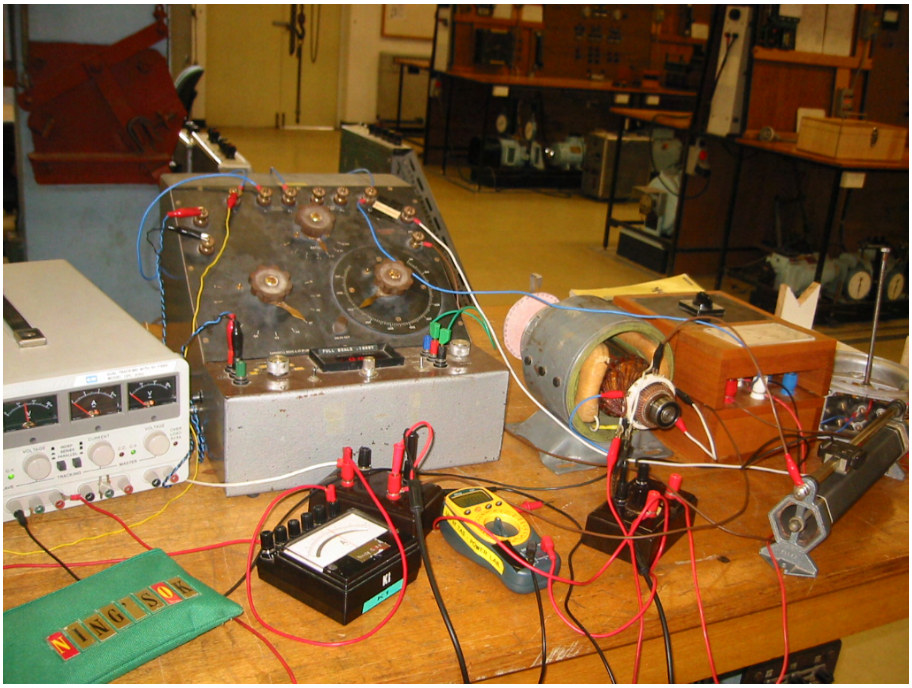

Figure 4.14 The unassembled Davey machine (inductances were measured on the machine while in this state)

Chapter 5

A mathematical model

5.1 Establishment of armature voltage equations

The basic construction of the Davey machine has been described in Chapter 3. If an external mechanical source rotates the shaft of the machine, then it is operating as a generator. This is the basic requirement for this machine to be simulated under the generating condition. Emfs are induced in the armature coils, and drive current through an external circuit. In Chapter 3 it was shown that the basic model of the Davey machine consists of two alternative equivalent circuits; either 7-coil circuit or 5-coil circuit at each instant of the rotation, as determined by whether each brush shorts out three or two segments on the armature winding during commutation.

It should be noted that the object of this model is a d-c generator rather than a d-c motor. This may impact its application, because d-c generators are no longer applicable in industry. The reason for modelling a d-c generator is because torque terms are not needed, and the speed can be set independently.

The voltage equations can now be written for the equivalent circuits as previously discussed. Recall Figure 3.5 of the 7-coil circuit with marked loop current directions from Chapter 3. It is shown here again as Figure 5.1.

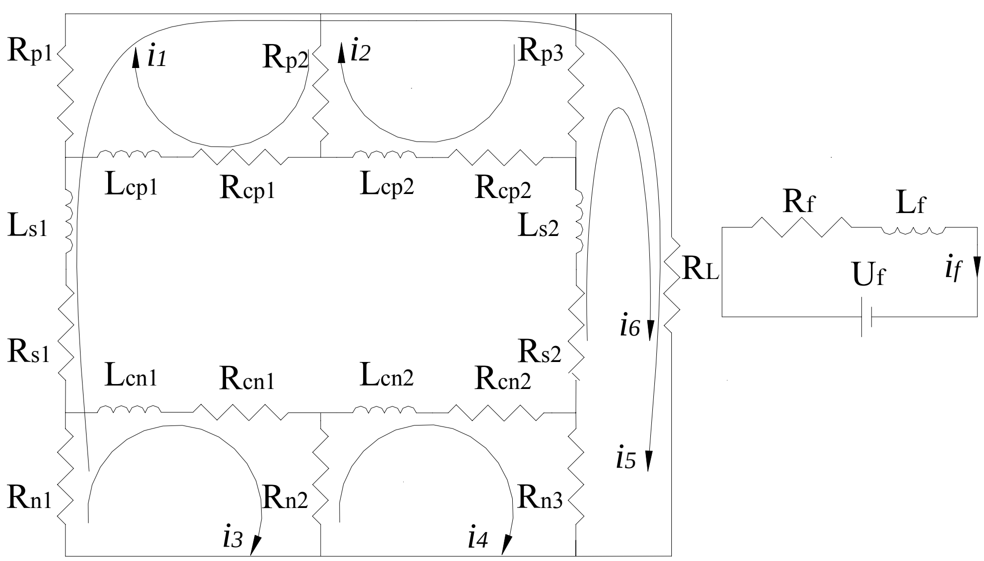

Figure 5.1 7-coil equivalent circuit of the Davey machine

In a loop analysis the loop currents in the 7-coil circuit are the variables denoted as i_1 to i_6 and i_f. It is important to note that there is only one coil in each loop. In other words, each loop only contains one self-inductance term. The reason for this arrangement will be stated later in this chapter. As it can be seen in Figure 5.1, the corresponding self-inductances to these seven loops are $\mathrm{L_{CP1}}$, $\mathrm{L_{CP2}}$, $\mathrm{L_{CN1}}$, $\mathrm{L_{CN2}}$, $\mathrm{L_{S1}}$, $\mathrm{L_{S2}}$ and $\mathrm{L_f}$ respectively. Using Kirchhoff's law, the voltage equations of the 7-coil circuit are:

Loop 1:

$$0 = i_1\,(R_{P1}+R_{P2}+R_{CP1})+i_5\,R_{P1}-i_2\,R_{P2}+M_{12}\frac{di_2}{\mathrm{dt}}-M_{13}\frac{di_3}{\mathrm{dt}}-M_{14}\frac{di_4}{\mathrm{dt}}-M_{1f}\frac{di_f}{\mathrm{dt}}+L_{CP1}\frac{di_1}{\mathrm{dt}}$$

Loop 2:

$$0 = i_2\,(R_{P2}+R_{P3}+R_{CP2})-i_6\,R_{P3}-i_1\,R_{P2}+M_{21}\frac{di_1}{\mathrm{dt}}-M_{23}\frac{di_3}{\mathrm{dt}}-M_{24}\frac{di_4}{\mathrm{dt}}-M_{2f}\frac{di_f}{\mathrm{dt}}+L_{CP2}\frac{di_2}{\mathrm{dt}}$$

Loop 3:

$$0 = i_3(R_{N1}+R_{N2}+R_{CN1})+i_5\,R_{N1}-i_4\,R_{N2}-M_{31}\frac{di_1}{\mathrm{dt}}-M_{32}\frac{di_2}{\mathrm{dt}}+M_{34}\frac{di_4}{\mathrm{dt}}+M_{3f}\frac{di_f}{\mathrm{dt}}+L_{CN1}\frac{di_3}{\mathrm{dt}}$$

Loop 4:

$$0 = i_4\,(R_{N2}+R_{N3}+R_{CN2})-i_6\,R_{N3}-i_3\,R_{N2}-M_{41}\frac{di_1}{\mathrm{dt}}-M_{42}\frac{di_2}{\mathrm{dt}}+M_{43}\frac{di_3}{\mathrm{dt}}+M_{4f}\frac{di_f}{\mathrm{dt}}+L_{CN2}\frac{di_4}{\mathrm{dt}}$$

Loop 5:

$$0 = i_5\,(R_{P1}+R_{N1}+R_{S1}+R_L)+i_1\,R_{P1}+i_3\,R_{N1}+i_6\,R_L+M_{66}\frac{di_6}{\mathrm{dt}}+i_f\,\omega_{\mathrm{r}}\frac{d_{M_{6f}}}{\mathrm{d}\theta}+L_{S1}\frac{di_5}{\mathrm{dt}}$$

Loop 6:

$$0 = i_6\,(R_{P3}+R_{N3}+R_{S2}+R_L)+i_2\,R_{P3}-i_4\,R_{N3}+i_5\,R_L+M_{66}\frac{di_5}{\mathrm{dt}}+i_f\,\omega_{\mathrm{r}}\frac{d_{M_{6f}}}{\mathrm{d}\theta}+L_{S2}\frac{di_6}{\mathrm{dt}}$$

Field:

$$U_f = i_f\,R_f+M_{1f}\frac{di_1}{\mathrm{dt}}+M_{2f}\frac{di_2}{\mathrm{dt}}-M_{3f}\frac{di_3}{\mathrm{dt}}-M_{4f}\frac{di_4}{\mathrm{dt}}+L_f\frac{di_f}{\mathrm{dt}}$$

Equation 5.1 7-coil equivalent circuit differential equations

In Equation 5.1, the parameter symbols are represented in the meaning as follows:

$\mathrm{L_{CP1}}$ = Self-inductance of the coil under the positive brush in Loop 1

$\mathrm{L_{CP2}}$ = Self-inductance of the coil under the positive brush in Loop 2

$\mathrm{L_{CN1}}$ = Self-inductance of the coil under the negative brush in Loop 3

$\mathrm{L_{CN2}}$ = Self-inductance of the coil under the negative brush in Loop 4

L_{S1} = Self-inductance of the 6 non-commutated coils in series in Loop 5

L_{S2} = Self-inductance of the 6 non-commutated coils in series in Loop 6

L_f = Self-inductance of the field circuit

$M_{12} = M_{21}$ = Mutual inductance between the coils in Loop 1 and Loop 2

$M_{13} = M_{31}$ = Mutual inductance between the coils in Loop 1 and Loop 3

$M_{14} = M_{41}$ = Mutual inductance between the coils in Loop 1 and Loop 4

$M_{23} = M_{32}$ = Mutual inductance between the coils in Loop 2 and Loop 3

$M_{24} = M_{42}$ = Mutual inductance between the coils in Loop 2 and Loop 4

$M_{34} = M_{43}$ = Mutual inductance between the coils in Loop 3 and Loop 4

M_{1f} = Mutual inductance between the coils in Loop 1 and Field

M_{2f} = Mutual inductance between the coils in Loop 2 and Field

M_{3f} = Mutual inductance between the coils in Loop 3 and Field

M_{4f} = Mutual inductance between the coils in Loop 4 and Field

M_{66} = Mutual inductance between the parallel paths in Loop 5 and Loop 6

M_{6f} = Mutual inductance in d-axis coupled between the 6 coils in series and Field

ω_r = Machine rated speed

R_{S1} and R_{S2} are the resistances of the 6 non-commutated coils in series

R_{p1}, R_{p2}, R_{p3}, R_{n1}, R_{n2}, R_{n3} are the positive or negative brush resistances respectively

Rc_{p1}, Rc_{p2}, Rc_{n1}, Rc_{n2} are the coil resistances under the positive or negative brush respectively.

Expressions have been derived for the voltages related to the resistances, self-inductances, mutual inductances and the machine's speed. These expressions were derived for the machine dynamic behaviour in the time domain, for which it can be assumed that the magnetic circuit is linear in order to solve these first order equations, as discussed in Chapter 3. Also elements in the armature circuit are symmetrically located at their physical positions in the machine. These dynamic equations couple the magnetic field and time. The functions of time involve 'dt' in the equations. This fixed time step was used as a time base for the integrators in all loops of the resulting SIMULINK model. A time base of 116 μs (equivalent to 1° of the rotation at the rated machine speed) was used for solving these differential equations. The author was interested in modelling the machine while running for six revolutions from switching it on. Equations 5.1 relate to the healthy machine. There will be need for a different treatment in the differential equations if the machine is modelled under faulted conditions as discussed in Chapter 7.

Refer to the 7-coil circuit again in Figure 5.1. The armature coils are approximately on two orthogonal axes (d and q). Each coil possesses resistance and inductance, and they are inductively coupled to the other coils in the same axis. The coils in the two parallel paths in the d-axis direction are coupled with each other, but are not coupled with any coils in the q-axis. However, these coils are generating the output voltage depending on the speed ω_r and the field mutual inductance against the rotor displaced position θ, shown as the term $i_f\ \omega_r\ \frac{d_{M6f}}{d\theta}$ in Equation 5.1. As a generator, there is only one voltage source U_f in the field voltage equation, but other loops contain no external source except mutual inductance terms.

The next step required is to determine how many loops have the mutual inductance linkages. Equation 5.1 shows that Loops 1, 2, 3 and 4, possess the mutual inductance only between them and the field circuit, as denoted by M_{12}, M_{13}, M_{14}, M_{23} ... to M_{43}. Also these loops (1-4) in the d-axis have the mutual inductance of M_{1f}, M_{2f} etc with the field. There is no flux linkage between Loops 1 to 4 and Loops 5 or 6, but these parallel paths of the six non-commutated coils in series still have mutual inductance with each other, denoted as M_{66} in both Loops 5 and 6. In other words, the coils in loops 5 and 6, and the field are in the q-axis, and all others are in the d-axis.

Futher interpretation of these equations requires these assumptions because the magnetic circuit of the machine is iron and coupling between the coils is very close. So it can be reasonably assumed that the unipolar flux and the effect of eddy current on the machine are negligible, and the armature windings are symmetrical in all cases to the discussion below. It is considered that the assumptions made were appropriate and also simplified the model.

Before further discussion of the model it is necessary first to adopt sign conventions with regard to the mutual inductances and associated currents directions (refer to Figure 5.2). Perhaps, the reader would already be familiar with Lenz's law that a minus sign mutual inductance indicates that the induced emf tends to circulate a current in such a direction as to oppose the increase of flux due to the growth of current in that coil. Therefore, the mutual inductances with a minus sign in the loop equations have been determined as the loop 1 or the loop 2 coil with the loop 3 or the loop 4, and the loop 1 or the loop 2 coil with the field coil. In the field circuit, the minus signs of the mutual inductances are only associated with Loop 3 and 4. Except these, the remainder of other mutual inductances have a plus sign. More clear explaination for the sign conventions can be seen in Equation 5.1, in which the minus signs used are only for the mutual inductances of M_{13} and M_{31}, M_{14} and M_{41}, M_{23} and M_{32}, M_{24} and M_{42}, M_{1f} and M_{2f}.

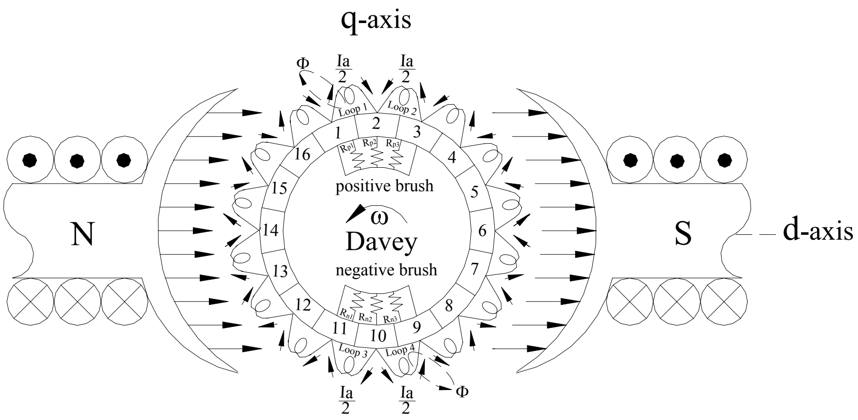

Figure 5.2 Flux direction in the 7-coil circuit

In order to explain how the sign of each mutual inductance is determined in the 7-coil circuit, another circuit diagram in Figure 5.3 may be useful. The load resistor R_L and the field loop are not included in this diagram.

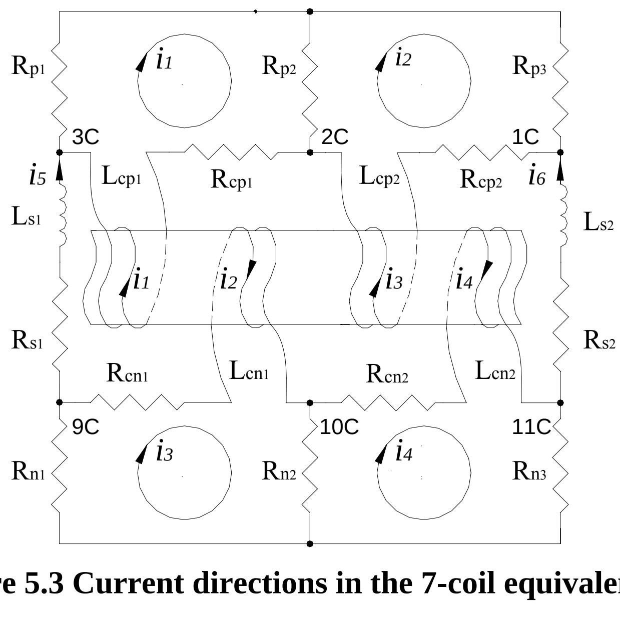

Figure 5.3 Current directions in the 7-coil equivalent circuit

In Figure 5.3, the six coils 11C to 1C, and another six coils 9C to 3C are defined as the armature coil number in this particular position of the 7-coil circuit. Other parameters are defined as per Equation 5.1. It should also be noted from the diagram, there is no such a bar wound by the currents i_1, i_2 , i_3 and i_4 in the actual motor. It is to be drawn only for understanding the related flux and current directions, which it shows better than the rotor in Figure 5.2.

The starting point is the currents from 1C to 3C defined as the loop 1 and 2 currents i_1 and i_2 , and the relevant flux is then produced in a d-axis toward 3C. In this case, the loop 3 and 4 currents i_3 and i_4 produce exactly opposite flux to the flux produced by i_1 and i_2 . The effect of the mutual inductances between loop currents i_1 to i_4 and the field coil has been taken into account, and their signs were also worked out following the direction of their m.m.f. Hence, it may be considered confidently that the signs of these mutual inductances chosen in the voltage equations are correct.

Similialy, the 5-coil equivalent circuit equations can also be built up in the same way from Figure 5.4.

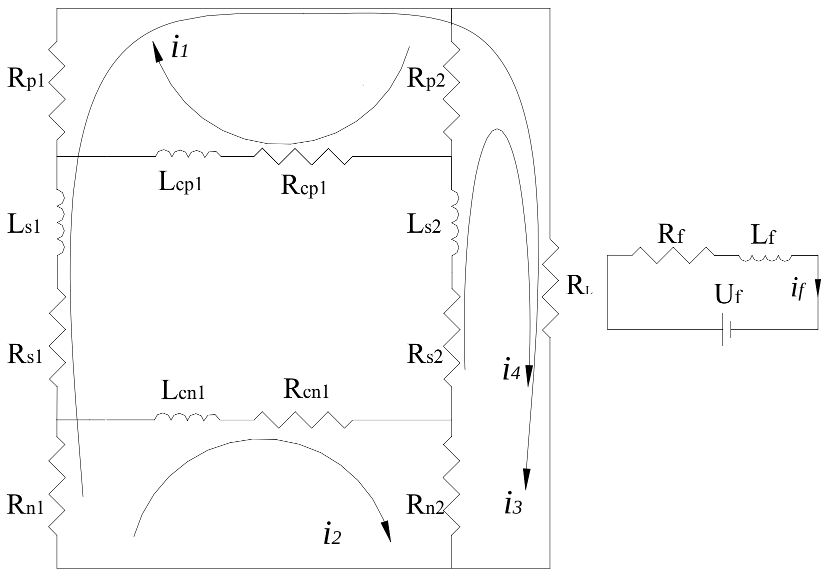

Figure 5.4 5-coil equivalent circuit of the Davey machine

Hence, the corresponding voltage equations of the 5-coil equivalent circuit are given in the following Equation 5.2.

Loop 1:

$$0 = i_1 (R_{P1} + R_{P2} + R_{CP1}) + i_3 R_{P1} - i_4 R_{P2} - M_{12} \frac{di_2}{dt} + M_{1f} \frac{di_f}{dt} + L_{CP1} \frac{di_1}{dt}$$

Loop 2:

$$0 = i_2 (R_{N1} + R_{N2} + R_{CN1}) + i_3 R_{N1} - i_4 R_{N2} - M_{21} \frac{di_1}{dt} - M_{2f} \frac{di_f}{dt} + L_{CN1} \frac{di_2}{dt}$$

Loop 3:

$$0 = i_3 (R_{P1} + R_{N1} + R_{S1} + R_L) + i_1 R_{P1} + i_2 R_{N1} + i_4 R_L + M_{77} \frac{di_4}{dt} + i_f \omega_r \frac{dM_{7f}}{d\theta} + L_{S1} \frac{di_3}{dt}$$

Loop 4:

$$0 = i_4 (R_{P2} + R_{N2} + R_{S2} + R_L) - i_1 R_{P2} - i_2 R_{N2} + i_3 R_L + M_{77} \frac{di_3}{dt} + i_f \omega_r \frac{dM_{7f}}{d\theta} + L_{S2} \frac{di_4}{dt}$$

Field:

$$U_f = i_f R_f - M_{1f} \frac{di_1}{dt} + M_{2f} \frac{di_2}{dt} + L_f \frac{di_f}{dt}$$

Equation 5.2 5-coil equivalent circuit differential equations

In Equation 5.2, the parameter symbols are represented in the meaning as follows:

L_{CP1} = Self-inductance of the coil under the positive brush in Loop 1

L_{CN1} = Self-inductance of the coil under the negative brush in Loop 2

L_{S1} = Self-inductance of the 7 non-commutated coils in series in Loop 3

L_{S2} = Self-inductance of the 7 non-commutated coils in series in Loop 4

L_f = Self-inductance of the field circuit

M_{12} = M_{21} = Mutual inductance between the coils in Loop 1 and Loop 2

M_{1f} = Mutual inductance between the coils in Loop 1 and Field

M_{2f} = Mutual inductance between the coils in Loop 2 and Field

M_{77} = Mutual inductance between the parallel paths in Loop 3 and Loop 4

M_{7f} = Mutual inductance in d-axis coupled between the 7 coils in series and Field

ω_r = Machine rated speed

R_{S1} and R_{S2} are the resistances of the 7 non-commutated coils in series

R_{p1}, R_{p2}, R_{n1}, R_{n2} are the positive or negative brush resistances respectively

Rc_{p1}, Rc_{n1} are the coil resistances under the positive or negative brush respectively

It is not necessary to go through the details for the 5-coil circuit equations here, as they are derived the same as the 7-coil circuit equations already discussed, but a bit simpler. The d-axis flux in the circuit is only in the loops 1 and 2 and their mutual inductance are given by a minus sign with each other. The terms of the generated voltage during the 5-coil operation are located on the seven armature coils in series while being not commutated, and the mutual inductance between them is M_{77} to replace M_{66} in the 7-coil circuit. Both currents i_1 and i_2 in the loops 1 and 2 are coupled with the field inductance. The sign conventions of the field mutual inductances in the 5-coil circuit also followed the rules as discussed for the 7-coil circuit, where the minus signed mutual inductance were located in the loop 2 with the field. In the field circuit, on the contrary, the minus sign was with Loop 1 and plus sign was with Loop 2. Both the 7-coil and 5-coil circuits definitely agree with the magnetic field flux relationship developed.

Before further progress can be made another question of fundamental importance has to be answered. In determining of the parameters in the model, are the coefficients of mutual inductance M_{12} and M_{21} always equal? If the equivalence is established for the inductors under saturated condition, it may be reasonable to accept it. This proof can be given from a test of a normal two-winding transformer, in which the secondary voltage on open-circuit is related to the primary current by the expression $V_2 = M_{21}(di_1/dt)$. On the other hand, $V_1 = M_{12}(di_2/dt)$ applies if the connection between the primary and secondary is reversed. Hence, such a conclusion can be obtained that M_{12} and M_{21} are equal, if they are determined under the same conditions of saturation. This condition has become important and critical for all the tests carried out to measure the inductances. Therefore, there is no conflict to believe that M_{12} equals to M_{21}. So that the assumption in both 7-coil and 5-coil equivalent circuits was made that each pair of mutual inductances are the same, such as $M_{12} = M_{21}$, $M_{13} = M_{31}$, $M_{14} = M_{41}$, etc, in the differential equations of the model.

5.2 Preliminary model design techniques

The following logic flow chart in Figure 5.5 explicitly shows how the model of the machine works.

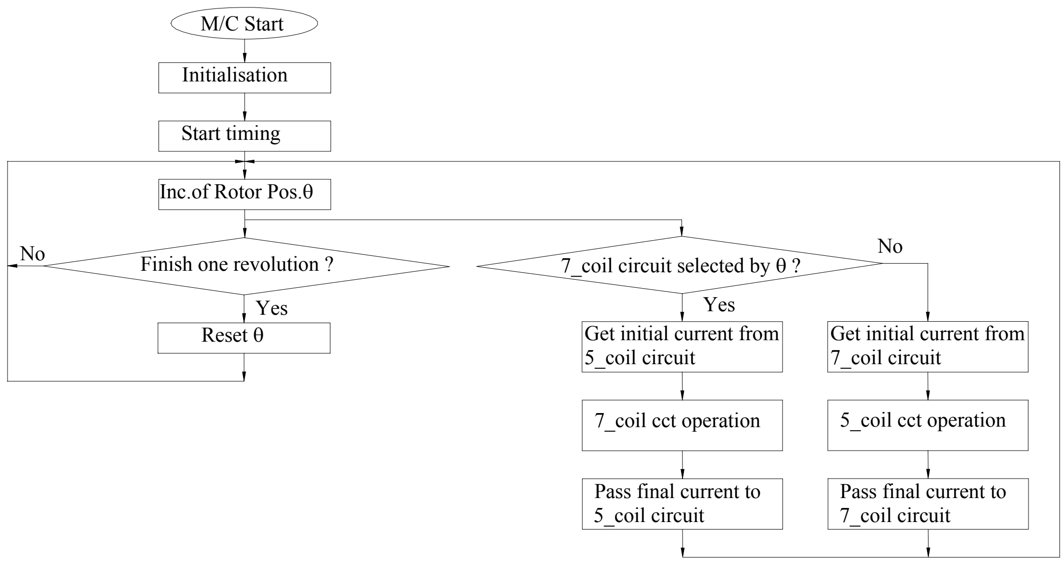

Figure 5.5 A logic flow chart for the model

From the chart, it can be seen that the machine is running in a time domain that logically determines the rotor's position at each time and also a selection to turn on either the 7-coil circuit or the 5-coil circuit. The increment of 1° rotor position is based on the machine's rated speed of 1440 rpm, and a per degree time of $116\,\mu s$ is therefore obtained. The simulating time was set up at a fixed step of $116\,\mu s$. During its operational sequence, the timing of the machine's rotation and the logical execution will be running in parallel and they do not affect each other at anytime. This would be an advantage for diagnosing the model if there is an error involved with any individual part in the model. Using MATLAB to debug in this way was found useful during moel implementation.

5.3 Varying brush resistance programming in the model

In this section, the author will discuss some components in the equivalent circuits, which were not able to be measured during the experimental tests. In the past a number of researchers (Ho [1], Krisch [38] and Linville[46]) have already contributed such a theory in varying of the brush resistance during the commutation on a d-c machine. They use an assumption that the commutating current is distributed uniformly over the brush surface to give a constant 1 Volt for the total brush voltage drop, based on their experimental tests.

They also found that the resistance value of the brush-segment contact was inversely proportional to the interfacing areas on the surface between segments and a brush. Figure 5.6 illustrates a position of the brush in the beginning of the 7-coil circuit.

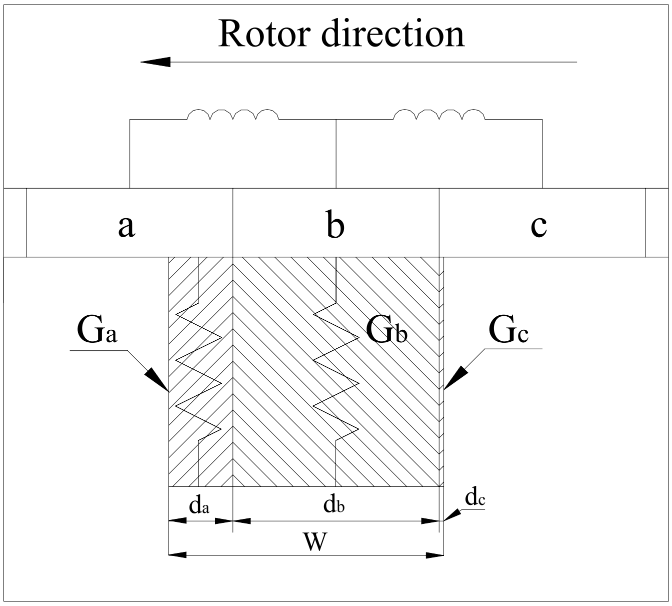

Figure 5.6 Brush segment contact resistance at the begin of 7-coil circuit

Figure 5.6 extracts a part from the 7-coil equivalent circuit as an example. Here G_w is the conductance of a total brush of a width W, obtained by:

$$G_w = \frac{\text{Rated current}}{\text{Total voltage drop on the brush}} = \frac{3.2\,\text{A}}{1\,\text{V}} = 3.2 \text{ mho}$$

Then, the relationship with G_w among the G_a, G_b and G_c are:

$$G_b = \frac{d_b}{W} G_w \qquad (5.3)$$

If the width of W is 30° and the width of one segment d_b is 22.5°, the above equation easily gives R_b, thus

$$R_b = \frac{1}{G_b} = \frac{W}{d_b G_W} \qquad (5.4)$$

Likewise, G_a and G_c can also be obtained in the same way, but it is not necessary to have a detailed discussion here. Because only the G_b is a fixed value as it is the segment in the middle with a fixed 22.5° width, but G_a and G_c will vary with the rotor's position, during commutation in the 7-coil circuit case. The various G_a and G_c will lead to R_a and R_c being varied corespondingly. Therefore, they must be considered individualy.

Having followed the basic rule of calculating the brush resistance in terms of the width on the contacted area between the brush and the segment, both G_a and G_c vary with the rotor's positions. It can be seen at the beginning of the 7-coil circuit. The corresponding movement in the mean time is that d_c covers only 0.5° of the segment and d_a is 7° of the segment under the commutator. The total width of three segments undergoing commutation is:

$$W = d_a + d_b + d_c = 7^\circ + 22.5^\circ + 0.5^\circ = 30^\circ$$

The 7-coil circuit starts from Figure 5.6 and ends with the shifted G_a and G_c while rotating, as shown in Figure 5.7.

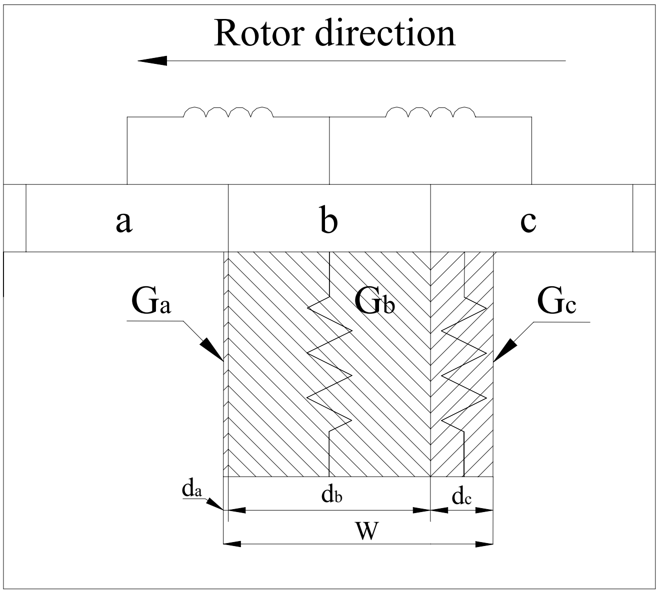

Figure 5.7 Brush segment contact resistance at the end of 7-coil circuit

It should be noticed that d_a has decreased from 7° to 0.5° and d_c has increased from 0.5° to 7° by the time when the rotor finishes the journey in the 7-coil circuit . So the total width of the three segments does not change and is still 30°, as d_b does not change during this time. Due to the resistances being inversely proportionally to segment width, R_a is increasing and R_c is decreasing within this period. Equations for R_a and R_c can be derived from Equation 5.4 as follows:

$$R_a = \frac{W}{d_a G_W} = \frac{30^\circ}{3.2 d_a} \tag{5.5}$$

$$R_c = \frac{W}{d_c G_W} = \frac{30^\circ}{3.2 d_c} \quad (5.6)$$

If a d_X is used to replace the d_a and d_c, the general equation for a varying brush resistance can then be written as

$$R_X = \frac{30^\circ}{3.2 d_x} \quad (5.7)$$

The importance is that R_X varies depending on d_X at each sampling time. To obtain R_a, d_X will be substituted by 7°, 6.5°, 6° etc, up to 0.5° at a 0.5° step decrement. On the contrary, for R_c, d_X is required to increase by 0.5^0 at each step from 0.5° up to 7°. This is part of a logic function created in the SIMULINK program, which fulfils the requirement of varying the brush resistance.

This method automatically provides varying accurate resistance value when running the MATLAB model, and it is also applicable for the 5-coil circuit. The only difference in the 5-coil circuit is that two segments are under commutation by the brush unlike the three segments in the 7-coil circuit. Therefore, there are only two brush resistances R_a and R_b in the 5-coil circuit, but both vary. Figure 5.8 illustrates how they are related to the rotor's position when the machine just turns into the 5-coil circuit.

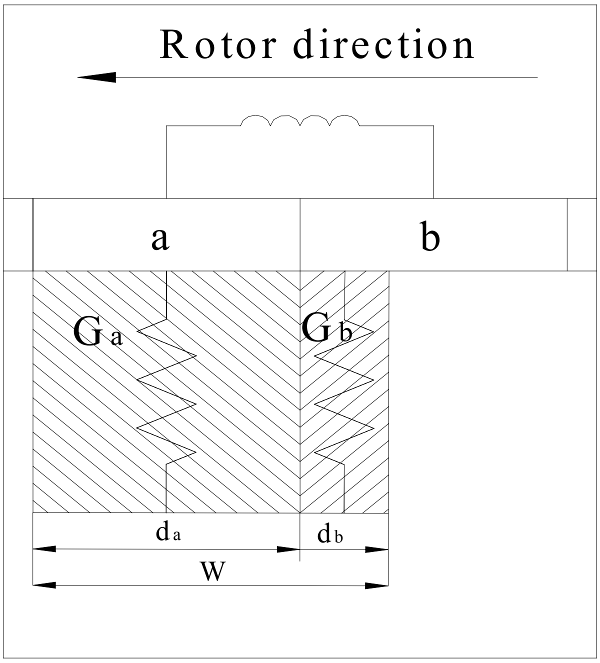

Figure 5.8 Brush segment contact resistance at the begin of 5-coil circuit

As previously defined, the 5-coil circuit runs for 15° of the rotor's displacement which is twice long as the 7-coil circuit. Figure 5.8 shows the two brush resistance R_a and R_b and their widths 22.5° and 7.5° respectively. When the 5-coil circuit starts active in the model, the d_a covers 22.5° of the full segment first, and then it reduces down to 7.5° by the end of this period. Similarly, d_b starts with 7.5° width of the segment and finally gets under 22.5° of the segment. Hence, the total width of two segments undergoing commutation is:

$W = d_a + d_b = 30^\circ$

At the end of the 5-coil circuit, the positions of the brush segment contacts d_a and d_b are just exchanged. Therefore the two brush resistance R_a and R_b are corespondingly exchanged, as shown in Figure 5.9.

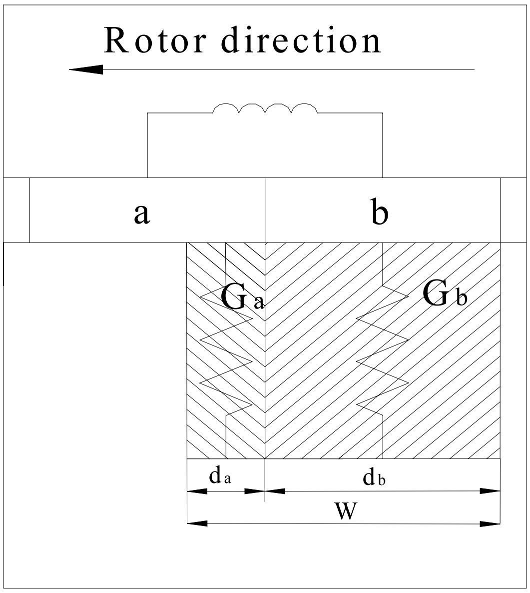

Figure 5.9 Brush segment contact resistance at the end of 5-coil circuit

Therefore, the calculation in Equation 5.7 for R_X is still satisfactory and the only change made in the 5-coil circuit is using twice longer sampling steps of the iteration than the 7-coil circuit. This is because the operation of the 5-coil circuit takes 15° of the rotating time which is doubled 7.5° of the 7-coil circuit time. However, the process in the SIMULINK program for calculating the varying brush resistances performed well throughout the model's tests.

Even though the function about the varying brush resistance in both the 7-coil and 5-coil equivalent circuits is understood, it is still not a complete procedure in the model. Because of the motion of the rotor, it is necessary to design two different blocks in order to identify whether the brush resistance is increasing or decreasing. For the 7-coil case in Figure 5.6 and Figure 5.7, the $R_a = \dfrac{30^\circ}{3.2d_a}$ is increasing with the decreasing d_a from 7° to 0.5°. Each 1° brush width is considered to have $30 \times \dfrac{1V}{3.2A} = 9.375\ \Omega$. This value of the 1° resistance was used as a base in two sub-systems in SIMULINK, for the increasing and decreasing brush resistances during the 7 coil operation, as shown in Figure 5.10 (a) and (b).

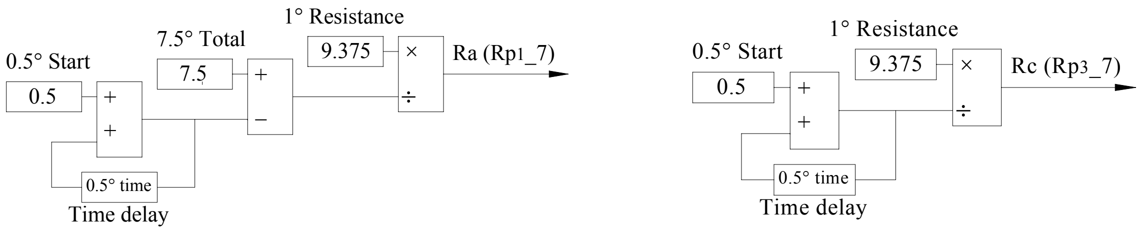

(a) increasing brush resistance **(b) decreasing brush resistance**

Figure 5.10 Varying brush resistance sub-systems in 7-coil circuit

5.4 Connection schemes

In the MATLAB environment, the nonlinear dynamics can be easily modeled. The designing and connecting schemes for the model have been regarded as a real exposure to SIMULINK over the research period. The major difficulty is due to the effect of those mutual inductances on the armature windings, and this is the ramification of linking each loop of the equivalent circuit with other loops. Therefore each loop current has to be fed from the mutual inductances with the derivatives of other loop currents everywhere in the model. It should be noted that care should be taken to avoid algebraic loops in MATLAB. The details of a connection diagram refer to Appendix B.

The first subsystem established in the model is about how to generate the rotor's position in degrees when the machine is running. This is straightforward with a few logic decisions. The output of this subsystem goes to the another subsystem called by "Position Selector" in Appendix B-2, which is logically controlled to select the 7-coil circuit only. The property from this output is a boolean type signal to determine whether the model operates the 7-coil circuit or the 5-coil circuit. It can be described by a logic block diagram in Figure 5.11.

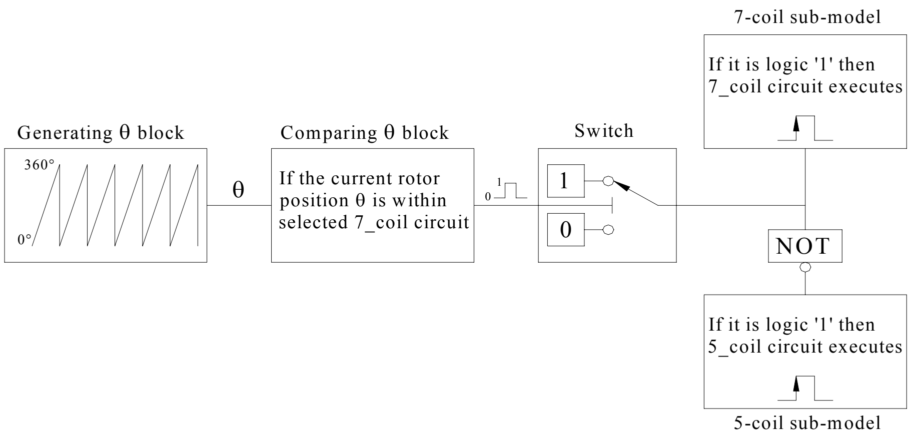

Figure 5.11 Logic block diagram of model execution

With the development in the SIMULINK for both 7-coil and 5-coil circuits' modelling, a great effort has been made to establish the complicated internal connections. One specific task of the model is to keep each loop's current continuous when changing from a 5-coil circuit to a 7-coil circuit, and vice verse.

Based on the previous discussion in Equation 5.1 and Equation 5.2, the 7-coil and 5-coil equivalent circuits need to be rewritten as Equation 5.8 and Equation 5.9, in which the self-inductance of each loop is relocated to the right side of the equation. The basic reason for this rearrangement is to configure the SIMULINK model as shown in Figure 5.12, with the output of the sum block being $\mathrm{L}\frac{\mathrm{di}}{\mathrm{dt}}$, allowing addition of a time delay and integrator to the feedback signal to get i .

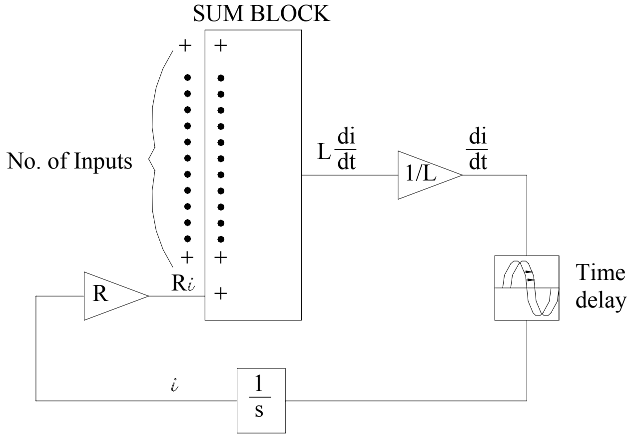

Figure 5.12 SIMULINK sum block used at each loop of the voltage equations

So there is only one term of the self-inductance L multiply with its own current derivative $\frac{\mathrm{di}}{\mathrm{dt}}$ on the right side of each equation, to anticipate as only one output of each sum block. Then the 7-coil circuit and 5-coil circuit have become like that in Equation 5.8 and Equation 5.9.

Loop 1:

$$-i_1\,(R_{P1}+R_{P2}+R_{CP1})-i_5\,R_{P1}-i_2\,R_{P2}-M_{12}\frac{di_2}{\mathrm{dt}}+M_{13}\frac{di_3}{\mathrm{dt}}+M_{14}\frac{di_4}{\mathrm{dt}}-M_{1f}\frac{di_f}{\mathrm{dt}}=L_{CP1}\frac{di_1}{\mathrm{dt}}$$

Loop 2:

$$-i_2\,(R_{P2}+R_{P3}+R_{CP2})+i_6\,R_{P3}+i_1\,R_{P2}-M_{21}\frac{di_1}{\mathrm{dt}}+M_{23}\frac{di_3}{\mathrm{dt}}+M_{24}\frac{di_4}{\mathrm{dt}}-M_{2f}\frac{di_f}{\mathrm{dt}}=L_{CP2}\frac{di_2}{\mathrm{dt}}$$

Loop 3:

$$-i_3\,(R_{N1}+R_{N2}+R_{CN1})-i_5\,R_{N1}+i_4\,R_{N2}+M_{31}\frac{di_1}{\mathrm{dt}}+M_{32}\frac{di_2}{\mathrm{dt}}-M_{34}\frac{di_4}{\mathrm{dt}}+M_{3f}\frac{di_f}{\mathrm{dt}}=L_{CN1}\frac{di_3}{\mathrm{dt}}$$

Loop 4:

$$-i_4\,(R_{N2}+R_{N3}+R_{CN2})+i_6\,R_{N3}-i_3\,R_{N2}+M_{41}\frac{di_1}{\mathrm{dt}}+M_{42}\frac{di_2}{\mathrm{dt}}-M_{43}\frac{di_3}{\mathrm{dt}}+M_{4f}\frac{di_f}{\mathrm{dt}}=L_{CN1}\frac{di_3}{\mathrm{dt}}$$

Loop 5:

$$-i_5(R_{P1}+R_{N1}+R_{S1}+R_L)-i_1\ R_{P1}-i_3\ R_{N1}-i_6\ R_L-M_{66}\frac{di_6}{\mathrm{dt}}-i_f\ \omega_r\frac{dM_{6f}}{\mathrm{d}\theta}=L_{S1}\frac{di_5}{\mathrm{dt}}$$

Loop 6:

$$-i_6(R_{P3}+R_{N3}+R_{S2}+R_L)-i_2\ R_{P3}+i_4\ R_{N3}-i_5\ R_L-M_{66}\frac{di_5}{\mathrm{dt}}-i_f\ \omega_r\frac{dM_{6f}}{\mathrm{d}\theta}=L_{S2}\frac{di_6}{\mathrm{dt}}$$

Field:

$$U_f-i_f\ R_f-M_{1f}\frac{di_1}{\mathrm{dt}}-M_{2f}\frac{di_2}{\mathrm{dt}}+M_{3f}\frac{di_3}{\mathrm{dt}}+M_{4f}\frac{di_4}{\mathrm{dt}}=L_f\frac{di_f}{\mathrm{dt}}$$

Equation 5.8 7-coil equivalent circuit presented in the SIMULINK

Loop 1:

$$-i_1(R_{P1}+R_{P2}+R_{CP1})-i_3\ R_{P1}+i_4\ R_{P2}+M_{12}\frac{di_2}{\mathrm{dt}}-M_{1f}\frac{di_f}{\mathrm{dt}}=L_{CP1}\frac{di_1}{\mathrm{dt}}$$

Loop 2:

$$-i_2\ (R_{N1}-R_{N2}-R_{CN1})-i_3\ R_{N1}+i_4\ R_{N2}+M_{21}\frac{di_1}{\mathrm{dt}}+M_{2f}\frac{di_f}{\mathrm{dt}}=L_{CN1}\frac{di_2}{\mathrm{dt}}$$

Loop 3:

$$-i_3(R_{P1}+R_{N1}+R_{S1}+R_L)-i_1\ R_{P1}-i_2\ R_{N1}-i_4\ R_L-M_{77}\frac{di_4}{\mathrm{dt}}-i_f\ \omega_r\frac{dM_{7f}}{\mathrm{d}\theta}=L_{S1}\frac{di_3}{\mathrm{dt}}$$

Loop 4:

$$-i_4(R_{P2}+R_{N2}+R_{S2}+R_L)+i_1\ R_{P2}+i_2\ R_{N2}-i_3\ R_L-M_{77}\frac{di_3}{\mathrm{dt}}-i_f\ \omega_r\frac{dM_{7f}}{\mathrm{d}\theta}=L_{S2}\frac{di_4}{\mathrm{dt}}$$

Field:

$$U_f-i_f\ R_f+M_{1f}\frac{di_1}{\mathrm{dt}}-M_{2f}\frac{di_2}{\mathrm{dt}}=L_f\frac{dif}{\mathrm{dt}}$$

Equation 5.9 5-coil equivalent circuit differential equations

These equations can be developed with same rearrangement from Equation 5.1 and Equation 5.2. The purpose is to add up the left side of each equation as the inputs to the sum blocks in the SIMULINK program, and the output of these blocks will be the loop's self-inductance multiplied by the derivative of the loop current. The key point here is how to join them together, and how to resolve problems if the continuity of the armature current or the loop currents cannot be met.

Nevertheless, it is worth trying with every option possible and some strategic thinking of using time delay would be of inherent benefit. The author has found that the time allocations within SIMULINK have time delay due to the operational sequence of the sub-systems. Although, it is absolutely correct from their logic relationship, the time delay will automatically occur and almost be inevitable in any case. It is, therefore, necessary to locate these time delays just in front the integrator of the loop current. In other words, the model would not work correctly without these important time delay. The reason is quite simple due to the numerical integration of the loop current while taking an external initial value at each step. Because these data cannot arrive at the same time as the internal integrator needs. So, only one fixed step time delay of the simulation has been employed to wait for the arrival of the external initial.

Another important thing in the model is that there is no further sub-system used within either the 7-coil circuit or the 5-coil circuit. That is because the more sub-systems used, the more difficult it is to match with required time. In the meantime, the varying brush resistances should also be located wherever they are needed within the loops. After these all have been worked out, the problem of the current continuity was finally solved.

5.5 Implementation of the model in MATLAB

The start position of the machine from the 7-coil circuit is taken as the reference. Each loop current is subject to give its value at each simulating step, but they will be disabled if their circuit is not enabled. In describing the magnetic-electric system, properties of this model must be introduced. The number of loop currents must be continuous at any time.

As required the last data of the loop currents while the equivalent circuit is enabled, is to be kept till another circuit has taken it as the first data of a loop's initial current. Such a process has been carried on for switching many times during the simulation. It may just simply be called a 'final-initial current passing process'. It is then needed to know where the destinations are for these currents. The preliminary assumption is still based on the coil numbers for the 7 and 5 equivalent circuits, as shown in Figure 5.13.

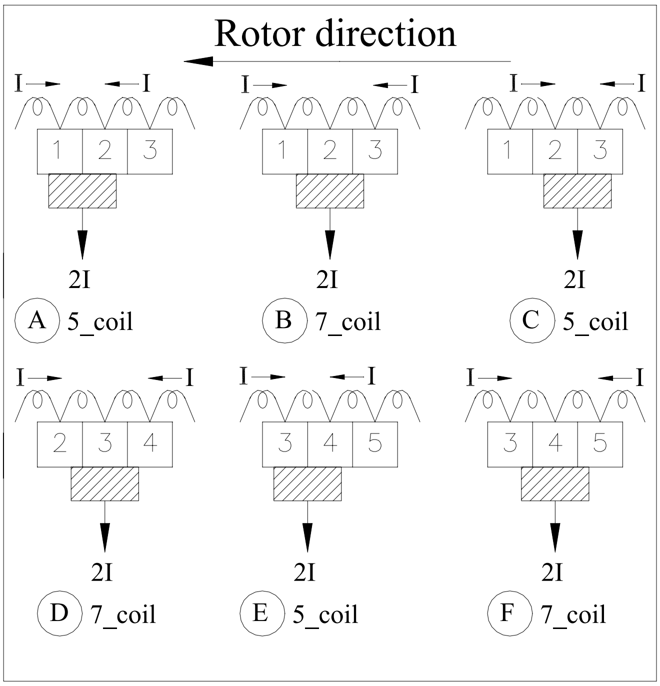

Figure 5.13 Armature winding of 7-coil and 5-coil equivalent circuits

While the machine is rotating, the current travelling tracks can be listed in Table 5.1

From 5-coil circuit	To 7-coil circuit	From 7-coil circuit	To 5-coil circuit
i_{1-5}	i_{1-7}	i_{1-7}	i_{1-5}
i_{2-5}	i_{4-7}	i_{3-7}	i_{1-5}
i_{3-5}	i_{3-7} and i_{5-7}	i_{5-7}	i_{3-5}
i_{4-5}	i_{2-7} and i_{6-7}	i_{6-7}	i_{4-5}
i_{f-5}	i_{f-7}	i_{f-7}	i_{f-5}

Table 5.1 Final-initial current passing process in the model

The two loop currents i_{1-7} and i_{4-7} seem missing during the 'final-initial current passing process'. It is assumed that they have become zero at the time when the machine changes from the end of the 7-coil circuit to the beginning of the 5-coil circuit. Unlike other loop currents of the 7-coil circuit, the final values of i_{1-7} and i_{4-7} are not passed to the 5-coil circuit.

5.6 Conclusion of the model

The other problem encountered at the beginning of the simulation in SIMULINK was the logic "switches". An initial value of 0.2A for the field current and zero for all other loop currents starting from the 7-coil circuit at t = 0 is required. The logic switches were supposed to allow the field and the loop currents to take other values (to be calculated) after the first iteration. The SIMULINK instructions were incorrect, and it turned out that they would never work in this way. Hence those switches had to be removed and replaced by another logic component such as a "product" in SIMULINK, and then the model worked after all.

Another problem was that many algebraic loops were produced within the model and there is no way that this problem could be avoided due to the effect of the mutual inductances. Then the extensive study was focussed on how to deal with these algebraic loops. The understanding that all the blocks in the model with zero algorithmic delay are connected in a feedback loop, and it was noticed that SIMULINK always reported each algebraic loop error and the model's performance could generally suffer. The solution to solve this problem was finally found by injecting a time delay into each feedback loop. This method might not prevent algebraic loops completely while running, but the model works eventually, which could possibly eliminate errors occurring. Prior to the test on the Davey machine, the model was implemented to solve the simultaneous differential equations for the healthy machine.

Chapter 6

Experimental results

6.1 Load testing on the Davey machine

The Davey machine was tested configured as a generator, as shown in Figure 6.1.

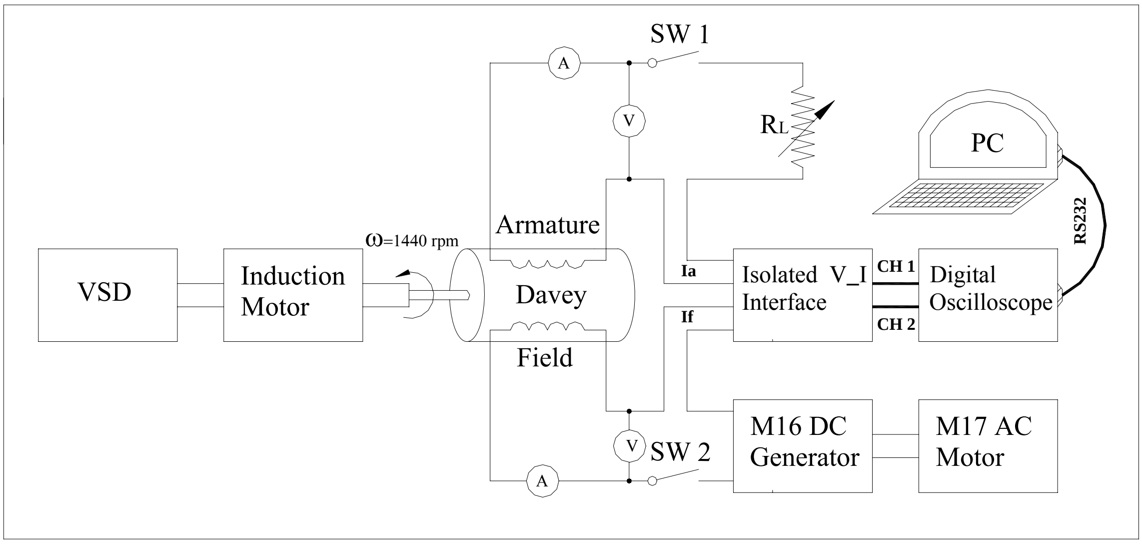

As it can be seen, another motor was needed which can be either a-c or d-c, to connect to the rotor's shaft of the Davey machine working as a generator. The requirement for this motor is that the speed should be adjustable to 1440 Rev/min (24 Rev/sec) as agreed with model's simulated speed. In the experimental test a 3 HP induction motor was controlled by a variable frequency supply. The Davey generator requires an external source of current for the field winding. This external current source can be another d-c generator, a controlled or uncontrolled rectifier, or simply a battery. However, the ideal field supply needs a zero ripple d-c output. Unfortunately, there is no suitable battery supply available in the Engineering School, and so another d-c generator in the power laboratory was used to generate a ripple-free rated field voltage of 220 Volts to the Davey machine. This gives rated field current I_f of approxmately 0.2A, which is required to saturate the iron magnetic circuit of the Davey machine.

6.2 Armature and field current waveforms comparison

It would be desirable to see the waveform of the armature current I_a to be measured under the same condition presumed as the model of the Davey machine. If everything is working correctly, the I_a should be equal or close to the output from the model on the computer. The measurement of I_a is shown in Figure 6.2.

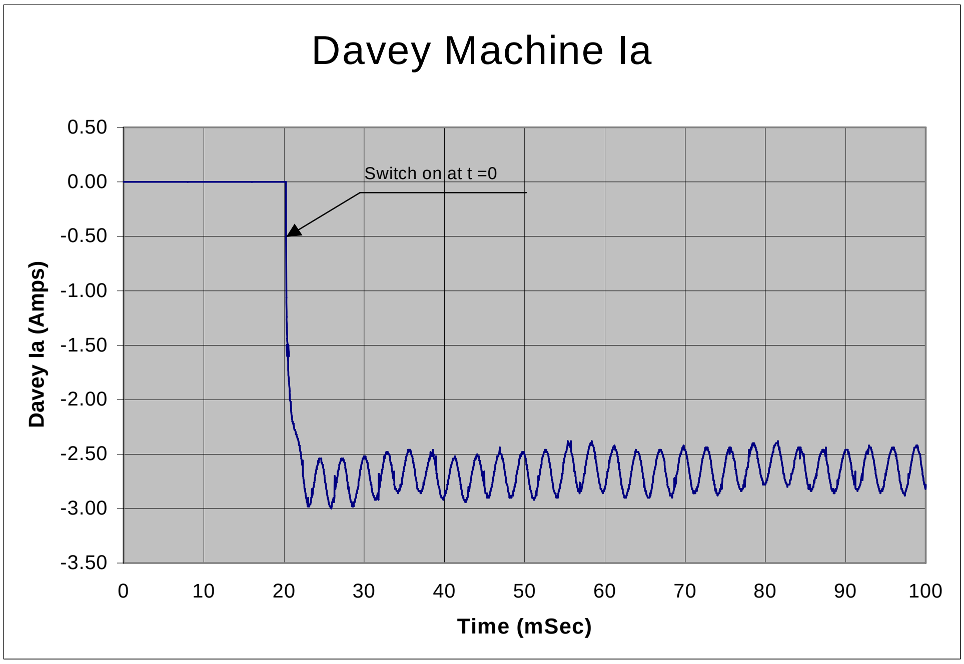

Figure 6.2 Measured I_a of the healthy Davey machine from being switched on

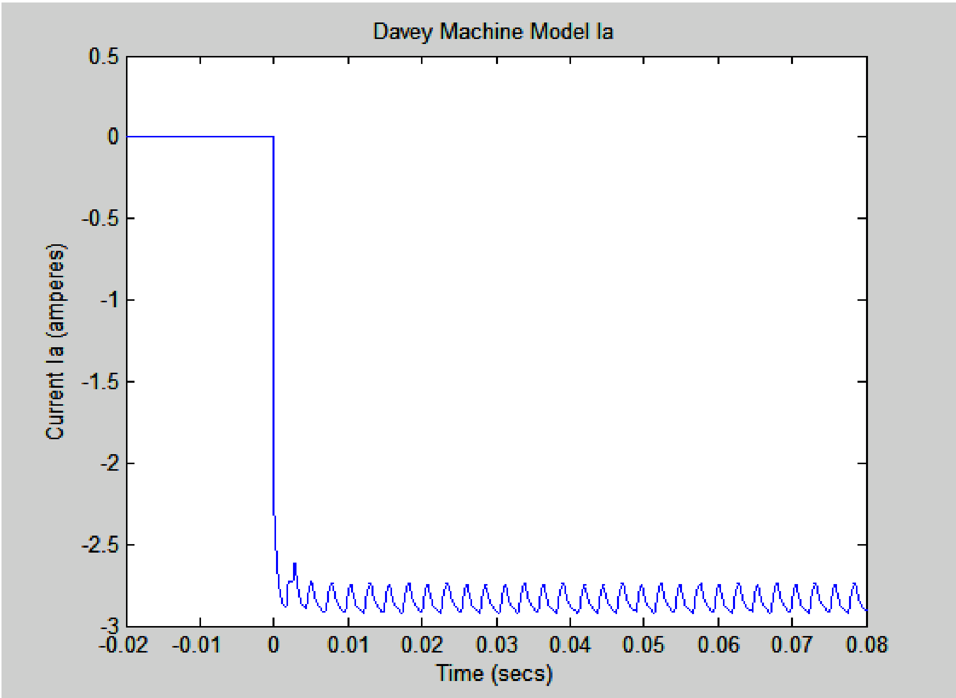

Figure 6.3 Simulated I_a of the healthy Davey machine from being switched on

Figure 6.2 shows a waveform of the measured I_a from being switched on, and Figure 6.3 gives a simulated result from the model. Both Figure 6.2 and Figure 6.3 display a 100 milliseconds period under the same switching operation. They both have proven that I_a reaches its steady state value in only a few milliseconds.

Then the probe on the digital oscilloscope is placed into the steady-state of I_a, to consider further the machine's performance. Both Figure 6.4 and Figure 6.5 represent this result in a zoomed version and a full version respectively, so that the I_a ripples can be enlarged clearly.

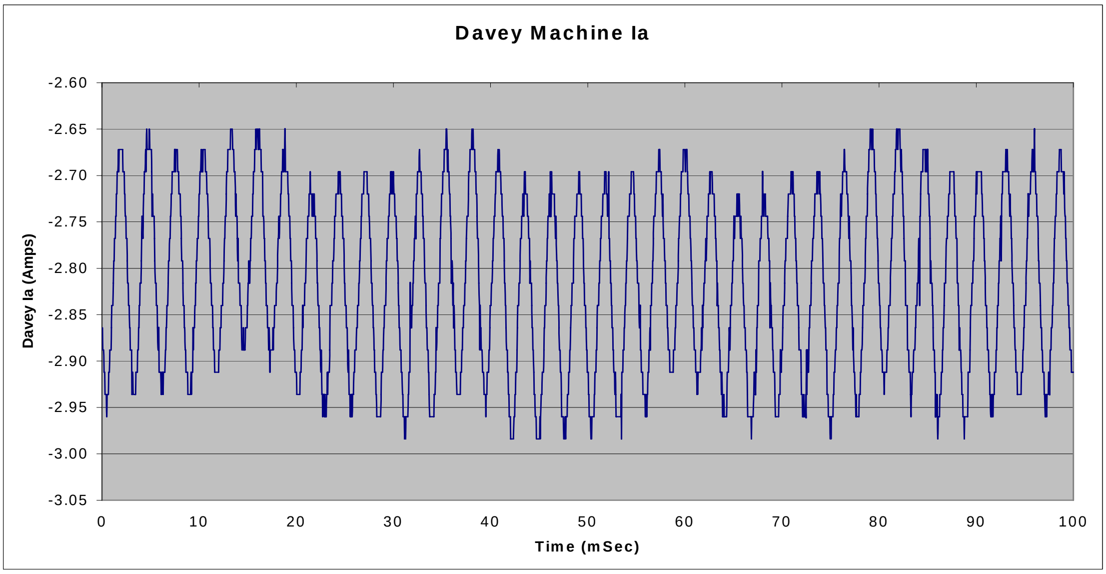

Figure 6.4 Measured I_a of the healthy Davey machine under steady-state (enlarged)

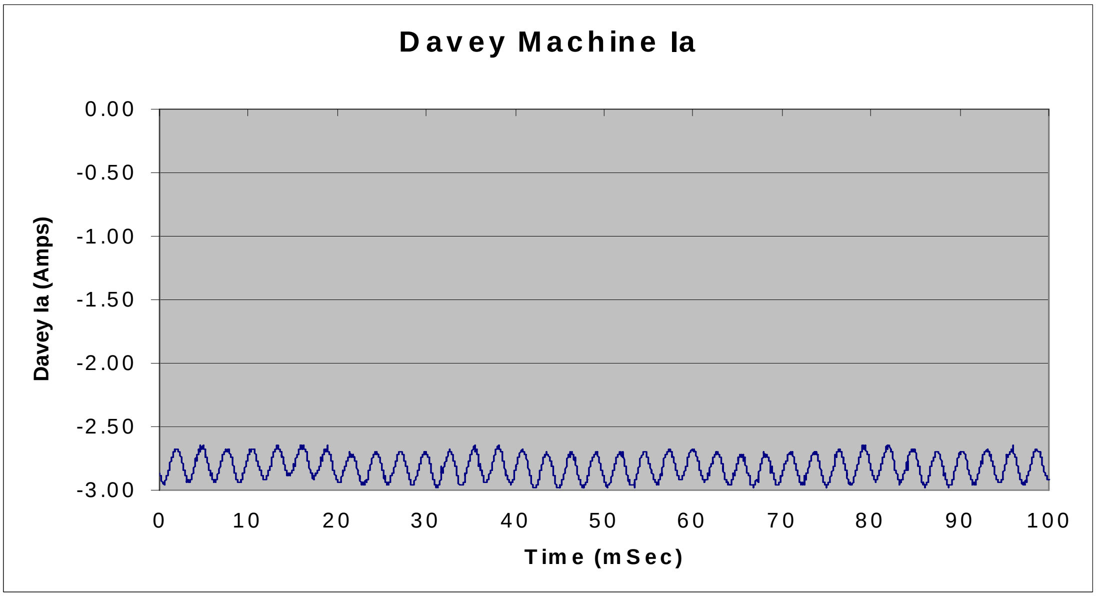

Figure 6.5 Measured I_a of the healthy Davey machine under steady-state

The following Figure 6.6 is an enlargement from the simulated model I_a and I_f of the Davey machine, so that the waveforms can be seen clearly. It has been confirmed that the ripple frequencies of I_a and I_f are the same.

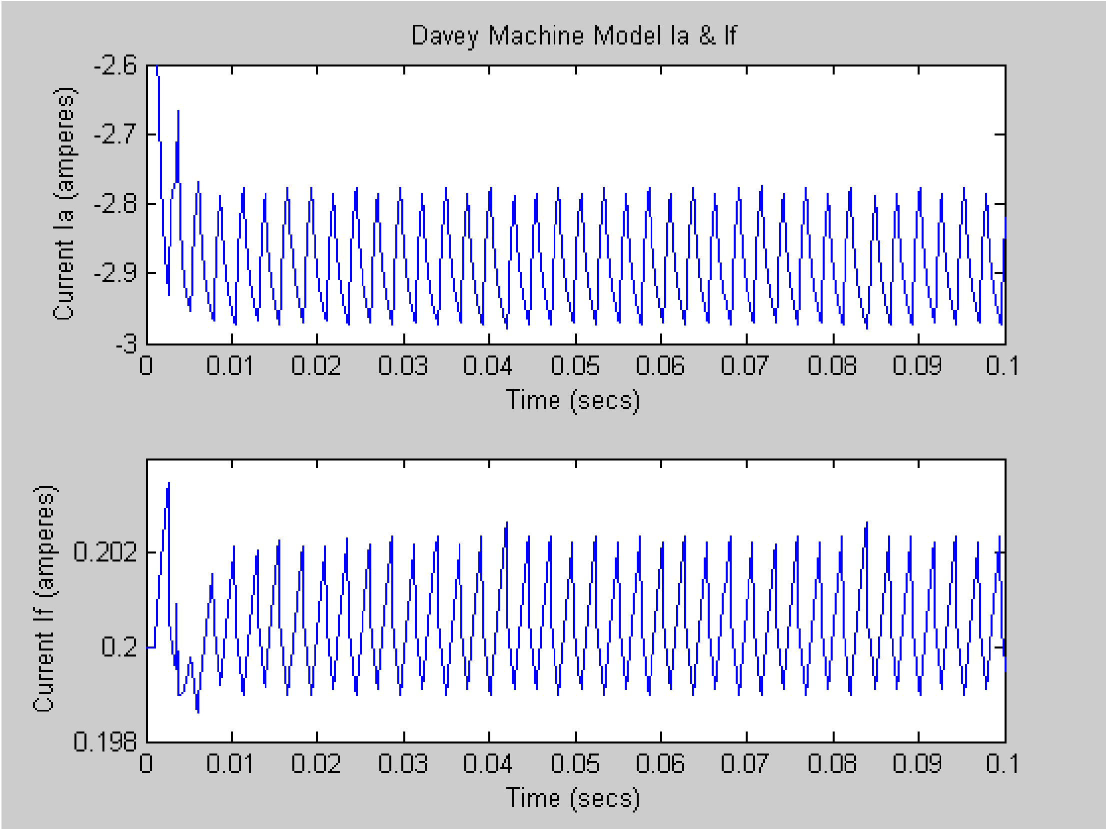

Figure 6.6 Enlargement of the simulated I_a and I_f from being switched on

The modulation of measured I_a (Figure 6.4) has a ripple of 36 periods within the first 100 milliseconds. According to our calculation in relation to 16 segments on the machine, it should have $16 \times \text{rated speed of rotor} = 16 \times 24\,\text{rev/sec} = 384$ Hz.

In Figure 6.6, the modelled armature current I_a shows about 38 periods in 100 milliseconds, in which is equivalent to 380 Hz even if there is distorted a bit by the initial transient state. So it is necessary to have a look at the second 100 milliseconds, as illustrated in Figure 6.7, which shows better performance in the steady-state of both I_a and I_f.

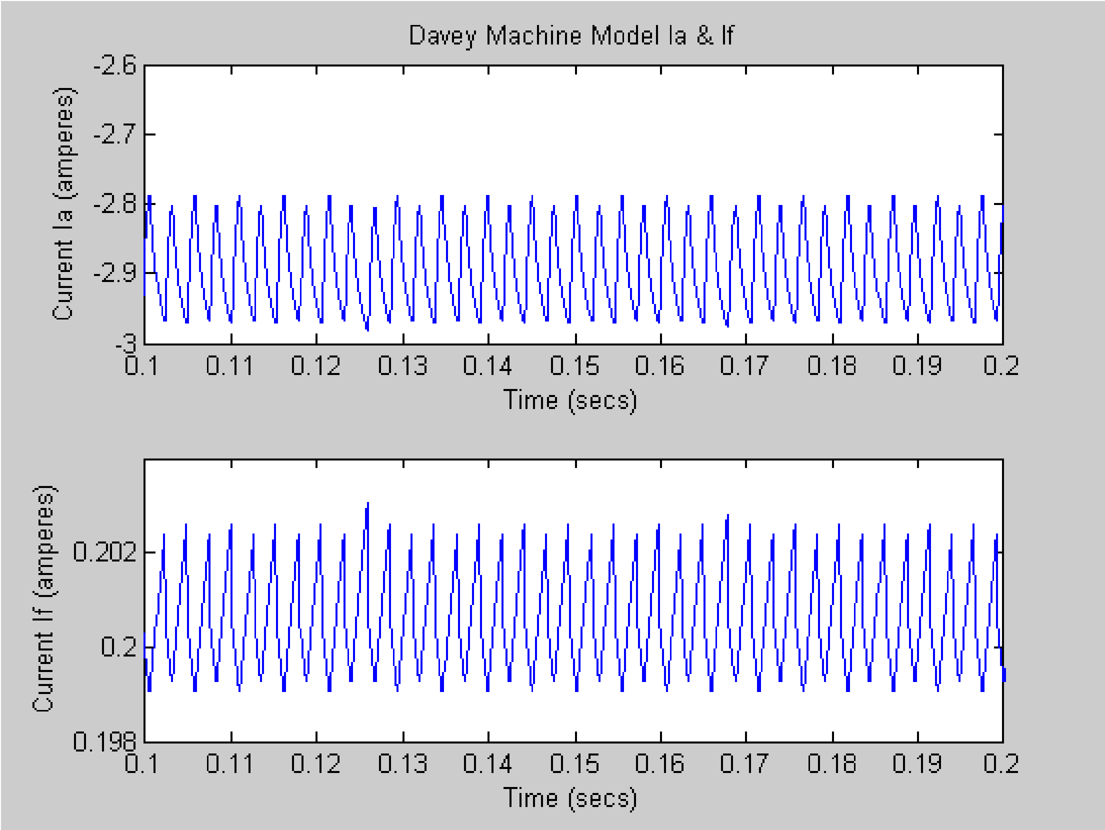

Figure 6.7 Enlargement of the simulated I_a and I_f under steady-state

Having been investigated and compared between the model outputs and experimental tests, one thing can certainly be confirmed that the ripple frequency of I_a is not due to 48 segments on the actual machine. Otherwise, the ripple frequency would be given as

$48 \times \text{rated speed of rotor} = 48 \times 24\,\text{rev/sec} = 1152\ \text{Hz}$

Therefore, the 48 segment armature winding is not the case for the modelling, regardless the machine is constructed like this. Hence, our assumption in establishing the equivalent circuits has been verified by the measured results on the machine.

Next step in the test was to view the waveform of the Davey machine's I_f. It was quite surprising to find that the measured I_f shown in Figure 6.8 looks quite different from the model's I_f. Note that the zero has been suppressed in order to show the ripple clearly.

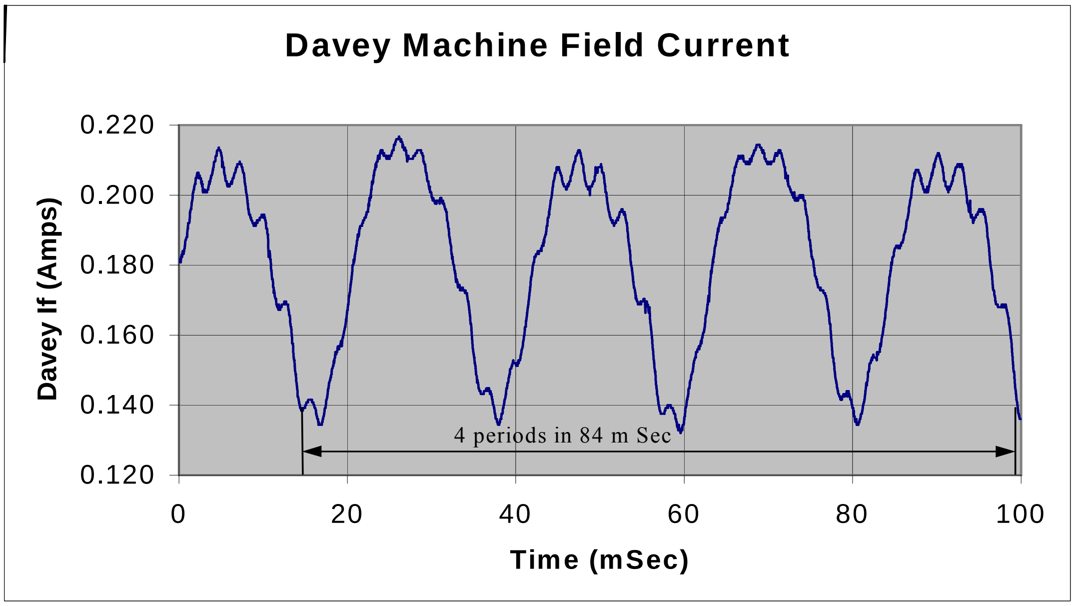

Figure 6.8 Measured I_f of the healthy Davey machine under steady-state

Figure 6.8 draws attention to the fact that the main frequency of the ripple in I_f is about 48 Hz (ie. 4 periods in 84 milliseconds), which is much less than the commutation ripple frequency of 380Hz.

To examine this phonemenon, the field current waveform was looked at more closely, as shown in Figure 6.9.

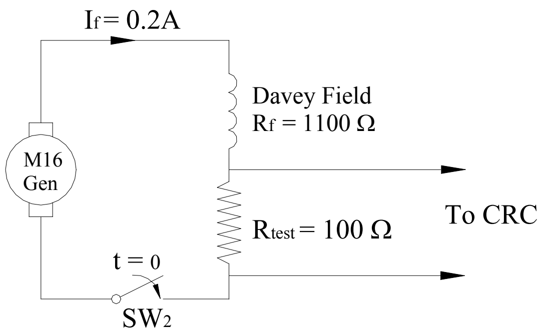

Figure 6.9 New connection for measuring I_f on the Davey machine

Unfortunately, the small ripples seem too small to see clearly in this waveform, but it is still countable approxmately about 36 ripples within 100 milliseconds. The connection in Figure 6.9 does not explain why the peak to peak ripple observed in Figure 6.8 is at 48 Hz. The discovery in the measured field current showes that the rotor might be a bit oval, it would modulate the I_f waveform at the double speed in Rev/sec which could give $2 \times 24\,\text{rev/sec} = 48\text{Hz}$.

6.3 Problem solving and sensitivity analysis

As electrical machines and transformers are sometimes sources of interference, the comparison has been undertaken to find out the best option for the measured signal coupling among the selectable settings on the oscilloscope. In order to display the required signals of a few hundred Hz in I_a and I_f and exclude any high frequency noise, a low pass filter of 5 kHz was used between the isolated V_I interface and the oscilloscope. Then the armature current on the Davey machine shown on the oscilloscope gives almost the same waveform as from the model.

In our measurement of the armature current I_a in Figure 6.4, the peak-to-peak ripple is about 10.5 %. However, the ripple percentage of the simulated I_a is about 8.5 %, which is slightly lower than the real situation from the test. The ripple percentage in the model should be affected by the inductances of the armature winding.

As the first step the changes made in the model was to double all the values of every self-inductances and mutual inductances. Figure 6.10 shows an output of the simulated I_a from doubling inductances.

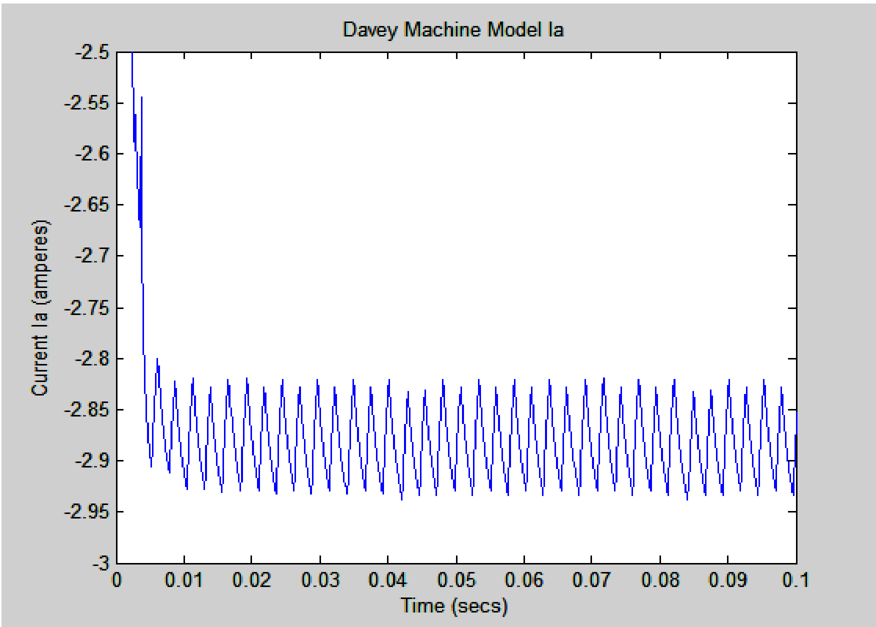

Figure 6.10 Simulated I_a with doubled inductances

Obviously, the I_a ripple becomes smaller by reducing to about 4.2 % peak-to-peak ripple, once all the inductance values have been doubled, as seen in Figure 6.10.

In the next step, the value of all inductances was halved. Figure 6.11 illustrates the result.

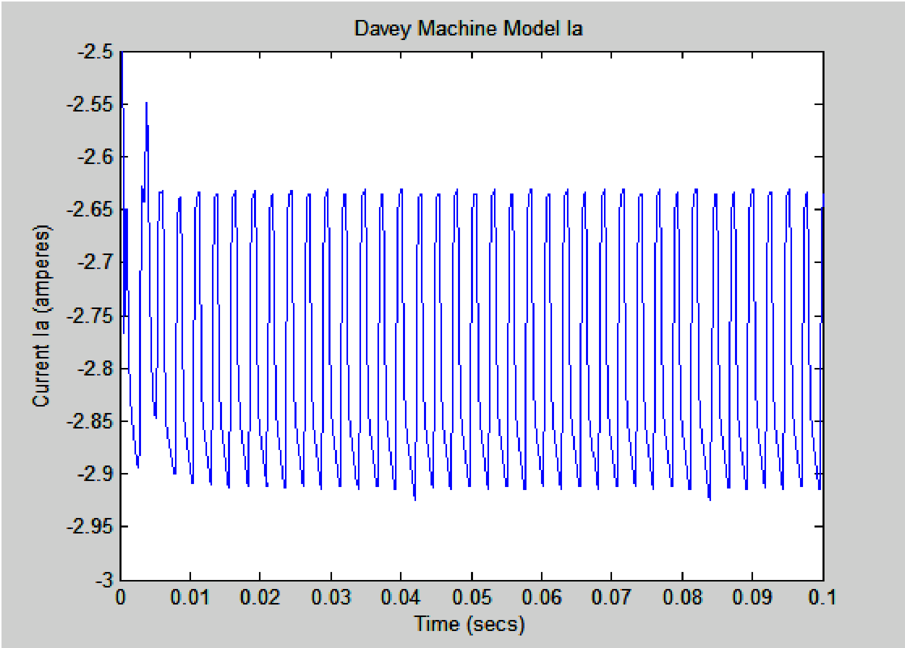

Figure 6.11 Simulated I_a with halved inductances

Now came the discovery that, although the value of all resistances on the armature winding have not been changed, there is an inverse relationship between the inductance values and the ripple amplitude in the current I_a. In other words, doubling inductances led to a 50% ripple in I_a, and halving the inductances led to a 200% ripple in I_a. This evidence indicates that the inductances obtained from the measurements on the Davey machine might be too high. There may be an error in inductance measurement, especially for the self-inductance of the sub-coils, which could be 20% too high.

6.4 Analysis and assessment on model's performance

Overall, the model's performance seems satisfactory comparing with the test results. Certainly, there may be errors involved in the inductance measurements, but a reasonable answer has been found in relation to the measured field current waveform.

It was also noticed that the waveform of the modeled I_f in Figure 6.7 has one ripple very slightly higher than others in every 16 ripples. Obviously, 16 segments (simulated in the model) in the armature winding would be related to this phenomenon of each machine revolution, but it is not clear how this has occurred during the simulation. The measurement cannot show this because of the oval rotor situation.

Figure 6.12 shows the Davey machine under the test.

Figure 6.12 The Davey machine being tested

Chapter 7

An armature shorted coil model

7.1 Armature winding with one shorted coil

The following model is based on the previous equivalent circuits for the Davey machine, but with one armature coil being shorted. The first position of the shorted coil is assumed at 3C in the 7-coil circuit (ie. the previous model of the healthy machine), as shown in Figure 7.1.

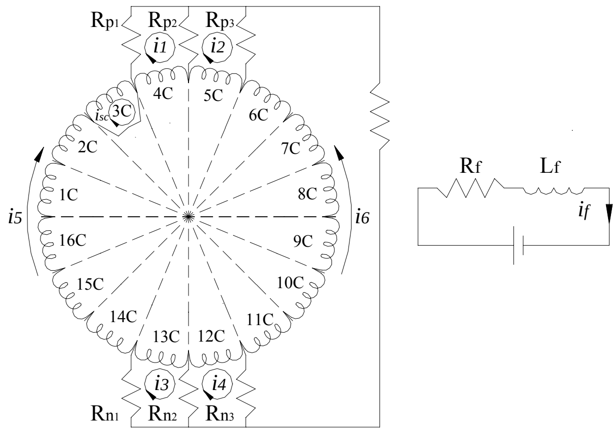

Figure 7.1 One coil shorted in the 7-coil circuit within first 7.5° rotation

By inserting a shorted coil into the 7-coil circuit it has become 8 coils all together. Figure 7.1 represents geographically the coil positions on the rotor, with the assumption of the shorted coil starting position at t = 0. The circuit diagram in Figure 7.2 shows all the components of the 8-coil circuit in detail.

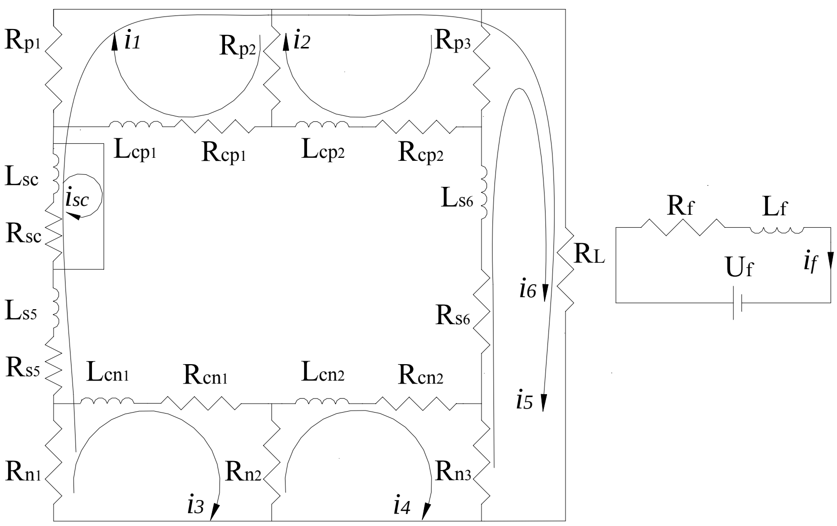

Figure 7.2 8-coil equivalent circuit of the Davey machine

The voltage equations for the 8-coil circuit still remain as first order differential for Loops 1 to 6, shorted-circuit loop (SC) and the field loop. They can be expressed as follows.

Loop 1: $0 = i_1(R_{P1} + R_{P2} + R_{CP1}) + i_5 R_{P1} - i_2 R_{P2} + M_{12}\frac{di_2}{dt} - M_{13}\frac{di_3}{dt} - M_{14}\frac{di_4}{dt} - M_{1f}\frac{di_f}{dt} + M_{1SC}\frac{di_{SC}}{dt} + L_{CP1}\frac{di_1}{dt}$

Loop 2: $0 = i_2(R_{P2} + R_{P3} + R_{CP2}) - i_6 R_{P3} - i_1 R_{P2} + M_{21}\frac{di_1}{dt} - M_{23}\frac{di_3}{dt} - M_{24}\frac{di_4}{dt} - M_{2f}\frac{di_f}{dt} + M_{2SC}\frac{di_{SC}}{dt} + L_{CP2}\frac{di_2}{dt}$

Loop 3: $0 = i_3(R_{N1} + R_{N2} + R_{CN1}) + i_5 R_{N1} - i_4 R_{N2} - M_{31}\frac{di_1}{dt} - M_{32}\frac{di_2}{dt} + M_{34}\frac{di_4}{dt} + M_{3f}\frac{di_f}{dt} - M_{3SC}\frac{di_{SC}}{dt} + L_{CN1}\frac{di_3}{dt}$

Loop 4: $0 = i_4(R_{N2} + R_{N3} + R_{CN2}) - i_6 R_{N3} - i_3 R_{N2} - M_{41}\frac{di_1}{dt} - M_{42}\frac{di_2}{dt} + M_{43}\frac{di_3}{dt} + M_{4f}\frac{di_f}{dt} - M_{4SC}\frac{di_{SC}}{dt} + L_{CN2}\frac{di_4}{dt}$

Loop 5: $0 = i_5(R_{P1} + R_{N1} + R_{S5} + R_{SC} + R_L) + i_{SC} R_{SC} + i_1 R_{P1} + i_3 R_{N1} + i_6 R_L + M_{66}\frac{di_6}{dt} + M_{S5SC}\frac{di_{SC}}{dt} + i_f\,\omega_r\frac{dM_{6f}}{d\theta} + L_{SC}\frac{di_{SC}}{dt} + (L_{S5} + L_{SC})\frac{di_5}{dt}$

Loop 6: $0 = i_6(R_{P3} + R_{N3} + R_{S6} + R_L) - i_2 R_{P3} - i_4 R_{N3} + i_5 R_L + M_{66}\frac{di_5}{dt} + M_{S6SC}\frac{di_{SC}}{dt} + i_f\,\omega_r\frac{dM_{6f}}{d\theta} + L_{S6}\frac{di_6}{dt}$

Loop SC: $0 = (i_{SC} + i_5) R_{SC} + L_{SC}\left(\frac{di_{SC}}{dt} + \frac{di_5}{dt}\right) + M_{1SC}\frac{di_1}{dt} + M_{2SC}\frac{di_2}{dt} - M_{3SC}\frac{di_3}{dt} - M_{4SC}\frac{di_4}{dt} + M_{SCf}\frac{di_f}{dt} + M_{S5SC}\frac{di_5}{dt} + M_{S6SC}\frac{di_6}{dt} + i_f\,\omega_r\frac{dM_{SCf}}{d\theta} + M_{SCf}\frac{di_f}{dt}$

Field: $U_f = i_f R_f + M_{1f}\frac{di_1}{dt} + M_{2f}\frac{di_2}{dt} - M_{3f}\frac{di_3}{dt} - M_{4f}\frac{di_4}{dt} + M_{SCf}\frac{di_{SC}}{dt} + L_f\frac{di_f}{dt}$

Equation 7.1 8-coil equivalent circuit differential equations

In Equation 7.1, the parameter symbols mean as follows:

L_{CP1} = Self-inductance of the coil under the positive brush in Loop 1

L_{CP2} = Self-inductance of the coil under the positive brush in Loop 2

L_{CN1} = Self-inductance of the coil under the negative brush in Loop 3

L_{CN2} = Self-inductance of the coil under the negative brush in Loop 4

L_{S5} = Self-inductance of the 5 non-commutated coils in series un-shorted in Loop 5

L_{S6} = Self-inductance of the 6 non-commutated coils in series in Loop 6

L_{SC} = Self-inductance of the shorted and non-commutated one coil in Loop SC

L_f = Self-inductance of the field circuit

$M_{12} = M_{21}$ = Mutual inductance between the coils in Loop 1 and Loop 2

$M_{13} = M_{31}$ = Mutual inductance between the coils in Loop 1 and Loop 3

$M_{14} = M_{41}$ = Mutual inductance between the coils in Loop 1 and Loop 4

$M_{23} = M_{32}$ = Mutual inductance between the coils in Loop 2 and Loop 3

$M_{24} = M_{42}$ = Mutual inductance between the coils in Loop 2 and Loop 4

$M_{34} = M_{43}$ = Mutual inductance between the coils in Loop 3 and Loop 4

M_{1f} = Mutual inductance between the coils in Loop 1 and Field

M_{2f} = Mutual inductance between the coils in Loop 2 and Field

M_{3f} = Mutual inductance between the coils in Loop 3 and Field

M_{4f} = Mutual inductance between the coils in Loop 4 and Field

M_{66} = Mutual inductance between the parallel paths in Loop 5 and Loop 6

M_{S6f} = Mutual inductance in d-axis coupled between the 6 coils in series and Field

M_{SCf} = Mutual inductance in d-axis coupled between SC loop and Field

M_{1SC} = Mutual inductance between Loop 1 and SC loop

M_{2SC} = Mutual inductance between Loop 2 and SC loop

M_{3SC} = Mutual inductance between Loop 3 and SC loop

M_{4SC} = Mutual inductance between Loop 4 and SC loop

M_{S5SC} = Mutual inductance between 5 un-shorted coils in series in Loop 5 and SC loop

M_{S6SC} = Mutual inductance between 6 coils in series in Loop 6 and SC loop

ω_r = Machine rated speed

R_{SC} is the resistance of the shorted (and non-commutated) coil

R_{S5} and R_{S6} are the resistances of the 5 and 6 non-commutated coils in series

R_{p1}, R_{p2}, R_{p3}, R_{n1}, R_{n2}, R_{n3} are the positive or negative brush resistances respectively

Rc_{p1}, Rc_{p2}, Rc_{n1}, Rc_{n2} are the coil resistances under the positive or negative brush respectively

After finishing the execution from the 8-coil circuit in the first 7.5° rotating time, the shorted coil (3C) will be moving into a 6-coil circuit, described in Figure 7.3.

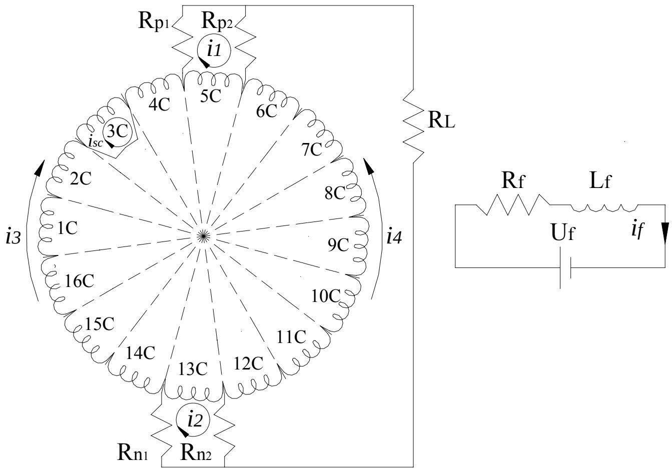

Figure 7.3 One coil shorted in the 5-coil circuit after 7.5° rotation

Likewise, the circuit diagram in Figure 7.4 represents an equivalent circuit of the 6-coil model.

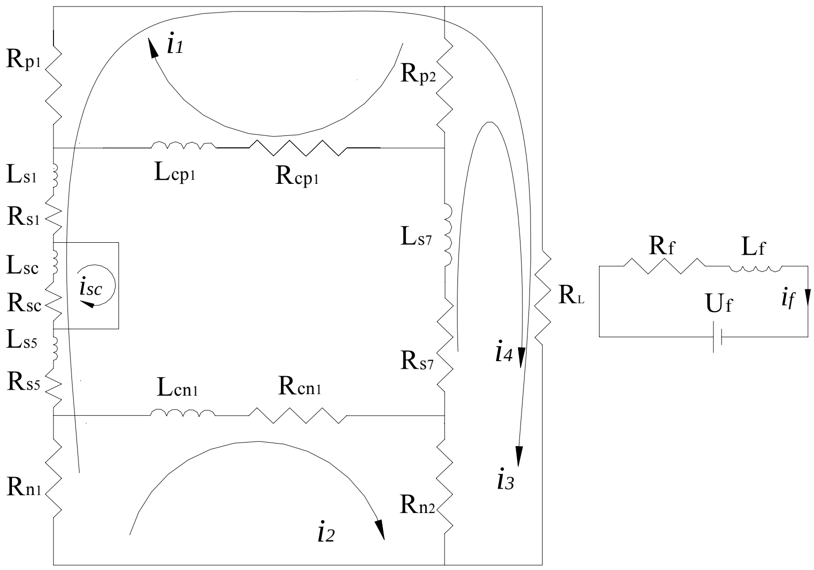

Figure 7.4 6-coil equivalent circuit of the Davey machine

The voltage equations for the 6-coil equivalent circuit, similar to the 8-coil circuit, are based on the previous 5-coil circuit by adding a shorted-circuit loop (SC). Hence, the number of the loops becomes 6, expressed in Equation 7.2.

Loop 1: $0 = i_1 (R_{P1} + R_{P2} + R_{CP1}) + i_3 R_{P1} - i_4 R_{P2} - M_{12}\frac{di_2}{\mathrm{dt}} - M_{1f}\frac{di_f}{\mathrm{dt}} + M_{1SC}\frac{di_{SC}}{\mathrm{dt}}$

$+ L_{CP1}\frac{di_1}{\mathrm{dt}}$

Loop 2: $0 = i_2 (R_{N1} + R_{N2} + R_{CN1}) + i_3 R_{N1} - i_4 R_{N2} - M_{21}\frac{di_1}{\mathrm{dt}} + M_{2f}\frac{di_f}{\mathrm{dt}} - M_{2SC}\frac{di_{SC}}{\mathrm{dt}}$

$+ L_{CN1}\frac{di_2}{\mathrm{dt}}$

Loop 3: $0 = i_3 (R_{P1} + R_{N1} + R_{S1} + R_{S5} + R_{SC} + R_L) + i_{SC} R_{SC} + i_1 R_{P1} + i_2 R_{N1} + i_4 R_L$

$+ M_{77}\frac{di_4}{\mathrm{dt}} + (M_{S5SC} + M_{S1SC} + L_{SC})\frac{di_{SC}}{\mathrm{dt}} + i_f\,\omega_d\frac{dM_{7f}}{\mathrm{d}\theta} + (L_{S1} + L_{S5} + L_{SC})\frac{di_3}{\mathrm{dt}}$

Loop 4: $0 = i_4 (R_{P2} + R_{N2} + R_{S7} + R_L) - i_1 R_{P2} - i_2 R_{N2} + i_3 R_L + M_{77}\frac{di_3}{\mathrm{dt}} + M_{S7SC}\frac{di_{SC}}{\mathrm{dt}}$

$+ i_f\,\omega_r\frac{dM_{7f}}{\mathrm{d}\theta} + L_{S7}\frac{di_4}{\mathrm{dt}}$

Loop SC: $0 = (i_{SC} + i_3) R_{SC} + L_{SC}\frac{di_3}{\mathrm{dt}} + M_{1SC}\frac{di_1}{\mathrm{dt}} - M_{2SC}\frac{di_2}{\mathrm{dt}} + M_{SCf}\frac{di_f}{\mathrm{dt}} + M_{S7SC}\frac{di_4}{\mathrm{dt}}$

$+ (M_{S5SC} + M_{S1SC})\frac{di_3}{\mathrm{dt}} + i_f\,\omega_r\frac{dM_{SCf}}{\mathrm{d}\theta} + L_{SC}\frac{di_{SC}}{\mathrm{dt}}$

Field: $U_f = i_f R_f + M_{1f}\frac{di_1}{\mathrm{dt}} - M_{2f}\frac{di_2}{\mathrm{dt}} + M_{SCf}\frac{di_{SC}}{\mathrm{dt}} + L_f\frac{di_f}{\mathrm{dt}}$

Equation 7.2 6-coil equivalent circuit differential equations

In Equation 7.2, the parameter symbols mean as follows:

L_{CP1} = Self-inductance of the coil under the positive brush in Loop 1

L_{CN1} = Self-inductance of the coil under the negative brush in Loop 2

L_{S5} = Self-inductance of the 5 non-commutated coils in series un-shorted in Loop 3

L_{S1} = Self-inductance of the one non-commutated coil beside the SC in Loop 3

L_{S7} = Self-inductance of the 7 non-commutated coils in series in Loop 4

L_{SC} = Self-inductance of the shorted and non-commutated one coil in Loop SC

L_f = Self-inductance of the field circuit

$M_{12} = M_{21}$ = Mutual inductance between the coils in Loop 1 and Loop 2

M_{1f} = Mutual inductance between the coils in Loop 1 and Field

M_{2f} = Mutual inductance between the coils in Loop 2 and Field

M_{77} = Mutual inductance between the parallel paths in Loop 3 and Loop 4

M_{S7f} = Mutual inductance in d-axis coupled between the 7 coils in series and Field

M_{SCf} = Mutual inductance in d-axis coupled between SC loop and Field

M_{1SC} = Mutual inductance between Loop 1 and SC loop

M_{2SC} = Mutual inductance between Loop 2 and SC loop

M_{S5SC} = Mutual inductance between 5 un-shorted coils in series in Loop 3 and SC loop

M_{S6SC} = Mutual inductance between 6 coils in series in Loop 4 and SC loop

M_{S1SC} = Mutual inductance between the one coil beside the SC and the SC coil in Loop 3

ω_r = Machine rated speed

R_{SC} is the resistances of the shorted and non-commutated one coil

R_{S6} and R_{S7} are the resistances of the 5 and 6 non-commutated coils in series

R_{p1}, R_{p2}, R_{n1}, R_{n2} are the positive or negative brush resistances respectively

Rc_{p1}, Rc_{n1} are the coil resistances under the positive or negative brush respectively

7.2 The shorted coil position after 22.5° rotation

It is assumed that the shorted coil starts at t = 0 with the armature position in Figure 7.1. Because of the rotation this shorted coil will move around. Therefore, the next position of the shorted coil after 22.5° is shown in Figure 7.5.

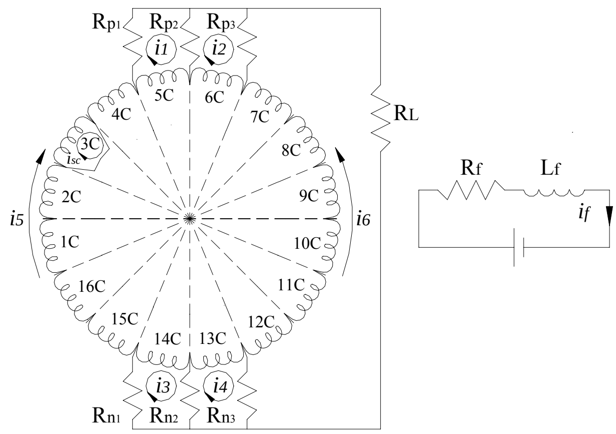

Figure 7.5 One coil shorted in the 7-coil circuit after 22.5° rotation

Hence, there should be another model of the 8-coil and 6-coil equivalent circuits corresponding to Figure 7.5. The shorted coil will have different mutual inductances with most of the other coils and the two sets of the differential equations for the 8-coil and 6-coil equivalent circuits will also be different. However, this has not been done during this research.

The last position of the coil (SC) in the 8-coil circuit on the left side of the non-commutated series path, as understood in Figure 7. 6.

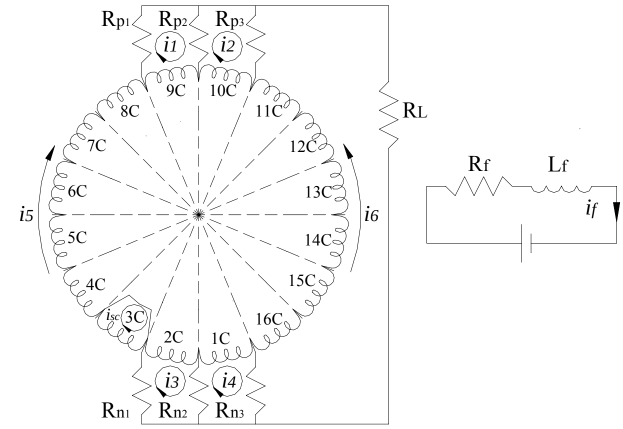

Figure 7.6 One coil shorted in the 7-coil circuit after 112.5° rotation

Then the shorted coil will move from the position in Figure 7.6 into the q-axis, where is under the negative brush, illustrated in Figure 7.7. In this particular position the shorted coil is shorting two negative brush resistance R_{n1} and R_{n2}, and therefore the armature winding may perform similarly to the healthy machine. In a case of the 8-coil circuit, the shorted coil will be under the either positive or negative brushes for 45° duration (ie. twice 22.5° time under the commutation under each brush).

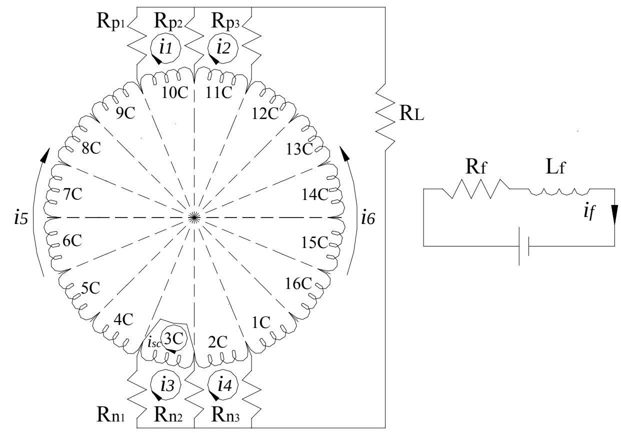

Figure 7.7 One coil shorted in the 7-coil circuit after 135° rotation

When the shorted coil has rotated 180 degrees from the starting position (Figure 7.1), it will be on the right side of the armature, located in Loop 6 of the 7-coil circuit. When the shorted coil moves further, its influence will repeat the same performance as in the previous 180 degrees. However, the further discussion about the shorted coil in other positions was not proposed within this research, but it may be possible for future development in modelling of d-c motors.

7.3 Implementation of the one shorted coil model for 22.5° of rotor movement

As previously stated for the healthy machine, the design of the one shorted coil machine model can also be established in the MATLAB/SIMULINK (refer to Appendix C). The model of the shorted coil also requires new inductance data from the measured parameters of the machine. The differential equations in Equation 7.1 and Equation 7.2 need to be rearranged using the rule of one self-inductance per loop established similarly as the healthy machine's model. Before considering the model, some particular relationship between the shorted coil and another coil in the same direction, such as Loop 5 in the 8-coil circuit or Loop 3 in the 6-coil circuit, needed to be understood and clarified, due to the movement of the shorted coil in these loops. This is because there are always two currents flowing through the shorted coil (ie. i_{5-7} and i_{sc-7} in the 8-coil circuit or i_{3-5} and i_{sc-5} in the 6-coil circuit). A single term including the self-inductance of each loop must be located on the right side of the voltage equations, as shown in Equation 7.3 and Equation 7.4.

Loop 1: $$-i_1(R_{P1}+R_{P2}+R_{CP1})-i_5 R_{P1}+i_2 R_{P2}-M_{12}\frac{di_2}{dt}+M_{13}\frac{di_3}{dt}+M_{14}\frac{di_4}{dt}+M_{1f}\frac{di_f}{dt}-M_{1SC}\frac{di_{SC}}{dt}=L_{CP1}\frac{di_1}{dt}$$

Loop 2: $$-i_2(R_{P2}+R_{P3}+R_{CP2})+i_6 R_{P3}+i_1 R_{P2}-M_{21}\frac{di_1}{dt}+M_{23}\frac{di_3}{dt}+M_{24}\frac{di_4}{dt}+M_{2f}\frac{di_f}{dt}-M_{2SC}\frac{di_{SC}}{dt}=L_{CP2}\frac{di_2}{dt}$$

Loop 3: $$-i_3(R_{N1}+R_{N2}+R_{CN1})-i_5 R_{N1}+i_4 R_{N2}+M_{31}\frac{di_1}{dt}+M_{32}\frac{di_2}{dt}-M_{34}\frac{di_4}{dt}-M_{3f}\frac{di_f}{dt}+M_{3SC}\frac{di_{SC}}{dt}=L_{CN1}\frac{di_3}{dt}$$

Loop 4: $$-i_4(R_{N2}+R_{N3}+R_{CN2})+i_6 R_{N3}+i_3 R_{N2}+M_{41}\frac{di_1}{dt}+M_{42}\frac{di_2}{dt}-M_{43}\frac{di_3}{dt}-M_{4f}\frac{di_f}{dt}+M_{4SC}\frac{di_{SC}}{dt}=L_{CN2}\frac{di_4}{dt}$$

Loop 5: $- i_5 (R_{P1} + R_{N1} + R_{S5} + R_{SC} + R_L) - i_{SC} \ R_{SC} - i_1 \ R_{P1} - i_3 R_{N1} - i_6 R_L - M_{66} \dfrac{di_6}{\mathrm{dt}}$

$$- M_{S5SC} \frac{di_{SC}}{\mathrm{dt}} - i_f \ \omega_r \frac{dM_{6f}}{d\theta} - L_{SC} \frac{di_{SC}}{\mathrm{dt}} = (L_{SC} + L_{S5}) \frac{di_5}{\mathrm{dt}}$$

Loop 6: $- i_6 (R_{P3} + R_{N3} + R_{S6} + R_L) + i_2 \ R_{P3} + i_4 \ R_{N3} - i_5 \ R_L - M_{66} \dfrac{di_5}{\mathrm{dt}} - M_{S6SC} \dfrac{di_{SC}}{\mathrm{dt}} -$

$$i_f \ \omega_r \frac{dM_{6f}}{d\theta} = L_{S6} \frac{di_6}{\mathrm{dt}}$$

Loop SC: $-(i_{SC} + i_5) \ R_{SC} - L_{SC} \ (\dfrac{di_{SC}}{\mathrm{dt}} + \dfrac{di_5}{\mathrm{dt}}) - M_{1SC} \dfrac{di_1}{\mathrm{dt}} - M_{2SC} \dfrac{di_2}{\mathrm{dt}} + M_{3SC} \dfrac{di_3}{\mathrm{dt}}$

$$+ M_{4SC} \frac{di_4}{\mathrm{dt}} - M_{SCf} \frac{di_f}{\mathrm{dt}} - M_{S5SC} \frac{di_5}{\mathrm{dt}} - M_{S6SC} \frac{di_6}{\mathrm{dt}} - i_f \ \omega_r \frac{dM_{SCf}}{d\theta} = M_{SCf} \frac{di_f}{\mathrm{dt}}$$

Field: $U_f - i_f \ R_f - M_{1f} \dfrac{di_1}{\mathrm{dt}} - M_{2f} \dfrac{di_2}{\mathrm{dt}} + M_{3f} \dfrac{di_3}{\mathrm{dt}} + M_{4f} \dfrac{di_4}{\mathrm{dt}} - M_{SCf} \dfrac{di_{SC}}{\mathrm{dt}} = L_f \dfrac{di_f}{\mathrm{dt}}$

Equation 7.3 8-coil equivalent circuit presented in the SIMULINK

Loop 1: $- i_1 (R_{P1} + R_{P2} + R_{CP1}) - i_3 \ R_{P1} + i_4 \ R_{P2} + M_{12} \dfrac{di_2}{\mathrm{dt}} + M_{1f} \dfrac{di_f}{\mathrm{dt}} - M_{1SC} \dfrac{di_{SC}}{\mathrm{dt}} = L_{CP1} \dfrac{di_1}{\mathrm{dt}}$

Loop 2: $- i_2 (R_{N1} + R_{N2} + R_{CN1}) - i_3 \ R_{N1} + i_4 \ R_{N2} + M_{21} \dfrac{di_1}{\mathrm{dt}} - M_{2f} \dfrac{di_f}{\mathrm{dt}} + M_{2SC} \dfrac{di_{SC}}{\mathrm{dt}} = L_{CN1} \dfrac{di_2}{\mathrm{dt}}$

Loop 3: $- i_3 (R_{P1} + R_{N1} + R_{S1} + R_{S5} + R_{SC} + R_L) - i_{SC} \ R_{SC} - i_1 \ R_{P1} - i_2 \ R_{N1} - i_4 \ R_L - M_{77} \dfrac{di_4}{\mathrm{dt}}$

$$- (M_{S5SC} + M_{S1SC} + L_{SC}) \frac{di_{SC}}{\mathrm{dt}} - i_f \ \omega_d \frac{dM_{7f}}{d\theta} = (L_{S1} + L_{S5} + L_{SC}) \frac{di_3}{\mathrm{dt}}$$

Loop 4: $- i_4 \ (R_{P2} + R_{N2} + R_{S7} + R_L) + i_1 \ R_{P2} + i_2 \ R_{N2} - i_3 \ R_L - M_{77} \dfrac{di_3}{\mathrm{dt}} - M_{S7SC} \dfrac{di_{SC}}{\mathrm{dt}}$

$$- i_f \ \omega_r \frac{dM_{7f}}{d\theta} = L_{S7} \frac{di_4}{\mathrm{dt}}$$

Loop SC: $- (i_{SC} + i_3) \ R_{SC} - L_{SC} \dfrac{di_3}{\mathrm{dt}} - M_{1SC} \dfrac{di_1}{\mathrm{dt}} + M_{2SC} \dfrac{di_2}{\mathrm{dt}} - M_{SCf} \dfrac{di_f}{\mathrm{dt}} - M_{S7SC} \dfrac{di_4}{\mathrm{dt}}$

$$-(M_{S5SC} + M_{S1SC}) \frac{di_3}{\mathrm{dt}} - i_f \ \omega_r \frac{dM_{SCf}}{d\theta} = L_{SC} \frac{di_{SC}}{\mathrm{dt}}$$

Field: $U_f - i_f \ R_f - M_{1f} \dfrac{di_1}{\mathrm{dt}} + M_{2f} \dfrac{di_2}{\mathrm{dt}} - M_{SCf} \dfrac{di_{SC}}{\mathrm{dt}} = L_f \dfrac{di_f}{\mathrm{dt}}$

Equation 7.4 6-coil equivalent circuit presented in the SIMULINK

In this model, the current dirrections of each loop and the signs with the mutual inductances are the same as the healthy machine's model in Chapter 5. Therefore the brush resistances are still varying as discussed previously. The model with the shorted coil requires the additional connections added to form the 8-coil and 6-coil circuits.

Another important fact must be noted in this model. The shorted coil is located in the d-axis and contains the generated voltage term $i_f \omega_r \frac{d_{MSCf}}{d\theta}$. As the shorted coil is only a portion (ie. one sixth in the 8-coil circuit and one seventh in the 6-coil circuit) compared within the non-commutated series path, the generated voltage in the shorted coil should be 1/6 or 1/7 of the total generated voltage.

The signs of the mutual inductances became even more complicated due to the shorted coil. The SC loop has the positive sign mutual inductances with all other loops including the field loop, except Loops 3 and 4 in the 8-coil circuit and Loop 2 in the 6-coil circuit.

7.4 Model's outputs for the shorted coil machine

There are three major outputs from running the model of the shorted one coil machine. They are the armature current I_a, the short circuit current I_{sc} and the field current I_f. The following waveforms in Figure 7.8 are for the model of the shorted coil, as given in Figure 7.1 and Figure 7.3, within the first 22.5°. It has been simulated for 100 milliseconds, in order to be certain that a steady state condition has been reached.

Note that the rotor (at 1440 rev/min) would have about 2.4 revolutions in 100 milliseconds. However, to simulate this would require a much more complicated SIMULINK model, which was not done due to the shortage of time. In fact, this would require a major extention to the project.

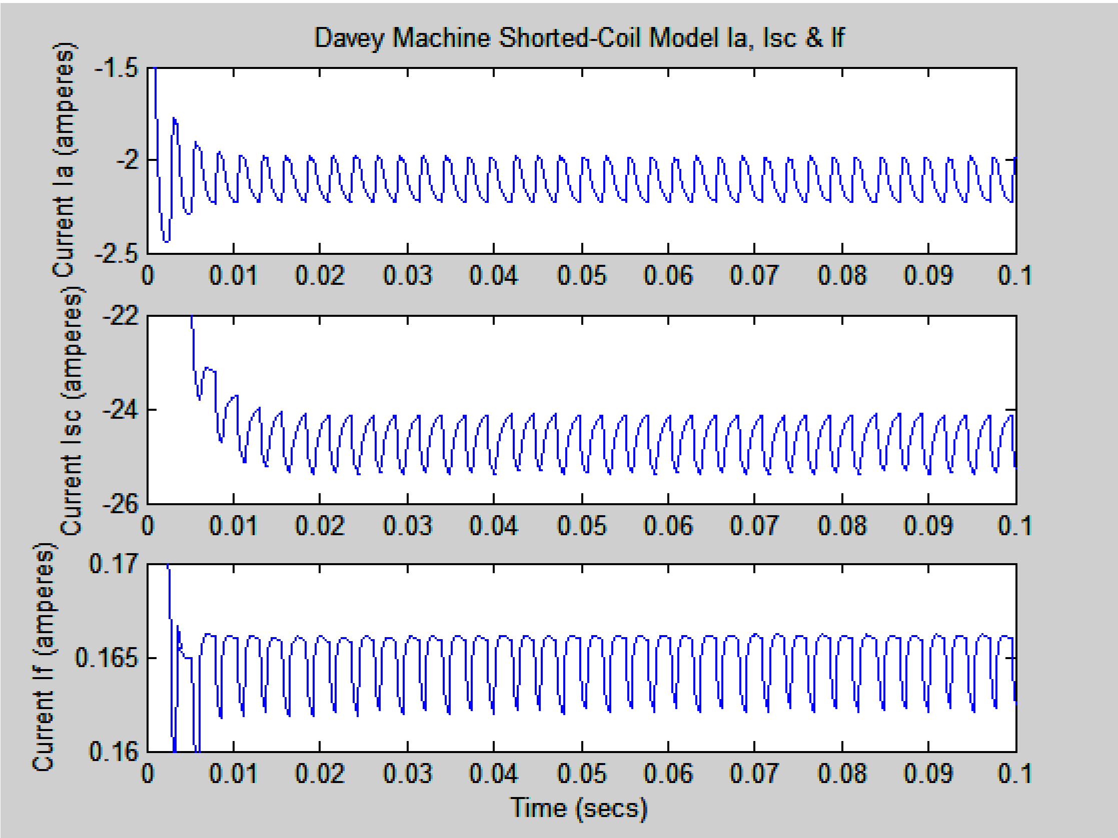

Figure 7.8 Model's outputs for the one coil shorted Davey machine

It can be seen that the waveforms of the I_a, I_{sc} and I_f are stable and are the same ripple frequency as in the healthy machine (about 38 periods in 100 milliseconds). The waveforms of the armature current I_a look quite similar to the healthy machine's I_a. Also, the I_a and I_{sc} appear symmetrical about the average value, but the field current I_f is not symmetrical. However, this predicted waveform is similar to the measure waveform of I_f, as shown in Figure 7.10.

It is apparent that the I_a and I_f d-c values from the shorted coil model are smaller than for the model of the healthy machine. The reduced magnitude of I_a is obviously affected by the shorted coil. There is a slightly larger ripple in I_a and a much large ripple in I_f.

It is worth checking why the short circuit current I_{sc} is about 25A d-c. The answer can be obtained from the calculation of the maximum possible value of I_{sc}, which is $\frac{U_1}{R_{sc}}$.

Where U_1 = voltage generated in the SC coil (ie, 1/6 or 1/7 of the rated voltage of 180V), and $R_{sc} = 0.9\ \Omega$.

Thus $I_{sc}\ (\text{Max}) \cong \frac{180/6.7}{0.9} = 29.8\text{A}$

Therefore, the model SC current of 25A d-c is reasonable.

Finally, a reminder that the model is only for 22.5° rotation of the SC coil.

7.5 Test results on the Davey machine with shorted coil

The measurement on the faulty machine was taken by shorting three segments on the rotor (assumed one segment in the model), in order to compare it with the model outputs. It should be understood that the shorted-circuit current I_{sc} could not be measured on the actual Davey machine. In order to reduce the risk of burning out the shorted coil, a reduced field current of 0.048A was used. The measured I_a and I_f waveforms are shown in Figure 7.9 and Figure 7.10.

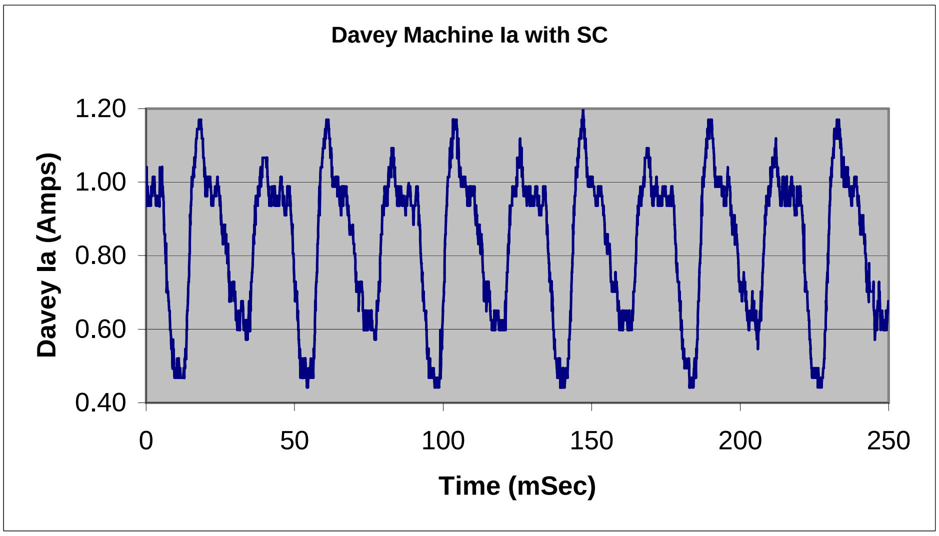

Figure 7.9 Measured Ia of the Davey machine with one shorted coil

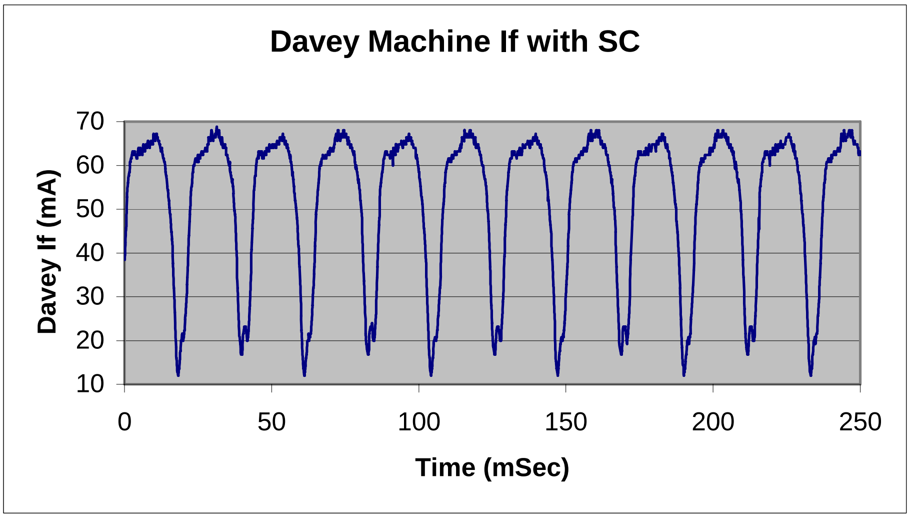

Figure 7.10 Measured I_f of the Davey machine with one shorted coil

The ripples on both Ia (75%) and If (115%) are much larger than in the healthy case, and not surprisingly do not correspond to the model, which is known to be inadequate.

The frequency of the ripple is approximately 48 Hz, so clearly it is not related to the commutator segment frequency of 380 Hz. 48Hz is double the rotor speed in rev/sec, and the dip in the field current occurs twice per revolution. This must be a result of the sudden reversal of current in the SC coil current that repeats every time the SC coil passes under a brush.

The measured I_a and I_f on Davey machine with a shorted coil were very convincing, as they looked very similar to the waveforms from the model. But the I_a and I_f on the actual machine are higher in the magnitudes than the model's output I_a and I_f. However, it was very surprising that the measured field current I_f shows almost the same waveform and the magnitude as given from the model I_f, even though it looks quite asymmetrical.

There is no doubt that the complete model of the shorted coil for 360° revolution could be achieved in a much more complicated way, and much longer research time will certainly be needed. Due to the limitation of the research time frame (about 12 months), the model of the short circuit armature coil cannot proceed any further than the results already obtained so far. However, the experience obtained during this research in dealing with electrical machines in MATLAB/SIMULINK might be useful for the future development.

The following Figure 7.11 displays the Davey machine testing site in the Power Laboratory.

Figure 7.11 Davey machine testing site in the Power Laboratory

Chapter 8

Conclusion of this research and further discussion

8.1 Overall review of the research work

The literature review of Chapter 2 was not able to provide any previous research directly related to this study except Ho [1]. The achievements in modelling a d-c machine can be summarised in three major sections:

- A new method of measuring self-inductance and mutual inductance in the machine;
- A model of the healthy d-c machine;
- A (incomplete) model of the machine with one shorted coil.

8.2 Measuring inductance method using a d-c source

Inductances are usually measured with alternating current in the coil. Commercial electronic RLC instruments use 1 kHz, but for a rotating machine 50 Hz could be more suitable. However, neither of these frequencies was suitable for the Davey machine. Reasons for this are explained in detail in Chapter 4 and Appendix A. Instead, a d-c method , based on Jones [22] was used, with some new modifications.

8.3 A model of the healthy Davey machine

Because of the complexity of dynamic-system problems, the usual simplifying assumptions made in many problems involving the behaviour of a d-c machine is to identify these problems using computer modelling. The detailed model of the healthy Davey machine was established with an assumption of varying brush resistances, and was implemented in SIMULINK. All inductances for the model were measured under the saturated flux conditions.

There was very good agreement between the model of the healthy machine and the experimental tests on the actual machine. Each output (ie. waveforms of the armature and field currents) obtained in the model was analysed and discussed.

8.4 A model of the faulty Davey machine with one shorted coil

Unfortunately, the complete model of the faulty machine could not be developed, simply because of lack of time. A shorted-coil was modelled for 22.5° of rotation only. Ripple frequency was as expected and the modelled currents were stable. Even though the current within the shorted coil on the actual machine cannot be measured, the value of I_{SC} in the model is close enough to what expected by calculation.

8.5 Working with models in MATLAB/SIMULINK

MATLAB is able to integrate computation, visualisation, and programming in flexible and user-friendly environments. SIMULINK was found to be one of the most useful tools available to efficiently model complex electric circuits. This research of a mathematical model for the Davey machine has improved the efficiency and accuracy of modeling a small d-c machine. It has been shown that either a healthy or faulty machine can be modelled with the methods developed.

The author found that the selection of an ODE (Ordinary Differential Equation) solver was very important, and ODE4 (Runge Kutta) was finally used for the models among a number of other available ODE solvers. The solver of ODE4 reduced the simulating time to about 5 seconds, compared with Ho's [1] model that took 26 hours to compute.

In using integrators to solve differential equations in SIMULINK, another important feature is a time delay which must be placed in front of the integrators, particularly in a model with multi-loops. Also, a time delay should be used in conjunction with two separate sub-systems, such as the 7-coil circuit and 5-coil circuit in the healthy machine model. Considerable experimentation was needed to achieve the correct time delay. Zero time delay sometimes could cause the model to be unstable.

The implementation of the simulation in SIMULINK is relatively straightforward, and allows observation of any component in the model at anytime. The model is also able to break down each part for individual tests if it is necessary. The author has no hesitation in endorsing the method for solving machine problems in SIMULINK to anyone if they are interested. There are enormous merits and advantages in using SIMULINK where more complicated machine problems could be solved efficiently.

8.6 Recommendations and future directions

The research outcomes have enabled the author to identify some key recommendations and to suggest future research directions. These are:

- Any type of d-c machine can be modelled using the method established in this research. It would be expected that modelling a machine with multi-poles would be more complicated.

- The basic principle in establishing equivalent circuits on an armature winding of d-c machines can be based on their commutation conditions. It is essential that two alternative equivalent circuits are used to simulate the commutating ripples in d-c currents.

- The d-c measuring inductance method can be used for measuring self-inductance and mutual inductance. This technique can be developed further to improve accuracy in measurement. D-c machine saturation conditions and coupling effects need to be known and set up during the measurement, so that all self and mutual inductances are measured under the same field flux.

- The research has provided good evidence that both healthy and faulty d-c machines can be modelled mathematically. Different technical treatments will be required to implement new models with different d-c machines with various operating or faulty conditions.

- MATLAB/SIMULINK proved to be a very useful tool for solving the complicated modelling required for this research and obviously has enormous potential for applications covering a wide range of Power Electrical Engineering.

References

[1] Ho S. Y. S., “ Condition Monitoring of Electric Motors” PhD thesis, the University of Tasmania, Australia, 1999.

[2] Srour JM and Cheng JKC, “Tools for DC machine diagnostic”, ICOMS 2000 Paper 18.

[3] Engelann R. H. and Middendorf W. H., “ Handbook of Electric Motors” Marcel Dekker, Inc, USA, 1995.

[4] Concordia C., “Synchronous machines”, John Wiley & Sons 1951.

[5] Hindmarsh J., “Commutation of Large D. C. Machines”, Electrical Times, 6 November 1958, pp. 187 –192.

[6] Hindmarsh J., “Electrical machines and their applications”, Pergamon Press 1977.

[7] Hindmarsh J. and Ghai N. K., “Objective methods of assessing commutation performance”, Proceeding IEE August 1961, Vol. 108, pp. 555-558.

[8] Hindmarsh J., “Fundamental Ideas on Large D. C. Machines”, Electrical Times, 7 August 1958, pp. 187 –192.

[9] Hindmarsh J., “Testing Large D. C. Machines”, Electrical Times, 12 March 1959, pp. 387 –390.

[10] Hindmarsh J., “Quick Response of Large D. C. Machines”, Electrical Times, 15 January 1959, pp. 79 –83.

[11] Hindmarsh J., “Volts per bar limit on large D. C. machines”, Electrical Times, 11 Sep. 1958, pp. 381 –85, and 25 Nov 1958, pp. 461 –463.

[12] Han Y. and Song Y. H., "Condition Monitoring Techniques for Electrical Equipment – A Literature Survey", IEEE Transactions on Power Delivery Vol. 18, No.1, January 2003.

[13] Ho S. and Langman R., "The Mathematical Model of a DC Motor", AUPEC Hobart Australia, 27 – 30 September 1998, pp. 389 – 394.

[14] Thompson J. E., "Problems of Brush Wear and Commutation", Electrical Times, 13 August 1964, pp. 227 –229.

[15] Tustin A. and Ward H., "The E.M.F.s induced in the armature coils of D. C. machines", IEE Monograph No. 511 U April 1962 pp. 456-474.

[16] Engelann R. H. and Middendorf W. H., " Handbook of Electric Motors" Marcel Dekker, Inc, USA, 1995.

[17] Clayton A. E. and Hancock N. N., "The performance and design of direct current machines", Pitman, 1959.

[18] Say M. G. and Taylor E. O., "Direct Current Machines", Pitman, Great Britain, 1980.

[19] Fitzgerald A. E., Kingsley Charles Jr. and Umans Stephen D. "Electric Machinery", McGraw Hill 2003.

[20] Sarma Mulukutla S., "Electrical Machines", WCB 1985.

[21] Slemon G. R. and Straughen A., "Electrical Machines", Addison-Wesley Publishing Company 1980.

[22] Jones C. V., "The unified theory of electrical machines", Butterworths, London, 1967.

[23] Spannhake S. and Filbert D., "A contribution to parameter estimation and model quality", Proceedings of the 25th University Power Engineering Conference, September 1990, pp. 767-770.

[24] Filbert D., "A contribution to the test of electric motors by parameter estimation methods", 25th Proceedings of UPEC Sept. 1990, Aberdeer-Scotland pp. 687-689.

[25] Filbert D., "Advanced fault diagnosis for the mass production of small power electric motors", SPIE Vol. 2101, Measurement Technology and Intelligent Instruments 1993, pp. 100-110.

[26] Guhmann C. and Filbert D., "Fault diagnosis of electrical low-power by analysis the motor current", IFAC/IMACS-Symposium on Fault Detection, Supervision and Safety for Technical Process, Vol.1, 1991, pp. 67-72.

[27] Filbert D. and Schneider C., "New methods for the testing of electric low power motors", 27th Proceedings of ISATA 31st Oct.-4th Nov. 1994, Aachen Germany.

[28] Filbert D., Schneider C. and Spannhake S, "Model equation and fault detection of electric motors", IFAC/IMACS-Symposium on Fault Detection, Supervision on Technical Diagnosis, Dresden, ISA Transactions 24 (3) 1985, pp. 67-72.

[29] Bradatsch T., Guhmann C., Ropke K. Schneider C. and Filbert D., "Analytical redundancy methods for diagnosing electric motors", Appl. Math. And Comp. Sci., 1993, Vol. 3, No.3, pp. 461-486.

[30] Filbert D., "Technical diagnosis and testing of electric motors in quality assurance", 8th IMECO Symposium on Technical Diagnostics, 23-25 Sept., 1992.

[31] Filbert D., "Technical diagnosis of electric drive systems", measurement Vol. 8, No.3, Jul.- Sept., 1990, pp. 121-127.

[32] Filbert D., “Quality testing systems with parameter estimation motor current spectral analysis for the detection of mechanical faults”, ISA Transaction Vol.24, No.3, pp.23-37.

[33] Diehl J. E., “Dissymmetry in D-C Rotating Electric Machines”, IEEE Transactions Power Apparatus System (USA) No.65, April 1963, pp. 57-67.

[34] Hughes E, “Fundamentals of Electrical Engineering in M.K.S. Units”, Longmans 1958.

[35] Hancock M., “Armature-conductor impedances and commutation in d. c. machines”, Proceeding IEE Vol.120, No.4, April 1973.

[36] Morley Arthur and Hughes Edward, “Principles of Electricity Based on the Rationalized M. K. S. System of Units”, Longmans 1958.

[37] Hughes Edward, “Fundamentals of Electrical Engineering”, Longmans 1954.

[38] Krisch E. and Smikal F., “Investigation of commutation of DC machines with wave winding”, International Conference of Electrical machines Proceeding, Budapest, Hungary, September 1982, Vol. 2, pp. 488-491.

[39] Sketch H. J. H., and Shaw P. A., “ A new method for observing the phenomena of commutation”, IEE Paper No. 2955 M June 1959.

[40] Schroeder T. W. and Aydelott J. C., “The ‘Black Band’ Method of Commutation Observation”, Proceeding IEE, Vol. 60, 1941.

[41] Johnson S., “ Commutation Adjustments on D. C. Machines”, Electrical Times, 21 September 1961, pp. 418 –420.

[42] Johnson S., “Testing D. C. Machines”, Electrical Times, 10 September 1964, pp. 379 - 416.

[43] Lundy R. T., "Measuring Commutation with An Indicating Instrument", AIEE Winter General Meeting, New York City, 31 January to 4 February 1949.

[44] Johnston H.R., "Blackzone measurement using photomultipliers", IEE Conference Publication No.11, 1964, pp. 171-177.

[45] Motter D. P., "Commutation of D-C Machines and Its Effects on Radio Influence Voltage Generation", AIEE Transactions Vol. 68, 1949, pp. 491-496.

[46] Linville T. M. and Rosenberry Jr G. M., "Commutation of Large D-C Motors and generators", AIEE Transaction, Part III Vol. 71 January 1952, pp 326-336.

[47] Walton A. P., "The effect of stationary parts on D. C. machine commutation", IEE Conference Publication No.11, 1964, pp. 159-163.

[48] Jones C. V., "A new theory of commutation", IEE Conference Publication No.11, 1964, pp. 6-10.

[49] Tarkanyi M., "The influence of the commutating coils on the main pole flux of a DC machine", IEE Conference Publication No.11, 1964, pp. 28-42.

[50] Taylor P. l., "Improving commutation in d. c. machines by the use of flux traps", Proceeding IEE, Vol. 117, No.7, July 1970.

[51] Schroder R. and Oberretl K., "Calculation of DC machine commutation taking brush contact resistance into account", Archiv fur Elektrotechnik Vol. 73, No.2, 1990, pp. 69-79. (In German).

[52] Doppelbauer M., "New results on the commutation of dc machines using harmonic field theory", Electrical Engineering, Springer-Verlag, Vol. 80, 1997, pp. 41-50. (In German).

[53] Goyet R. and Benalla H., "Commutations of DC machine by means of external assistance", Journal de Physique III, France, Vol.4, No.12, Dec. 1994, pp. 2583-2592. (In French).

[54] Ramboz J. D., "Machinable Rogowski Coil, Design, and Calibration", IEEE Transactions on Instrumentation and Measurement, Vol.45, No. 2, April 1996, pp. 511-515.

[55] Destefan D. E., "Calibration and Testing facility for Resistance Welding Current Monitors", IEEE Transactions on Instrumentation and Measurement, Vol.45, No. 2, April 1996, pp. 453-456.

[56] Krause P. C., "Analysis of Electric Machinery", McGraw Hill 1987.

[57] Langman R., "The manual of the Direct Current Inductance Bridge", School of Engineering, The University of Tasmania.

[58] Jones C. V., "An analysis of commutation for the unified-machine theory", Trans. American IEE Part III Vol. 79, February 1960, pp. 476-488.

[59] Thaler G. J. and Wilcox M. L., "Electric Machines: Dynamics and Steady State", Wiley International Edition, 1966.

[60] Messerle H. K., "Dynamic circuit theory", AIEE Transactions Part III. Power Apparatus and Systems, April 1960 pp. 1-12.

[61] Glowacz Z., "Analysis of failure states of DC machine", Proceedings of International Conference on Electrical Machines, ICEM'96, September 10-12, 1996, Vigo, Span, Vol. 2, pp. 464-469.

[62] Burth M., Filbert D, Guhmann C., Ropke K. and Schneider C., "Non-linear Approach to the Fault Diagnosis of Low Power Motors", Elektronnoe Modelirovanie Vol. 17, No.6, Nov.-Dec. 1995, pp. 73-78.

[63] Filbert D. and Guhmann C., "Fault diagnosis on bearings of electrical motor by estimating the current spectrum", IFAC/IMACS-Symposium on Fault Detection, Supervision and Safety for Technical Process, Vol.2, 1994, pp. 714-719.

[64] Bradatsch T. and Filbert D., "A personal computer based system for fault detection in electric motors", 25th UPEC Conference Proceeding 1990, pp. 703-706.

[65] Poignet P., Gautier M., Khalil W. and Pham M.T., "Modeling, simulation and control of high speed machine tools using robotics formalism", Mechatronics, 2002, pp. 461-487.

[66] Ghoneim W. A. M., Fletcher J. E. and Williams B. W., "Matrix approach for the generalised theory of doubly salient reluctance machines", IEE Proc, Elect. Power Appl. Vol. 149, No.1, January 2002, pp. 65-80.

[67] Lyshevski S. E., "Electromechanical systems, electric machines, and applied mechatronics", CRC Press 2000.

[68] Cathey J. J., "Electric machines analysis and design applying MATLAB", McGraw Hill International Edition.

Measurements of armature inductance using an a-c source

A. 1 Measurement errors in the a-c method

Chapter 4 describes the Direct Current Inductance Bridge (DCIB) technique to measure self and mutual inductances of the Davey motor. The DCIB was necessary because the (more usual) a-c or impedance technique gave us misleading results. It was attempted to use an a-c method before using the DCIB. This appendix describes some of the results, and also shows the theory as to why the a-c method was not used for this research.

The a-c method induces currents in any other (closed) circuits that are magnetically coupled with the circuit whose inductance is to be measured. Take the armature inductance L_a. The armature coil is coupled with the field coil and probably also with undefined eddy current circuits in the aluminum end covers. The form of the circuit is shown in Figure A.1.

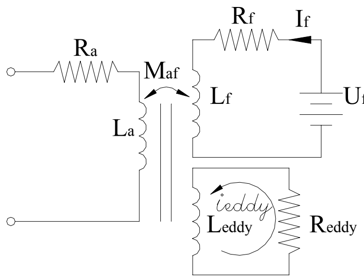

Figure A.1 Eddy current generated by the field current

For the required data in the SIMULINK model, it was necessary to measure all inductances under the rated operating conditions. The rated field current of 0.2A caused magnetic saturation in the field poles. In order to achieve this, the circuit in Figure A.2 was derived from Figure A.1 for the a-c measuring method.

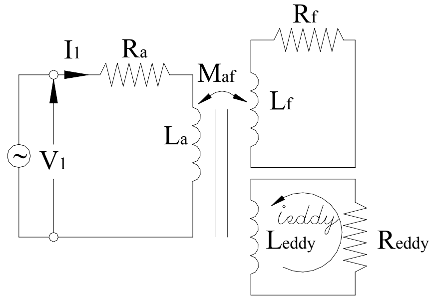

Figure A.2 Eddy current generated by the a-c supply

The quantitative effect of the eddy current is unknown, but presumably, since a d-c method is able to "ignore" their effect, then a sufficiently low a-c frequency would mean that the eddy currents do not affect the armature inductance measurement. The theory is given for only one coupled circuit, as shown in Figure A.3, in order to simplify the mathematics in the calculation, but it is adequate to predict the trends.

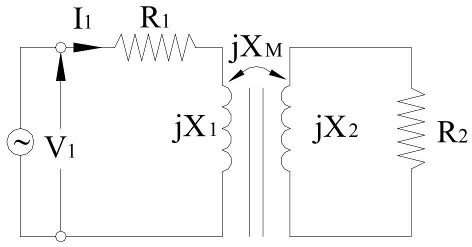

Figure A.3 Equivalent circuit of the a-c measuring method

From the circuit in Figure A.3, input impedance Z_{in} can be obtained by

$$Zin = \frac{U_1}{I_1} = R_1 + jX_1 - \frac{X_M{}^2\,(jX_2 - R_2)}{X_2{}^2 + R_2{}^2}$$

The imaginary part of Z_{in} is the apparent reactance

$$X_{in}' = X_1 - \frac{X_M{}^2 \times X_2}{X_2{}^2 + R_2{}^2}$$

Let $X_1 = X_2$, $X_1 = \omega L_1$, and $X_M = KL_1$, where K is a coupling factor.

$$\text{Then, } \omega L_{in} = \left[\omega L_1 - \frac{K^3 \times \omega^2 \times L_1{}^2}{K^2 \times \omega^2 \times L_1{}^2 + R_2{}^2} \right]$$

To make the second term on the RH side insignificant (say 1%) of ωL_1 , requires

$$\frac{K^3 \times \omega^2 \times L_1{}^2}{K^2 \times \omega^2 \times L_1{}^2 + R_2{}^2} = 0.01$$

Consider $K \cong 1.0$, and assume that for a frequency of 50 Hz, $\omega L_1 = R_2$.

If the required low value of ω is $\omega' = x\omega$, then $1 + \frac{1}{x^2} = 100$

Hence x = 0.1, coresponding to a frequency of 5 Hz.

The coupling factor K is of course less than 1.0 and later measurement showed it to be approximately 0.9 for the armature and field coils. This does not significantly affect the value of the low frequency to be uesd.

The armature impendance was measured under a varying frequency from 70Hz down to 5Hz. The set-up is shown in Figure A.4, in which the field coil was open circuit and the supply was an Agilent 6813B electronic power conditioner. The measurement of voltage, current and power was done with a Voltech PM100 power meter.

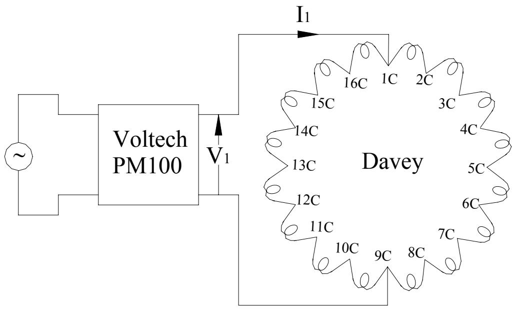

Figure A.4 Set-up of the a-c measuring method

Figure A.5 shows the assumed equivalent circuit (Ref. Jones [5])

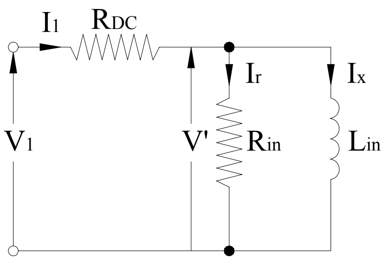

Figure A.5 Set-up of the a-c measuring method

R_{DC} is the d-c resistance of the complete armature. L_{in} is the apparent inductance, to be calculated from the Voltech data, and R_{in} represents losses that may be from the hysteresis and eddy currents. The results of this a-c method are shown in Figure A.6.

.

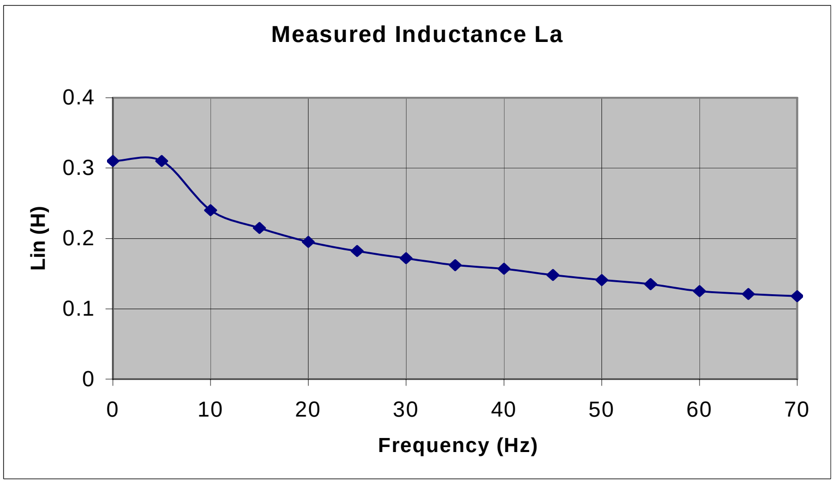

Figure A.6 Measured Lin in the a-c circuit

The inductance of 0.31H at the frequency of 0 Hz was measured with the DCIB. It was the same as the 5 Hz value within the limits of experimental error. It was mentioned earlier in this appendix that a field current of 0.18A should be presented for all inductance measurements, which, if an a-c method were to be used, would effectively give the circuit of Figure A.2. Subsequent DCIB data showed that the ratio $\omega L_2/R_2$ was about 13 at 50 Hz. This would require a supply frequency of about 1.2 Hz to give an apparent inductance of only 1% less than the true value.

Both the Agilent supply and the Voltech power meter had a lower limit at 5 Hz. It was thus apparent that a d-c method must be used, as the accompanying errors in the a-c method cannot be tolerated.

A. 2 Saturated and unsaturated inductance data

Some miscellaneous inductance data given here were measured in the course of trying to ascertain the appropriate flux condition, and they were all done with the DCIB. The following data show the different results, with and without magnetic saturation.

The measured field self-inductance L_f = 185H with $I_f = \pm$ 0.18A

Incremental field self-inductance ΔL_f = 47H; I_f altered from 0.20A to 0.18A.

Armature complete self-inductance L_a at $I_a = \pm$ 2.0A. The unsaturated value varies sinusoidally with rotor position from a maximum of 0.31H to a minimum of 0.15H. The saturated value (at $I_a = \pm$ 2.0A, I_f = 0.18A) is almost constant with rotor position (70 ± 10) mH.

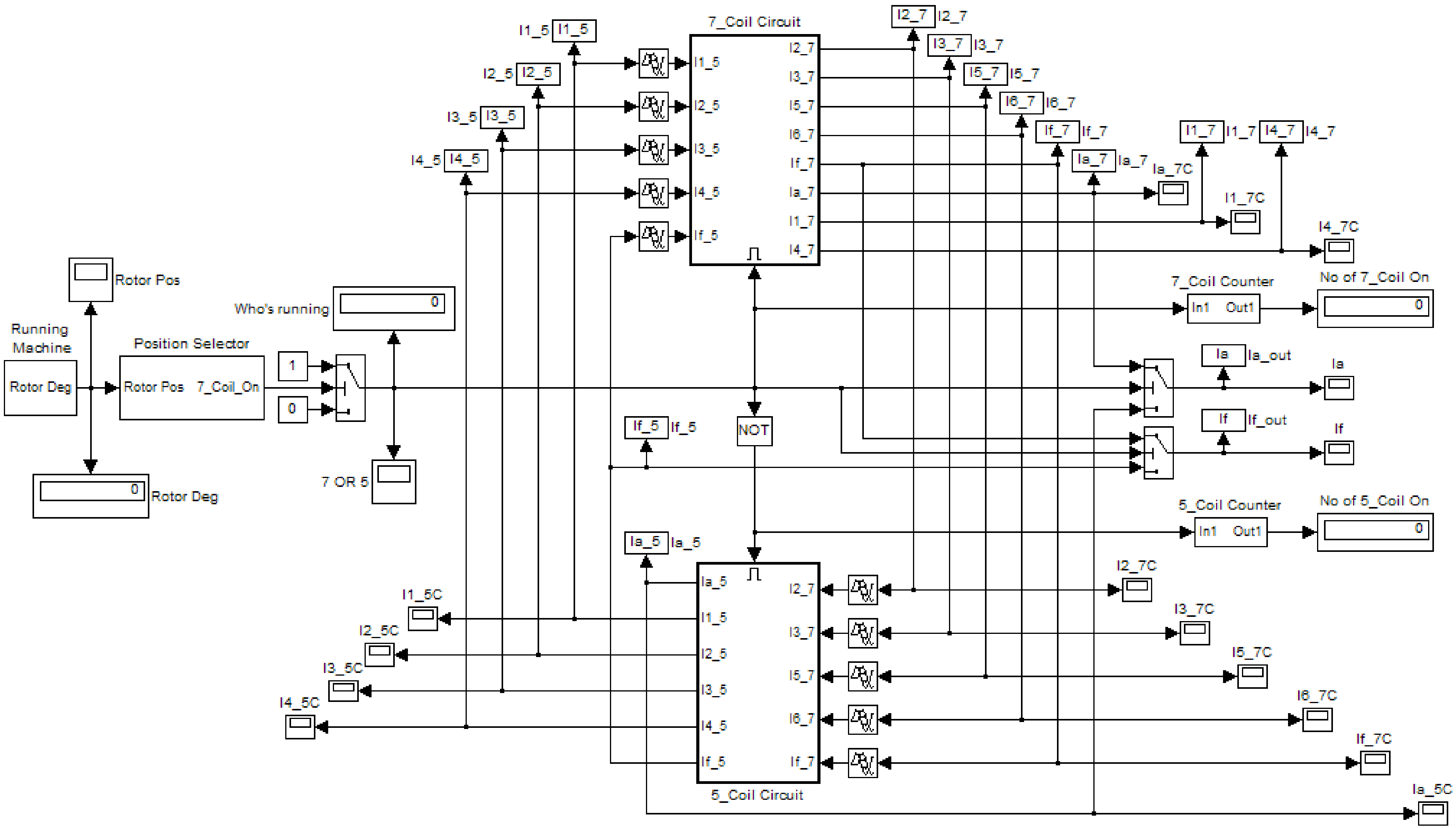
7_Coil Circuit
5_Coil Circuit
Running Machine
Rotor Deg
Position Selector
Rotor Pos
7_Coil_On
Who's running
7 OR 5
NOT
7_Coil Counter
No of 7_Coil On
5_Coil Counter
No of 5_Coil On
In1 Out1
Ia_out
If_out

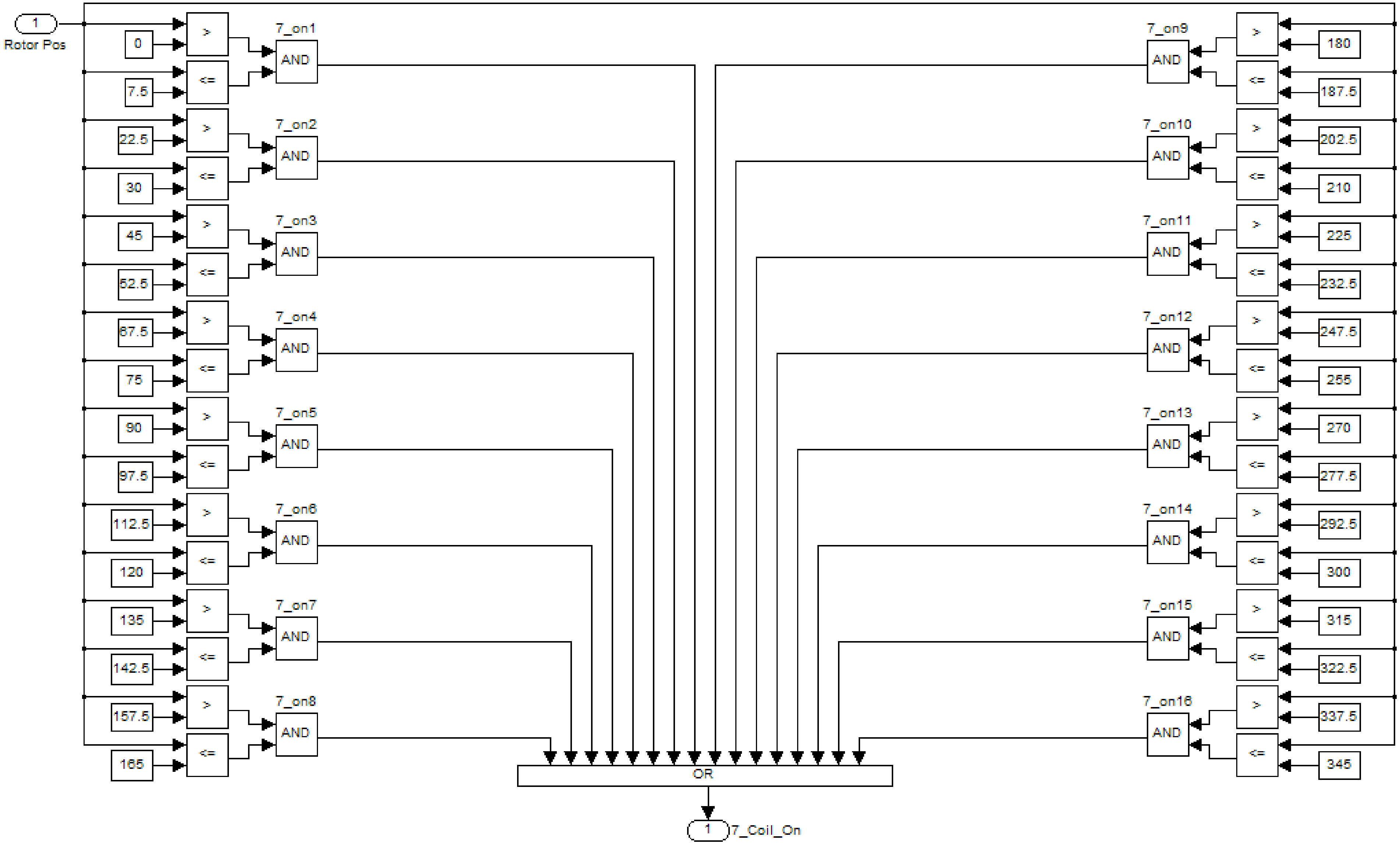
1
Rotor Pos
0
7.5
22.5
30
45
52.5
67.5
75
90
97.5
112.5
120
135
142.5
157.5
165
180
187.5
202.5
210
225
232.5
247.5
255
270
277.5
292.5
300
315
322.5
337.5
345
7_on1
7_on2
7_on3
7_on4
7_on5
7_on6
7_on7
7_on8
7_on9
7_on10
7_on11
7_on12
7_on13
7_on14
7_on15
7_on16
AND
OR
1
7_Coil_On

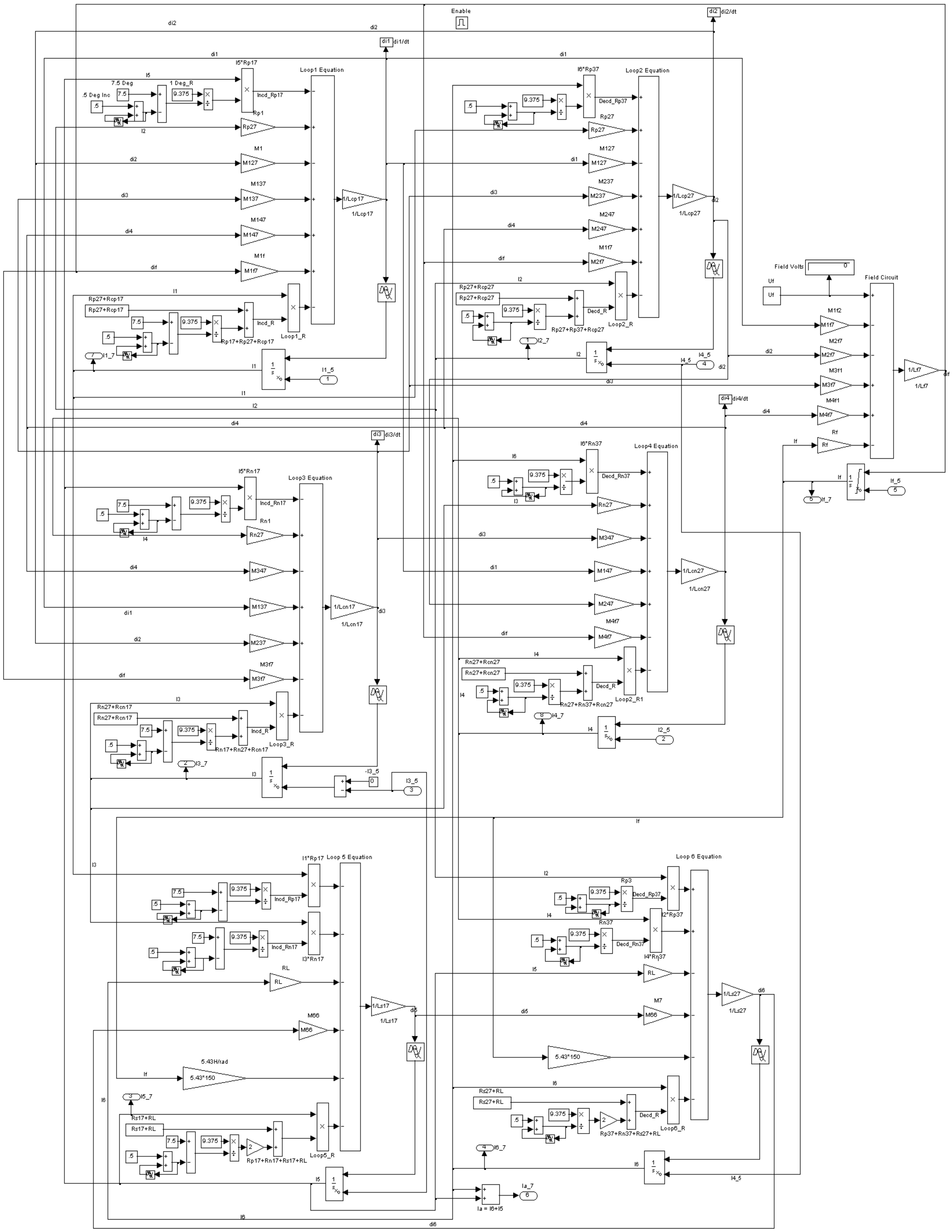
Enable
Loop1 Equation
Loop2 Equation
Loop3 Equation
Loop4 Equation
Loop 5 Equation
Loop 6 Equation
Field Circuit
Field Volts
1/Lcp17
1/Lcp27
1/Lcn17
1/Lcn27
1/Ls17
1/Ls27
1/Lf7
di1/dt
di2/dt
di3/dt
di4/dt
Rp27+Rcp17
Rp27+Rcp27
Rn27+Rcn17
Rn27+Rcn27
Rs17+RL
Rs27+RL
Rp17+Rp27+Rcp17
Rp27+Rp37+Rcp27
Rn17+Rn27+Rcn17
Rn27+Rn37+Rcn27
Rp17+Rn17+Rs17+RL
Rp37+Rn37+Rs27+RL
5.43H/rad
5.43*150
Ia = I6+I5

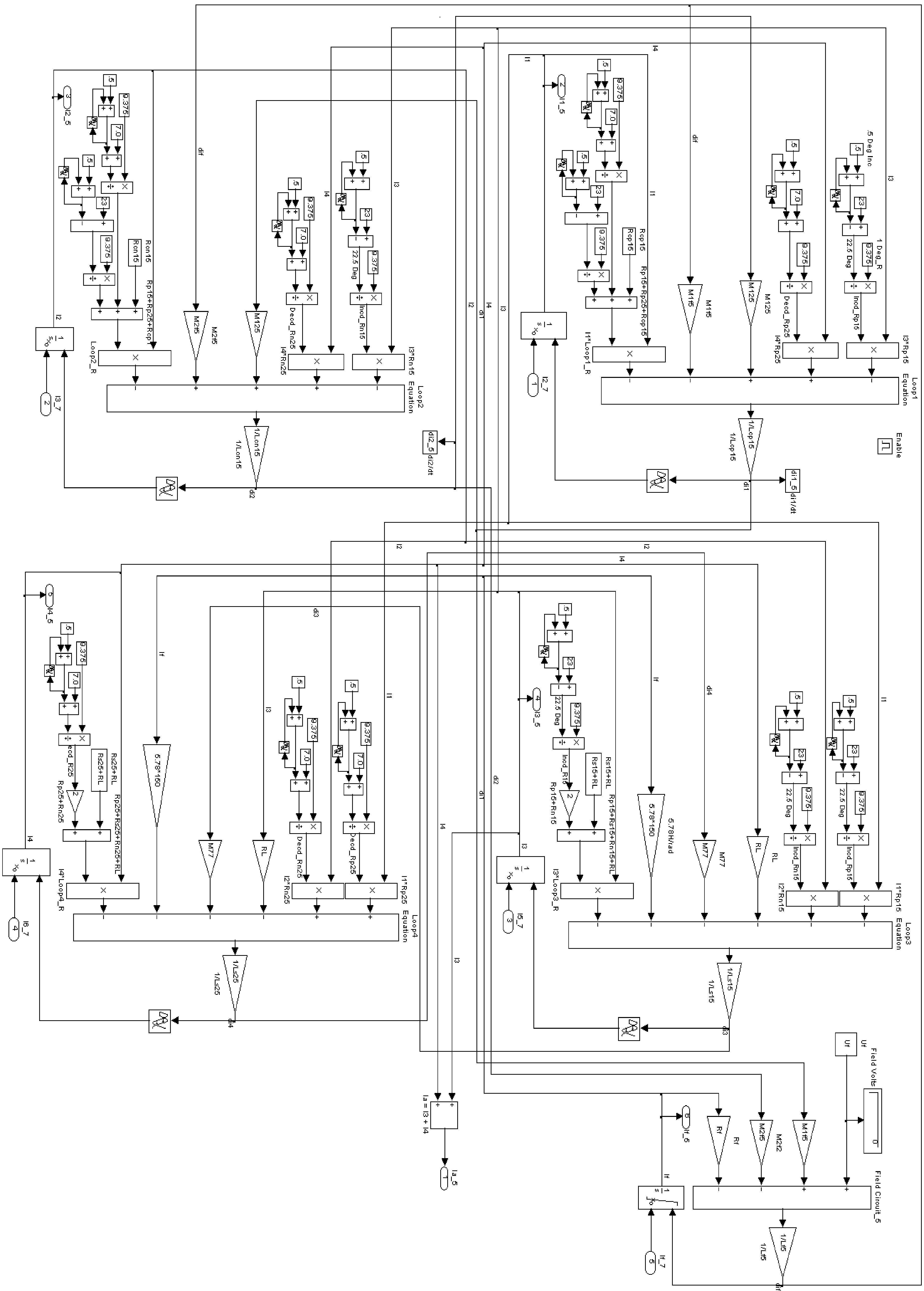

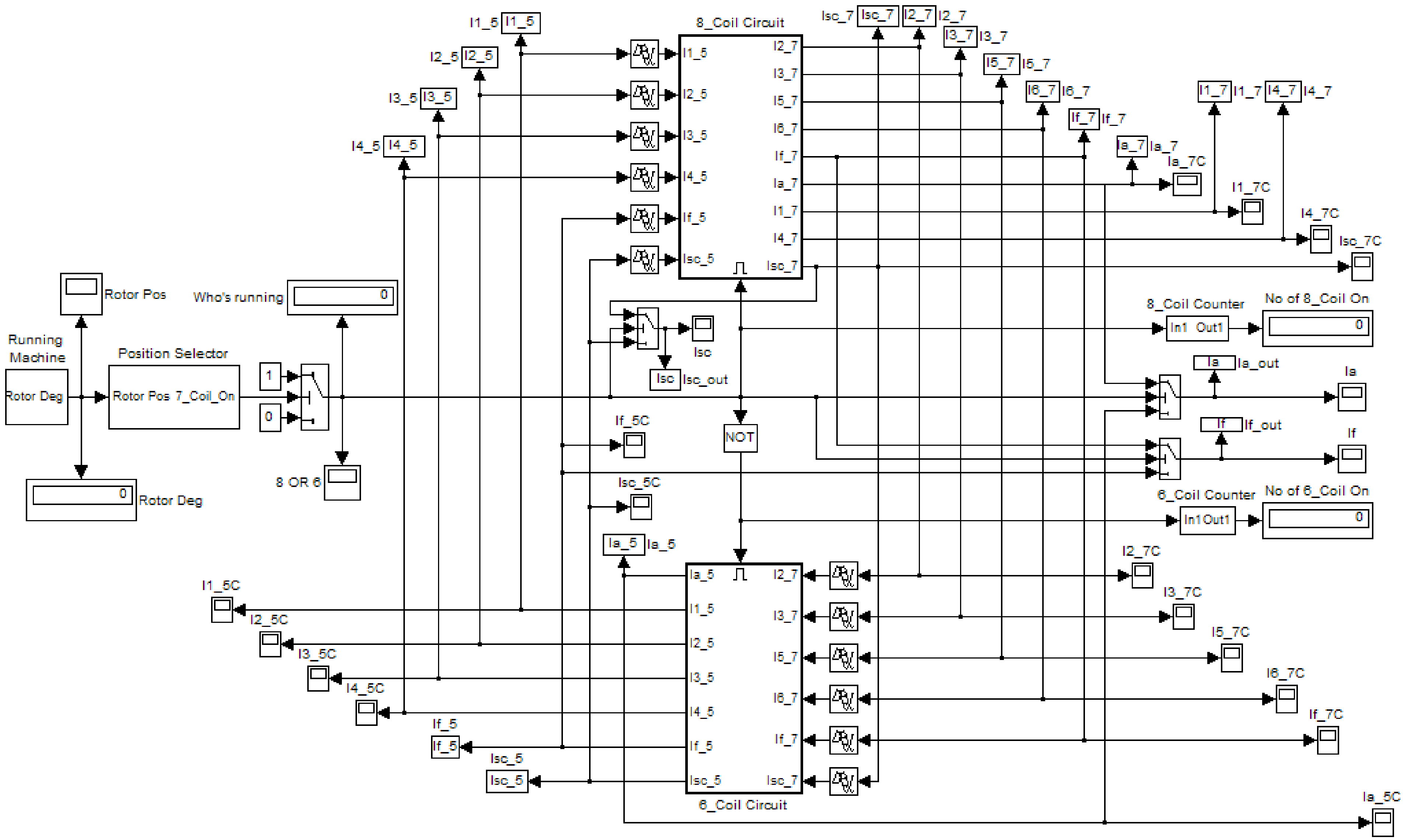
8_Coil Circuit
I1_5
I2_5
I3_5
I4_5
If_5
Isc_5
I2_7
I3_7
I5_7
I6_7
If_7
Ia_7
I1_7
I4_7
Isc_7
Ia_7C
I1_7C
I4_7C
Isc_7C
Rotor Pos
Who's running
0
Running Machine
Rotor Deg
Position Selector
Rotor Pos 7_Coil_On
1
0
8 OR 6
Rotor Deg
Isc
Isc_out
NOT
If_5C
Isc_5C
Ia_5
8_Coil Counter
In1 Out1
No of 8_Coil On
Ia
Ia_out
If
If_out
6_Coil Counter
No of 6_Coil On
I1_5C
I2_5C
I3_5C
I4_5C
I2_7C
I3_7C
I5_7C
I6_7C
If_7C
Ia_5C
6_Coil Circuit

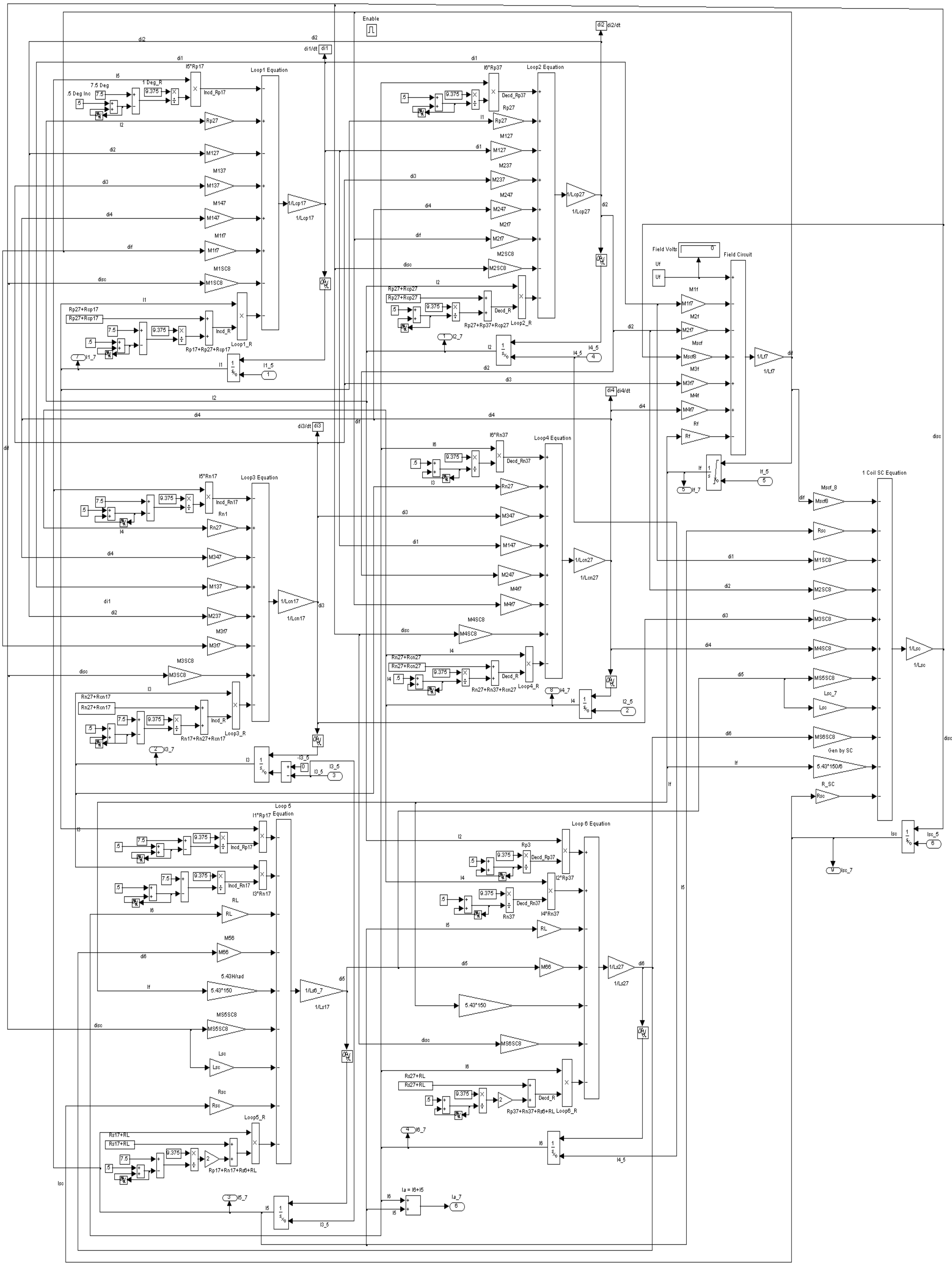

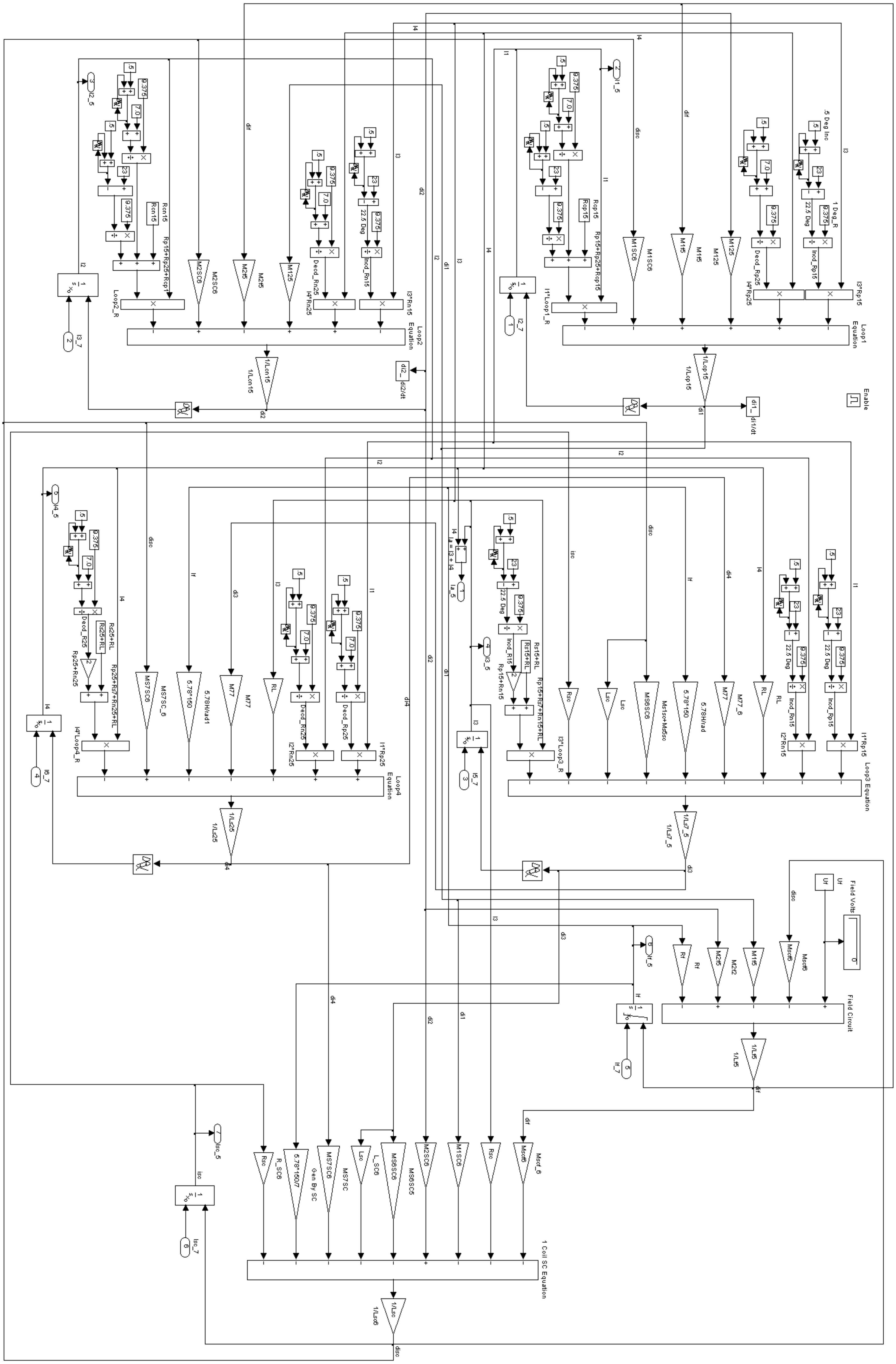
Loop1 Equation
Loop2 Equation
Loop3 Equation
Loop4 Equation
Field Circuit
1 Coil SC Equation
Field Volts
Enable

Appendix D-1

Data for the model of the healthy Davey machine

U_f	220 Volt
R_f	1100 Ohm
L_f	47.7 H
R_L	56.25 Ohm
7-coil equivalent circuit sub-model	
$R_{p2} = R_{n2}$	0.4167 Ohm
$R_{cp1} = R_{cp2} = R_{cn1} = R_{cn2}$	0.9 Ohm
$R_{S1} = R_{S2}$	5.4 Ohm
$M_{1f} = M_{2f} = M_{3f} = M_{4f}$	0.27 H
$M_{12} = M_{13} = M_{14} = M_{23} = M_{24} = M_{34}$	0.002 H
M_{66}	0.025 H
$L_{cp1} = L_{cp2} = L_{cn1} = L_{cn2}$	0.0025 H
$L_{S1} = L_{S2}$	0.03 H
Note: R_{p1}, R_{p3}, R_{n1} and R_{n3} are varying in the model	
5-coil equivalent circuit sub-model	
$R_{cp1} = R_{cn1}$	1.8 Ohm
$R_{S1} = R_{S2}$	6.3 Ohm
$M_{1f} = M_{2f}$	0.54 H
M_{12}	0.002 H
M_{77}	0.03 H
$L_{cp1} = L_{cn1}$	0.009 H
$L_{S1} = L_{S2}$	0.034 H
Note: R_{p1}, R_{p2}, R_{n1} and R_{n2} are varying in the model	

Appendix D-2

Data for the model of the Davey machine with one shorted coil

U_f	220 Volt
R_f	1100 Ohm
L_f	47.7 H
R_L	56.25 Ohm
8-coil equivalent circuit sub-model	
$R_{p2} = R_{n2}$	0.4167 Ohm
$R_{cp1} = R_{cp2} = R_{cn1} = R_{cn2} = R_{SC}$	0.9 Ohm
$R_{S1} = R_{S2}$	5.4 Ohm
$M_{1f} = M_{2f} = M_{3f} = M_{4f}$	0.27 H
$M_{1SC} = M_{2SC} = M_{3SC} = M_{4SC} = M_{5SC}$	0.002 H
$M_{12} = M_{13} = M_{14} = M_{23} = M_{24} = M_{34}$	0.002 H
M_{6SC}	0.0025 H
M_{66}	0.025 H
$L_{cp1} = L_{cp2} = L_{cn1} = L_{cn2}$	0.0025 H
$L_{S1} = L_{S2}$	0.03 H
Note: R_{p1}, R_{p3}, R_{n1} and R_{n3} are varying in the model	
6-coil equivalent circuit sub-model	
$R_{cp1} = R_{cn1}$	1.8 Ohm
R_{SC}	0.9 Ohm
$R_{S1} = R_{S2}$	6.3 Ohm
$M_{1f} = M_{2f}$	0.54 H
M_{12}	0.002 H
M_{77}	0.03 H
$M_{1SC} = M_{2SC}$	0.002 H
M_{S6_SC}	0.025 H
M_{S6_SC}	0.025 H
M_{SCf}	0.02 H
$L_{cp1} = L_{cn1}$	0.009 H
$L_{S1} = L_{S2}$	0.034 H
Note: R_{p1}, R_{p2}, R_{n1} and R_{n2} are varying in the model	